

AN ABSTRACT OF THE THESIS OF

Sean Kissick for the degree of Master of Science in Mechanical Engineering presented on June 20, 2018.

Title: Power Cycle Selection and Optimization for a Small Modular Reactor

Abstract approved: _____

Hailei Wang

As a way to improve safety and economics, one area of research and commercialization of new nuclear power plants has focused on the development of small modular reactors (SMRs). NuScale Power has developed a 50 MWe natural convection cooling SMR coupled with a regenerative Rankine cycle. Current estimates place the NuScale SMR plant at a competitive levelized cost of electricity (LCOE), but there is continued interest to improve the economics of the system. This paper provides a research review and analysis of alternative power cycle designs well suited for the NuScale SMR. Alternative cycles are analyzed for overall cycle efficiency, 2nd law exergy efficiencies, capital cost, and plant (LCOE). These results are compared to the baseline regenerative Rankine cycle via optimization techniques. Results reveal two cycles, regenerative reheat Rankine and transcritical ethanol, have promise as alternative cycles. While both cycles had higher estimated capital costs, the additional power produced reduced the LCOE by $5.1 \pm 4.0\%$ for the regenerative reheat Rankine cycle and $4.8 \pm 4.8\%$ for the transcritical ethanol cycle, when compared to the regenerative Rankine cycle. The regenerative reheat Rankine cycle would be the simplest cycle to integrate into the NuScale SMR as it is similar to the baseline regenerative Rankine cycle. Conversely, the transcritical ethanol cycle would require more research to assess the viability, but has greater potential to improve the economics of the system.

©Copyright by Sean Kissick
June 20, 2018
All Rights Reserved

Power Cycle Selection and Optimization for a Small Modular
Reactor

by

Sean Kissick

A THESIS

submitted to

Oregon State University

in partial fulfillment of
the requirements for the
degree of

Master of Science

Presented June 20, 2018
Commencement June 2019

Master of Science thesis of Sean Kissick presented on June 20, 2018.

APPROVED:

Major Professor, representing Mechanical Engineering

Head of the School of Mechanical, Industrial, and Manufacturing Engineering

Dean of the Graduate School

I understand that my thesis will become part of the permanent collection of Oregon State University libraries. My signature below authorizes release of my thesis to any reader upon request.

Sean Kissick, Author

ACKNOWLEDGEMENTS

I would like to recognize and express my gratitude to my advisor Dr. Hailei Wang, who if not for the guidance, patience, and opportunities he presented me with, I would not have pursued a graduate program. My education was strengthened by your knowledge and leadership.

Besides my advisor, I would like to thank the rest of my thesis committee. If not for the excellent teachings of Dr. Brian Fronk and Dr. Chris Hoyle this work would have been insufficient. For Dr. Goran Jovanovic, thank you for performing the thankless job of graduate council representative, I am grateful you did not turn me down as many others had.

I would like to thank NuScale Power and specifically Derick Botha for both funding my program and providing me with a very interesting and challenging topic of study. I hope this work provides some valuable insight on your future developments.

Most importantly I wholeheartedly thank my wife Kate. Without her I would never have had the courage, commitment, and belief in myself to pursue this new journey. And although I am terrible at communicating my appreciation, please know I recognize all of the support and patience you provided during this process. I am forever grateful and will love you forever.

TABLE OF CONTENTS

	<u>Page</u>
1 Introduction	1
1.1 Overview	1
1.2 Project Scope	5
1.3 Design Problem	5
2 Literature Review	7
2.1 Regenerative Rankine Cycle	7
2.2 Rankine Reheat Cycle	8
2.3 Supercritical CO2 Cycles	10
2.4 Transcritical Cycle	14
2.5 Kalina Cycle	15
2.6 Combined Cycle	17
2.7 Trilateral Flash Cycle	19
3 Methods	22
3.1 Overview	22
3.2 1st Law Analysis	23
3.2.1 Equations	23
3.2.1.1 Turbine	24
3.2.1.2 Pumps and Compressors	25
3.2.1.3 Heat Exchangers	25
3.2.1.4 Throttle Valves	27
3.2.1.5 Mixing Valves	27
3.2.1.6 Flow Splitting	28
3.2.1.7 Cycle Efficiency	28
3.3 Exergy Analysis	28
3.4 Component Costing Models	30
3.4.1 Costing Model Comparison	31
3.4.1.1 Turbine and Compressor Cost Model	31
3.4.1.2 Heat Exchanger Cost Model	33
3.4.1.3 Pump Cost Model	36
3.4.2 Costing Model Selection	37
3.4.3 Heat Exchange Surface Area	39

TABLE OF CONTENTS (Continued)

		<u>Page</u>
3.4.3.1	Heat Transfer Area Equations	40
3.4.3.2	Different Heat Transfer Modes In Single Heat Exchanger	40
3.5	Levelized Cost of Electricity	43
3.6	Assumptions	44
3.7	Software	46
3.8	Solution Process	47
3.9	Cycle Optimization	48
3.10	Uncertainty	50
4	Results	52
4.1	1st Law Analysis	52
4.1.1	Cycles	53
4.1.1.1	Regenerative Rankine Cycle	53
4.1.1.2	Reheat Regenerative Rankine Cycle	56
4.1.1.3	Transcritical Cycle	59
4.1.1.4	sCO_2 Regenerative Cycle	62
4.1.1.5	sCO_2 Recompression Cycle	65
4.1.1.6	Combined Cycle	69
4.1.2	Cycle Comparison	73
4.2	Exergy Analysis	74
4.3	Costing and LCOE Analysis	78
4.3.1	Cycles	79
4.3.1.1	Regenerative Rankine Cycle	79
4.3.1.2	Regenerative Reheat Rankine Cycle	80
4.3.1.3	Transcritical Ethanol Cycle	82
4.3.1.4	sCO_2 Recompression Cycle	84
4.3.2	Cycle Comparison	86
5	Discussion	88
5.0.1	Cycle Efficiency	90
5.0.2	Exergy Efficiency	90
5.0.3	Levelized Cost of Energy (LCOE)	91
5.0.4	Efficiency vs. LCOE	92
5.0.5	Reactor Power	93

TABLE OF CONTENTS (Continued)

	<u>Page</u>
6 Conclusion	96

LIST OF FIGURES

<u>Figure</u>		<u>Page</u>
1.1	Diagram of NuScale small modular reactor.	2
1.2	NuScale small modular reactor portability.	3
1.3	Estimated levelized cost of electricity comparison of NuScale SMR plant versus other common power plants.	4
2.1	Cycle and temperature-entropy diagram of the NuScale regenerative Rankine cycle.	8
2.2	Cycle and temperature-entropy diagram of a regenerative reheat Rankine cycle.	9
2.3	Cycle and temperature-entropy diagrams for a sCO_2 regenerative cycle.	11
2.4	Cycle and T-s diagrams for a sCO_2 recompression cycle.	12
2.5	Power cycle efficiency for selected cycles.	13
2.6	Cycle and T-s diagrams for a transcritical cycle.	15
2.7	Temperature-entropy diagrams of the Rankine and Kalina cycles.	16
2.8	Diagram for a combined cycle with a sCO_2 regenerative topping cycle and a ORC bottoming cycle.	18
2.9	Heat addition temperature profile for different cycles.	20
2.10	T-s diagram for trilateral flash cycle.	21
3.1	Diagram of cycle selection process.	22
3.2	Comparison of turbine costing models.	32
3.3	Comparison of sCO_2 turbine and compressor costing models.	33
3.4	Comparison of shell and tube heat exchanger costing models.	34
3.5	Comparison of PCHE costing models.	36
3.6	Temperature/enthalpy diagram of a two fluid heat exchange in counterflow orientation.	41

LIST OF FIGURES (Continued)

<u>Figure</u>	<u>Page</u>
4.1 Cycle diagram of the NuScale regenerative Rankine cycle.	54
4.2 Cycle diagram of two regenerative reheat Rankine cycles.	57
4.3 Diagram of transcritical cycle.	61
4.4 sCO_2 regenerative cycle diagram.	64
4.5 sCO_2 regenerative cycle efficiency vs. minimum pressure.	65
4.6 sCO_2 recompression cycle diagram.	67
4.7 sCO_2 recompression cycle efficiency vs. flow split ratio.	68
4.8 sCO_2 recompression cycle efficiency vs. minimum cycle pressure.	69
4.9 Diagram for a combined cycle with a sCO_2 regenerative topping cycle and an ORC bottoming cycle.	71
4.10 Overall first law cycle efficiency comparison.	74
4.11 Percentage of exergy destroyed by cycle and component.	75
4.12 Percentage of exergy destroyed for heat exchangers.	76
4.13 Percentage of exergy destroyed for turbines and pumps.	77
4.14 Percentage of exergy destroyed for flow mergers and throttle valves.	78
4.15 Regenerative Rankine cycle estimated cost by component.	79
4.16 Regenerative Rankine cycle levelized cost of electricity and 1st law effi- ciency vs. average regenerator effectiveness.	80
4.17 Regenerative reheat Rankine cycle estimated cost by component.	81
4.18 Regenerative reheat Rankine cycle levelized cost of electricity and 1st law efficiency vs. average regenerator effectiveness.	81
4.19 Transcritical cycle estimated cost by component.	82
4.20 Transcritical cycle levelized cost of electricity and 1st law efficiency vs. average regenerator effectiveness.	83

LIST OF FIGURES (Continued)

<u>Figure</u>		<u>Page</u>
4.21	<i>sCO</i> ₂ recompression cycle estimated cost by component.	84
4.22	<i>sCO</i> ₂ recompression cycle levelized cost of electricity and 1st law efficiency vs. average regenerator effectiveness.	85
4.23	Estimated levelized cost of electricity (LCOE) and cycle efficiency comparison.	87
5.1	Temperature profile within the high temperature regenerator in the transcritical ethanol cycle.	92
5.2	Temperature profile of the baseline regenerative Rankine and regenerative reheat Rankine cycles during heat exchange within the primary heat exchanger.	94
5.3	Temperature profile of the transcritical ethanol and <i>sCO</i> ₂ recompression cycle during heat exchange within the primary heat exchanger.	95

LIST OF TABLES

Table	Page
1.1 NuScale Power SMR parameters used to evaluate alternative power cycle options.	6
3.1 Printed circuit geometry assumptions used to determine heat exchanger weight.	35
3.2 Pump cost estimates for three first order costing methods.	37
3.3 Costing model selection for power cycle analysis.	38
3.4 Overall assumptions used in the analysis of potential replacement power cycles.	45
3.5 Overall efficiency of turbines, compressors, and pumps used in the analysis of potential replacement power cycles.	46
3.6 References to equations of state used to determine thermophysical properties in EES.	47
3.7 Uncertainty values for independent variables used to determine overall uncertainty of LCOE and cycle efficiency.	51
4.1 Regenerative Rankine cycle overall values for 1st law analysis.	53
4.2 Independent variables used to solve the regenerative Rankine cycle for maximum efficiency.	55
4.3 Regenerative reheat Rankine cycle values optimized for maximum efficiency.	58
4.4 Independent variables used to solve the regenerative reheat Rankine cycle for maximum efficiency.	59
4.5 Transcritical cycle overall values for optimized maximum efficiency.	60
4.6 Independent variables used to solve the transcritical cycle for maximum efficiency.	62
4.7 sCO_2 regenerative cycle overall values optimized for maximum efficiency.	63

4.8	Independent variables used to solve the sCO_2 regenerative cycle for maximum efficiency.	64
4.9	sCO_2 recompression cycle overall values optimized for maximum efficiency.	66
4.10	Independent variables used to solve the sCO_2 recompression cycle for maximum efficiency.	67
4.11	sCO_2 regenerative topping cycle input values used for combined cycle analysis.	70
4.12	Combined cycle overall 1st law analysis values for different working fluids.	72
4.13	Independent variables used to solve the combined cycle for maximum efficiency with different working fluids.	73
4.14	Independent variables used to solve the transcritical ethanol cycle for minimum LCOE.	84
4.15	Independent variables used to solve the sCO_2 recompression cycle for minimum LCOE.	86
5.1	Summary of potential NuScale power cycles to replace the current regenerative Rankine cycle.	89

Nomenclature

Variables

$\%c$	Percent change fraction.
Δi	Specific enthalpy change [$\frac{kJ}{kg}$].
ΔT	Temperature difference [$^{\circ}C$].
ΔT_{lm}	Log mean temperature difference [$^{\circ}C$].
\dot{C}	Heat capacity rate [$\frac{kW}{K}$].
\dot{E}	Exergy of fluid stream [kW].
\dot{E}_d	Exergy destroyed [kW].
\dot{m}	Working fluid mass flow rate [$\frac{kg}{s}$].
\dot{Q}	Heat transfer [kW].
\dot{W}_p	Power consumed by pumps or compressors [kW].
\dot{W}_t	Power produced by turbine [kW].
\dot{W}_{net}	Net power produced by the cycle [kW].
ϵ	Heat exchanger effectiveness.
η_a	Turbine efficiency accounting for moisture.
η_I	First law cycle efficiency.

η_p	Isentropic efficiency of pump or compressor.
η_t	Isentropic efficiency of turbine.
ϕ	Fluid flow split ratio.
ρ	Density [$\frac{kg}{m^3}$].
A	Heat transfer surface area [m^2].
a	Baumann factor for adjusting turbine efficiency when moisture is present.
A/V	Heat exchanger area to volume ratio [$\frac{m^2}{m^3}$].
C	Component cost [\$].
C_r	Heat capacity ratio.
d	Diameter [m].
f_m	Heat exchanger volume metal fraction.
f_{cap}	Fraction of plant capital costs contributing to the levelized cost of electricity (LCOE).
f_{equip}	Fraction of power cycle component costs contributing to overnight plant costs.
h	Convection heat transfer coefficient [$\frac{kW}{m^2K}$].
I	Cost index.
i	Specific enthalpy [$\frac{kJ}{kg}$].
k	Thermal conductivity [$\frac{kW}{mK}$].
$LCOE$	Levelized cost of electricity.
N	Total number of discretized sections.
NTU	Number of transfer units.
P	Pressure [bar].

T	Temperature [$^{\circ}C$].
T_o	Dead state temperature [K].
T_r	Reactor temperature [K].
U	Overall heat transfer coefficient [$\frac{kW}{m^2K}$].
UA	Heat exchanger conductance [$\frac{kW}{K}$].
W_{metal}	Weight of PCHE heat exchanger [kg].
x	Saturated fluid quality.
x_a	Adjusted quality used to determine turbine efficiency when moisture is present.
Σ	Summation.
\vec{x}	Independent variables for optimization problem.
$f(\vec{x})$	Objective function for optimization.
g	Gravity [$\frac{m}{s^2}$].
g_i	Optimization problem inequality constraints.
g_i^+	Penalty method inequality constraints.
R	Penalty method scaling penalty parameter.
$T(\vec{x})$	Transformed objective function from a constrained optimization problem to an unconstrained optimization problem.
u	Uncertainty of variable.
V	Velocity [$\frac{m}{s}$].
z	Height [m].

Subscripts









baseline Baseline value.

<i>c</i>	Cold fluid.
<i>d</i>	Exergy destroyed.
<i>h</i>	Hot fluid.
<i>I</i>	First law efficiency.
<i>i</i>	Inner surface or index.
<i>in</i>	Fluid inlet.
<i>isen</i>	Isentropic.
<i>m</i>	Metal.
<i>max</i>	Maximum.
<i>min</i>	Minimum.
<i>new</i>	New value.
<i>o</i>	Outer surface or dead state.
<i>out</i>	Fluid outlet.
<i>p</i>	Pump or compressor.
<i>r</i>	Reactor.
<i>SMR</i>	Small Modular Reactor.
<i>t</i>	Turbine.
<i>w</i>	Wall.

Superscripts

<i>j</i>	Index for discretized section.
----------	--------------------------------

Diagram Legend

Name	Description	Icon
Primary Heat Exchanger	Primary heat source for power cycle. Also referred to as the steam generator.	
Regenerator	Heat exchanger used for internal heat transfer within the power cycle	
Condenser/Precooler	Heat exchanger that rejects heat to the environment	
Turbine	Component used to generate work	
Compressor	Component used to compress gases or supercritical fluids	
Pump	Component used to pressurize liquids	
Fluid Flow Merger/Splitter Valve	Valves used to direct flow from 2 streams to one (merger), or 1 stream to 2 (splitter)	
Throttle Valve	Valves used to reduce the pressure of the fluid	

Chapter 1 Introduction

1.1 Overview

Nuclear power generation has been around since the 1950s, and is considered free of greenhouse gas emissions while being a reliable source for base electrical loads. Even with these advantages, production of new plants has slowed with both economic factors and accidents occurring at plants such as Fukushima, Three Mile Island, and Chernobyl playing a large role [1]. To combat these issues, research and commercialization has focused on the development and production of small modular reactors (SMRs) handling thermal capacities of 50-200 MW_{th} [2].

SMRs have the advantage of offering lower capital investment, greater site flexibility, modular design, and enhanced safety features when compared to large scale nuclear plants [3]. One specific company currently working on the commercialization of a SMR is NuScale Power (NuScale). NuScale has designed a 160 MW_{th} SMR to provide 50 MWe of electrical power generation for each module.

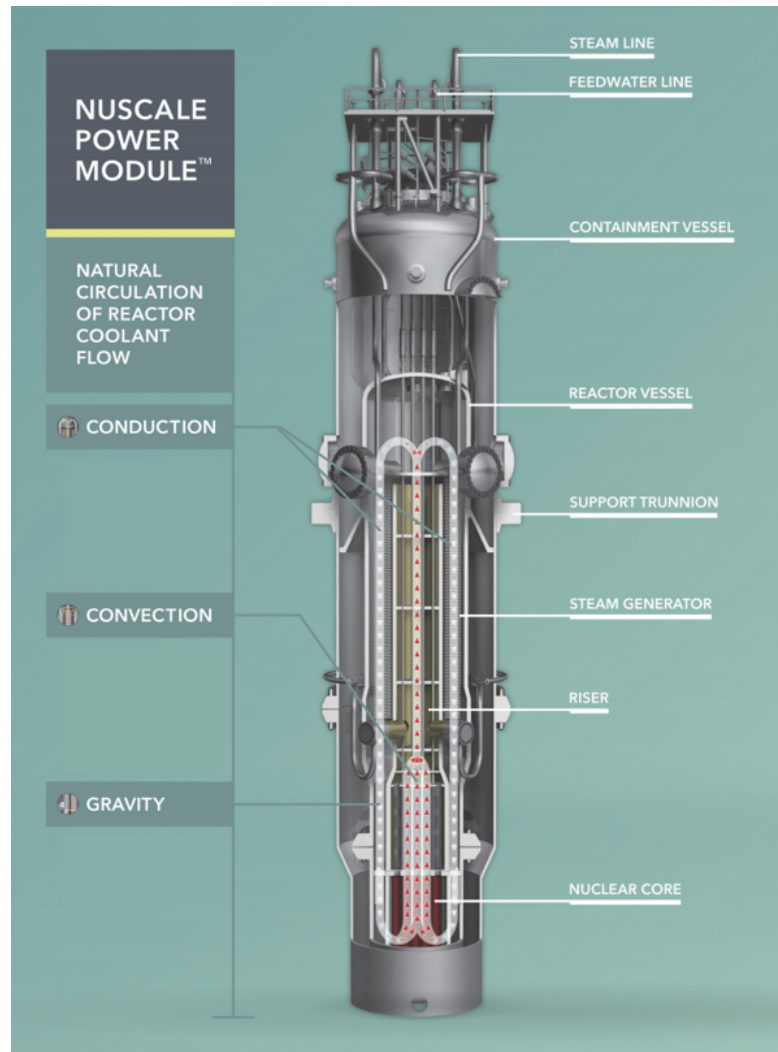


Figure 1.1: Diagram of NuScale small modular reactor. Image from NuScale Power [4].

The NuScale SMR has a passive cooling system designed to use natural convection to cool the reactor core. The cooling process is shown in figure 1.1, where the NuScale reactor is cooled with pressurized water. As the coolant is heated within the core, the coolant density decreases causing it to rise within the center of the module and flow outward radially. The coolant then enters a heat exchanger referred to as a steam generator to cool, but for the purposes of this paper will be referred to as the primary

heat exchanger. The cooling causes the fluid density to increase driving it back down into the reactor core. To enhance safety, the entire reactor module is placed within a pool of water which allows the module to passively and safely cool down in the advent of a plant malfunction or natural disaster.

The NuScale reactor module is 23 m tall and 4.6 m wide. The term "small" in SMR is relative to standard reactors with a containment building that is typically 200 m tall and 37 m wide [5]. The smaller design allows for the SMR to be manufactured at the factory and then shipped to the plant as shown in figure 1.2



Figure 1.2: NuScale small modular reactor portability. Image from NuScale Power [5].

For electrical power production the NuScale SMR is currently designed to be combined with a regenerative Rankine cycle. The Rankine cycle is a simple water-steam based cycle that was first introduced in the 1800s. This cycle is well understood and used in many large scale thermal power plants.

The SMR technology is expected to make nuclear power generation more attractive financially. NuScale currently estimates a 12-module plant will have a levelized cost of electricity of 89 \$/MWh (figure 1.3). This places the SMR plant in the mid-range of costs and will make it a reasonably attractive investment when considering all of the other benefits to nuclear power.

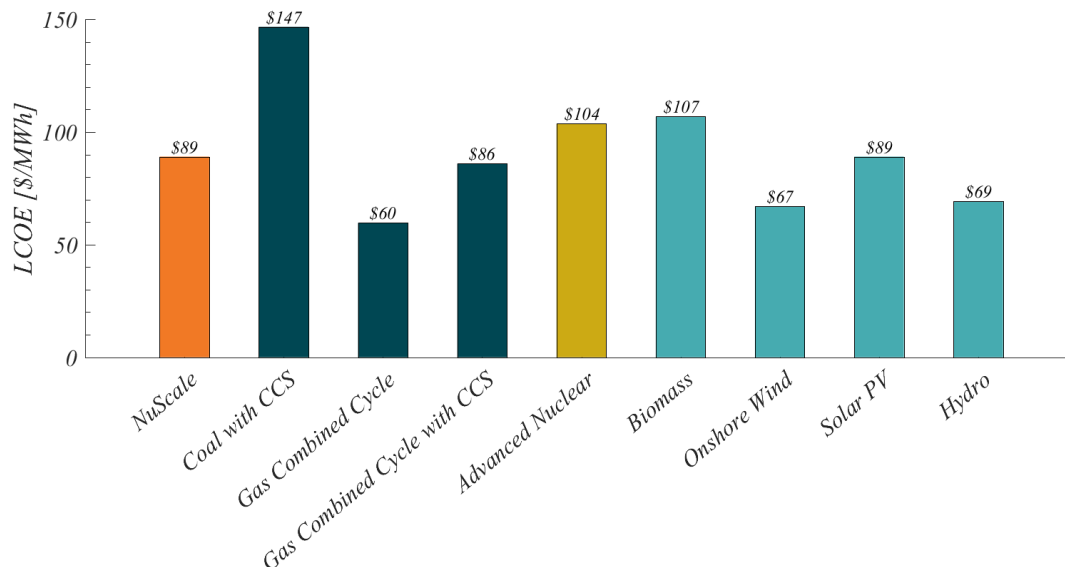


Figure 1.3: Estimated levelized cost of electricity comparison of NuScale SMR plant versus other common power plants. Data from [6] and adjusted to 2018 dollars. The CCS cycles include carbon capture and sequestration processes.

NuScale’s first plant is to be located at the Idaho National Laboratory (INL) and will contain 12 SMR modules [7]. This plant is part of the Western initiative for nuclear (Program WIN), where a series of potential other projects are possible. With initiatives like Program WIN, the NuScale SMR design is demonstrating its economic potential when compared to alternatives, but there is still desire to improve the economics and efficiency of the cycle.

The paper provides an analysis of potential power cycle alternatives to the current regenerative Rankine cycle in place for NuScale’s SMR. The focus on the analysis is to research alternative cycles and assess their potential to benefit NuScale’s SMR design by either improving efficiency, lowering cost, or increasing reactor power.

The organization of this paper first provides an overview of the project which has been presented in chapter one and continues with the project scope and problem definition. The second chapter examines potential alternative power cycles by presenting a current review of literature. The third chapter describes the methods used in the analysis, and the final chapters cover the results, discussion, and conclusion.

1.2 Project Scope

The scope of this project is to assess if alternative power cycles exist as potential replacements to the current regenerative Rankine cycle coupled with the NuScale SMR design. To meet the criteria of an alternative cycle, the new cycle would need to demonstrate a reduced levelized cost of electricity (LCOE) by meeting one or more of the following criteria:

- Increase power generation efficiency
- Decrease the cost of plant equipment
- Increase the reactor power output

The first two bullets are the main focus of this paper and include detailed analysis of potential cycle efficiencies using the 1st law of thermodynamics. Based on the 1st law analysis results, low performing cycles were removed and first order costing methods were used to estimate the cost of major power cycle components. The cycle efficiencies and costs were then used to assess an overall levelized cost of electricity (LCOE) to compare with the baseline regenerative Rankine cycle currently used in NuScale's design.

The last bullet of assessing an increase in the reactor power is not quantitatively analyzed within this paper, but alternative cycles are qualitatively discussed in terms of their potential to handle increased reactor heat loads.

1.3 Design Problem

For this paper only near term replacement options for alternative power cycles were considered. This means the cycle pressures and temperatures can not exceed the design pressures and temperatures of the reactor. Additionally, working fluids must be compatible with the materials and coolant.

Another constraint is the primary heat source for the power cycle is a sensibly cooled source setup in a counterflow orientation with the power cycle working fluid. This means the coolant temperature lowers as heat is extracted within the heat exchanger. The change in temperature of the primary coolant is required to maintain a maximum temperature of $310\text{ }^{\circ}\text{C}$ and no higher than a minimum temperature of $258\text{ }^{\circ}\text{C}$. This is

due to the natural convection cooling process which requires a minimum temperature difference to maintain flow rates.

The overall design parameters from the NuScale SMR used in this analysis are listed in table 1.1. These values constrain the design and dictate which alternative cycles are best suited for the NuScale SMR.

Table 1.1: NuScale Power SMR parameters used to evaluate alternative power cycle options. Data from [8], [9].

Parameter	Variable	Value
Heat Transfer [MW]	\dot{Q}_{in}	160
Maximum Coolant Temperature [C]	$T_{max,SMR}$	310
Minimum Coolant Temperature [C]	$T_{min,SMR}$	258
Coolant Mass Flow Rate [kg/s]	\dot{m}_{SMR}	587
Coolant Pressure [bar]	P_{SMR}	128
Coolant Type	-	Pressurized Water

Outside of the scope of this paper are longer term options for alternative power cycles. These options may include recommendations for higher pressures and temperatures which generally lead to higher cycle efficiencies. This would have to be considered against the additional costs to redesign the SMR, which would require thicker pressure vessel walls and potentially more expensive materials.

Chapter 2 Literature Review

This chapter reviews current literature to assess potential power cycle alternatives for the NuScale SMR design. From the cycles discussed in the sections below attractive alternatives were selected for additional analysis.

2.1 Regenerative Rankine Cycle

A regenerative Rankine cycle is a standard Rankine cycle with the addition of feedwater heat exchangers or regenerators. The regenerators reduce exergy losses by preheating the water before undergoing heat exchange with the primary heat source. The preheating is performed by heating the incoming liquid water stream with lower temperature heat sources generated by bleeding off a portion of the expanded saturated fluid at designed stages within the turbine [10].

The current NuScale power cycle is based on a regenerative Rankine cycle where the heat source is the primary heat exchanger contained within the nuclear reactor pressure vessel. The efficiency of NuScale's regeneration Rankine cycle was determined to be 31.8% based on the parameters from [8], [9].

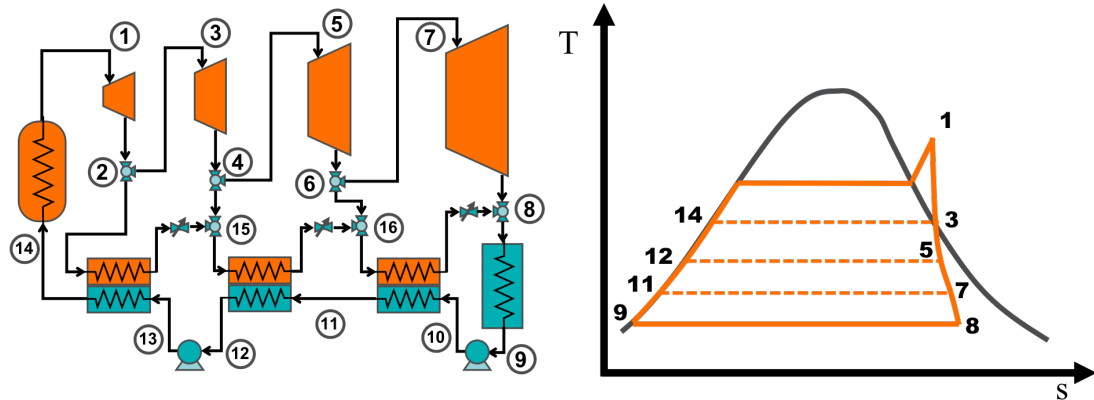


Figure 2.1: Cycle and temperature-entropy diagram of the NuScale regenerative Rankine cycle.

A simplified diagram of NuScale’s regenerative Rankine cycle and temperature-entropy plot is shown in figure 2.1. The simplified diagram was generated from the NRC reports NuScale is required to provide for regulatory approval [9]. As shown in figure 2.1 the NuScale design bleeds off steam from the turbine at intermediate pressures (states 2,4,6), and directs the saturated water into the regenerators. After heating the feedwater, the bleed stream is then throttled to next stage pressure where it is combined with the next turbine bleed stream (states 15, 16). In the last regenerator (state 16), the bleed stream is throttled to the minimum pressure and combined with the turbine outlet stream and sent to the condenser (state 8).

The efficiency of the cycle can be continually increased by adding additional regenerators to the cycle. An analysis by Srinivas et al. [11] demonstrated this effect on cycle efficiency for ‘n’ number of regenerators. As ‘n’ was increased, so did cycle efficiency, but at a decreasing rate, with most gains coming from 3 - 4 regenerators. NuScale’s design includes 3 regenerators, which suggest the efficiency gain from adding additional units does not justify the additional costs.

2.2 Rankine Reheat Cycle

The Rankine reheat cycle is a standard Rankine power cycle in which the working fluid is reheated at an intermediate pressure during the turbine expansion process. The rea-

soning for this implementation is to increase cycle efficiency and prevent turbine blade erosion [10].

Rankine reheat cycles improve cycle efficiency in two different ways. The first reason is higher boiling pressures can be achieved as the reheat process prevents moisture development during turbine expansion due to low degrees of superheated vapor. This is shown in the T-s diagram in figure 2.2, where the vapor is reheated prior to reaching the saturation point during turbine expansion in states 1-6.

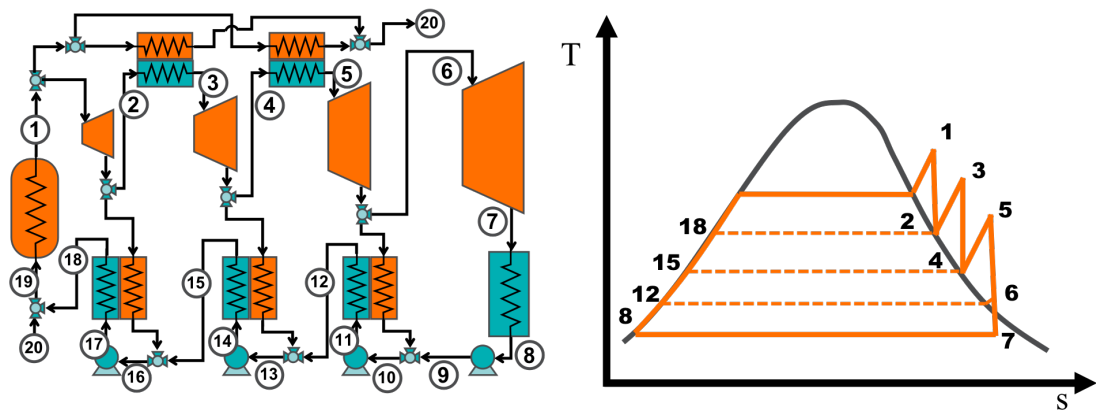


Figure 2.2: Cycle and temperature-entropy diagram of a regenerative reheat Rankine cycle.

The second way the reheat process improves cycle efficiency is by keeping the working fluid as a superheated vapor during turbine expansion. Expanding a saturated fluid in a turbine has been demonstrated to lower isentropic efficiency of the turbine [12], [13]. This is due to the velocity differences between the vapor and liquid when impacting the turbine blades. The impact on turbine efficiency degradation is typically modeled as a function of fluid quality. As the fluid quality is reduced, so to is the efficiency of the turbine.

The current NuScale design could benefit by adding reheating to the saturated vapor during the expansion stages. Most reheat cycles are performed by sending the partially expanded vapor stream back to the primary heat source, but the NuScale design could instead split part of the main fluid stream exiting out of the steam generator. One of the split streams would be used for turbine expansion, and the other for reheating as shown in states 1-5 in figure 2.2. This reheat design would not dramatically alter the current

setup, but does require additional heat exchangers and piping for the reheating process.

One other potential advantage of the reheat setup is a reduction in the heat exchanger surface area required in the primary heat exchanger. This is due to the increased boiling pressure and reduced degree of superheat required. As vapor heating convection coefficients are typically an order of magnitude less than boiling convection coefficients [14], the heat transfer process would be more effective. This could result in a reduction in size of the primary heat exchanger or the thermal power from the reactor could be increased.

As both the regenerative and reheat Rankine cycles improve on cycle efficiency in different ways, a higher efficiency cycle is expected when combining both. For the NuScale setup this would likely include 1-2 reheaters with 3 regenerators. Figure 2.2 depicts a cycle with 2 reheaters (between states 2-3 and 4-5) and 3 regenerators (between states 10-11, 14-15, and 17-18). Also included is an addition of mixing the regeneration streams directly into the feedwater streams as shown in states 10, 13, and 16. As noted in NuScale’s design, the regenerative streams are throttle down into the condenser. This design eliminates the throttling to minimize exergy losses, but at the expense of additional pumps.

2.3 Supercritical CO₂ Cycles

Power cycles operating with supercritical CO₂ (*sCO*₂) have garnered new research intensity due wide applicability, lower cost potential, safety enhancements, and low global warming potential [15]–[17]. *sCO*₂ is produced when pressurizing and heating carbon dioxide above the critical point at 31.1 °C and 73.9 bar. A supercritical fluid only has one phase in which it is neither a gas or a liquid, but exhibits properties seen in both [18].

The *sCO*₂ cycle was first proposed by Feher [19] in 1968 as an alternative to gas Brayton and steam Rankine cycles. Feher concluded the *sCO*₂ supercritical cycle has advantages over the standard cycles as some of the best features of each cycle could be combined. The high densities found near the critical point would reduce the power needed by the compressor, and the small expansion ratio leads to smaller and simpler turbines. Feher also concluded that CO₂ was an optimal fluid due to its low critical pressure, chemical stability, and abundance. Since Feher’s introduction, many variations of *sCO*₂ power cycles have been proposed. The layouts are designed to maximize advantages such

as low pumping/compression power and better temperature matching in the primary heat source, while minimizing drawbacks such as pinch points within the recuperators [20].

The most basic sCO_2 cycle design is the regenerative cycle as shown in figure 2.3. This cycle, first proposed by Fehr, only employs a recuperator/regenerator at state 5-6. The cycle can operate as a supercritical cycle or a transcritical cycle by swapping out the compressor for a pump. Regenerative cycles have lower efficiencies when compared to other more advanced sCO_2 cycles. This is primarily caused by the pinch points found in the regenerator as large differences in the fluid stream's heat capacities form when the low pressure stream is near the critical point [21].

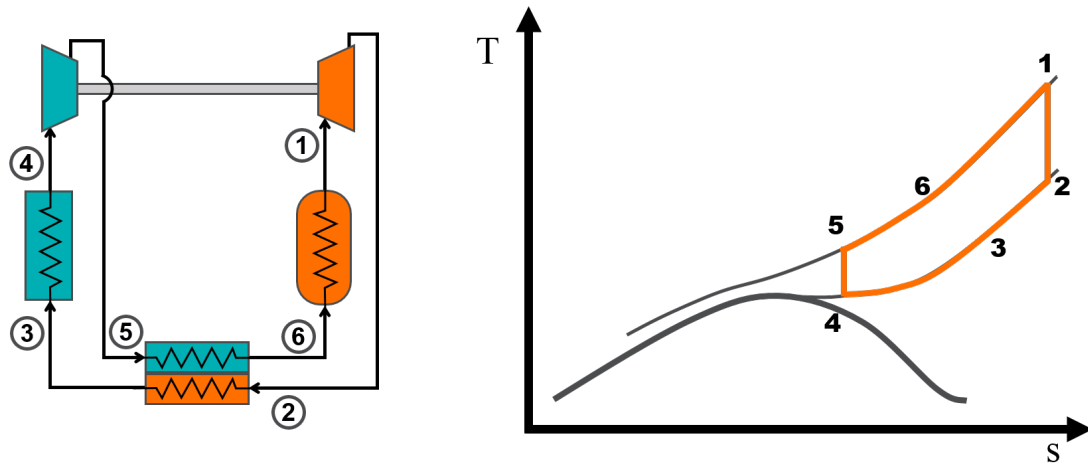


Figure 2.3: Cycle and temperature-entropy diagrams for a sCO_2 regenerative cycle.

To combat the pinch point problem in the regenerative cycle, a recompression cycle was proposed by Angelino in 1969 [22]. The recompression cycle adds a second regenerator (LTR) and compressor as shown in figure 2.4. After the low pressure stream exits the LTR at state 4, the flow is split with a portion being directly re-compressed, while the other is cooled prior to flowing through the main compressor (state 6). The flow exiting the main compressor is heated in the LTR and then merged with the re-compressed flow at state 11 prior to additional heat recuperation in the HTR.

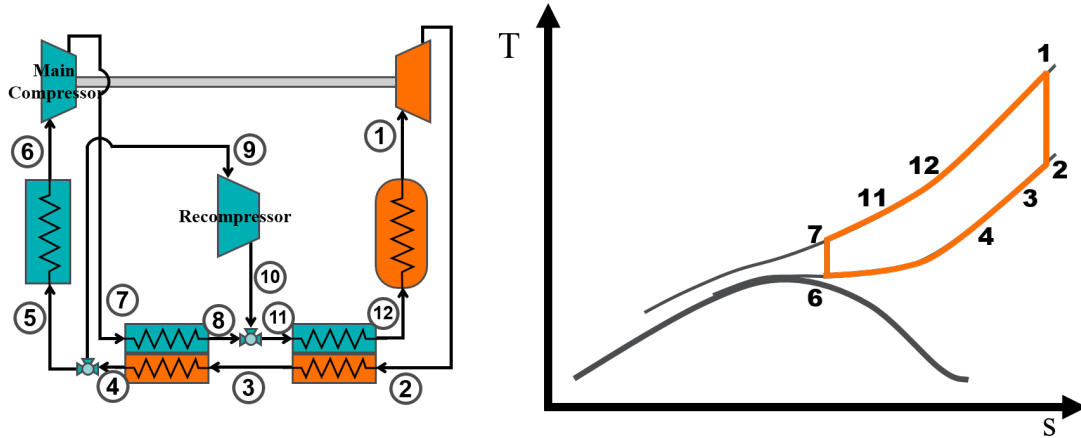


Figure 2.4: Cycle and T-s diagrams for a sCO_2 recompression cycle.

The split flow and two regenerators allows for better heat capacitance matching within the heat exchangers. This alleviates pinch points, which increase the cycle efficiency, but at the cost of large regenerators [21].

Other compelling cycles layouts include the recompression reheat cycle, which is similar to the recompression cycle but includes a intermediate reheat stage during turbine expansion. Dostal et al. showed the cycle was more efficient than the recompression cycle, but works best when the reheat stream is sent back to the primary heat source [15]. Another novel cycle proposed by Kimzey [23] looked to better match sensible heat sources such as those found in NuScale's SMR. Kimzey's cycles, named a cascaded closed Brayton cycle (CCBC), were developed as a bottoming cycle to replace standard Rankine cycles. The CCBC cycles had excellent heat recovery from the high temperature source, but the overall cycle efficiency was much lower than steam Rankine cycles.

The optimal operating ranges for sCO_2 cycles have been explored by Dostal et al. [15], [24] and is shown in figure 2.5. Compared to other common cycles in the range of 350-950 °C it was concluded that sCO_2 cycles perform best in temperature ranges of 500 - 700 °C. Conversely superheated steam cycles outperformed the sCO_2 cycle at temperatures lower than 500 °C.

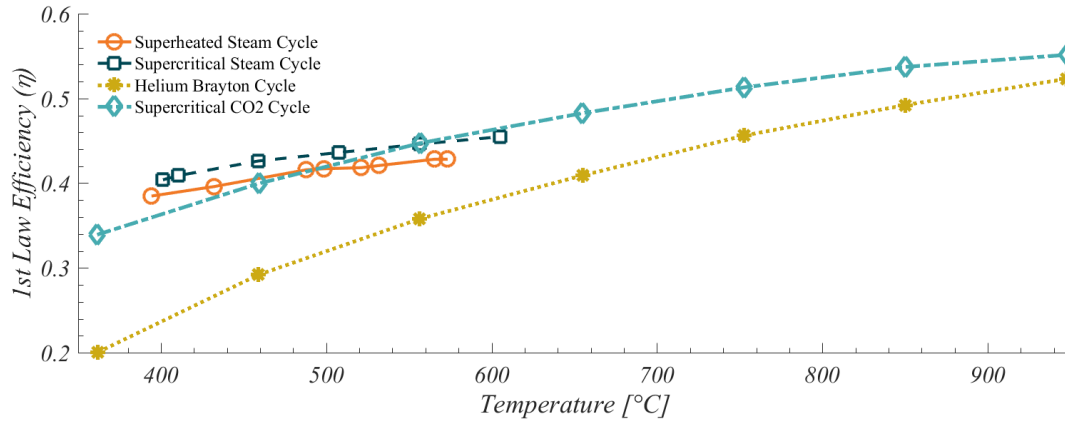


Figure 2.5: Power cycle efficiency for selected cycles based on data from Dostal et al. [15].

As Dostal et al. did not provide much analysis in the lower temperature range for SMR applications, Yoon et al. [2] conducted a study for a sCO_2 cycle coupled with a SMR at the operating temperature of 310 °C. Optimized efficiency for a sCO_2 recompression cycle was found at a pressure ratio around 2.4, but cycle efficiency is minimally impacted when the pressure ratio is at least 2.0. The NuScale design puts the maximum pressure ratio of a sCO_2 cycle around 1.7, increasing the likelihood of a significant negative impact on efficiency. Overall, Yoon et al. concluded the sCO_2 cycle efficiency is slightly lower than superheated steam cycles, but the reduction in power cycle footprint could still make the cycle an attractive option.

Conversely Santini et al. [17] looked at sCO_2 cycle efficiency in a similar 300 °C range for 3 different setups operating both supercritical and transcritical operating points. Santini et al. concluded that even though cycle efficiencies were similar to the superheated steam cycles, a transcritical sCO_2 recompression reheated cycle was slightly higher at 34.0% (steam cycle at 33.5%). These efficiencies were obtained with a cooling water temperature of 19 °C and pressure ratio of 4.1 (max pressure 250 bar). When looking at more comparable conditions of cooling water temperature of 25 °C and maximum pressure of 150 bar the overall cycle efficiency reduced to 30.9%.

One of the touted main benefits of the sCO_2 cycles is due to the cycle's overall size being much less than the steam Rankine cycles. Ahn et al. estimates the size to be four times less than that of steam Rankine cycles [25]. Dostal et al. provided a size reduction

estimate based on an increase in the power density of the cycle. With the sCO_2 cycle being 46% more dense than that of a similar helium Brayton cycle. The reduced footprint of sCO_2 cycles is mostly attributed to the turbine where an sCO_2 cycle will have 1 to 2 turbine stages and a comparable steam Rankine cycle can have up to 30 [19].

In addition to size reduction in turbomachinery, high efficiency of such devices is achievable when compared to Rankine cycles [15]. Based on the work from Dostal et al., most research assumes turbine and compressor efficiencies of 90% and 89% respectively [2], [17], [21], [26]. These values selected by Dostal et al. were considered to be conservative as their models showed efficiencies can reach upwards of 95% for compressors and 93% for turbines, due to limited expansion stages when compared to Rankine cycles and helium Brayton cycles.

2.4 Transcritical Cycle

This paper refers to a transcritical cycle as a power cycle that transitions from a supercritical fluid to a subcritical fluid with both liquid and vapor phases. A diagram of a regenerative transcritical cycle is shown in figure 4.3. One main advantage of the transcritical cycle is the variable temperature change during heat addition in the primary heat source. As seen in the T-s diagram at states 21-1 in figure 2.6, the fluid exhibits a temperature glide during the heat addition process. This allows the transcritical cycle to better match with sensible heat sources and reduce entropy generation. The other primary advantage is the cycle is a liquid at the minimum pressure which requires significantly less power to pressurize the cycle compared to gas and supercritical cycles.

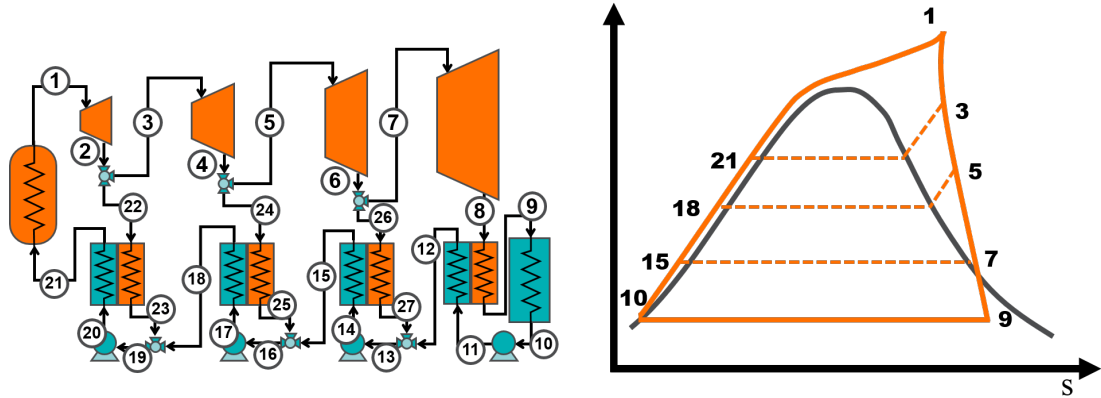


Figure 2.6: Cycle and T-s diagrams for a transcritical cycle.

One widely used transcritical cycle is the "supercritical" Rankine cycle. This is a water-based cycle that is pumped to pressures greater than 221 bar and then heated before turbine expansion [27]. The high critical pressure of the "supercritical" Rankine cycle prevents it from being considered for the NuScale SMR design, but other fluids with lower critical pressures and temperatures can be evaluated.

Two potential fluids are ethanol and ammonia. These fluids are readily available, cost effective, and well understood. Ammonia is commonly used in commercial refrigeration, but does have safety concerns due to health hazards when inhaled at larger concentrations [28]. Ammonia has a critical pressure and temperature of 48.7 bar and 132.4 °C which would make it an ideal candidate for the NuScale SMR.

Ethanol is another abundant fluid that has low critical pressures and temperatures of 63 bar and 241 °C. Ethanol is a flammable substance and therefore could pose safety issues as well.

2.5 Kalina Cycle

The Kalina cycle was first introduced by Kalina in 1984 [29] and was proposed as a higher efficiency cycle compared to steam Rankine cycles due to increased thermal efficiencies from sensible heat sources and sinks. The increase in thermal efficiency was achieved by using a zeotropic, or two mixtures, working fluid with different boiling points. The

zeotropic fluid typically used in Kalina cycles is a mixture of ammonia and water. The effect of a zeotropic fluid on a power cycle can be seen in the temperature-entropy diagram comparing Rankine and Kalina cycle in figure 2.7. As the Rankine cycle consists of water only, it undergoes an isothermal phase change when boiling and condensing. Conversely, the Kalina cycle will have a temperature glide during boiling and condensation due to the mixture of fluids with differing boiling points. The temperature glide in the Kalina cycle reduces entropy generation in the primary heat exchanger and condensers.

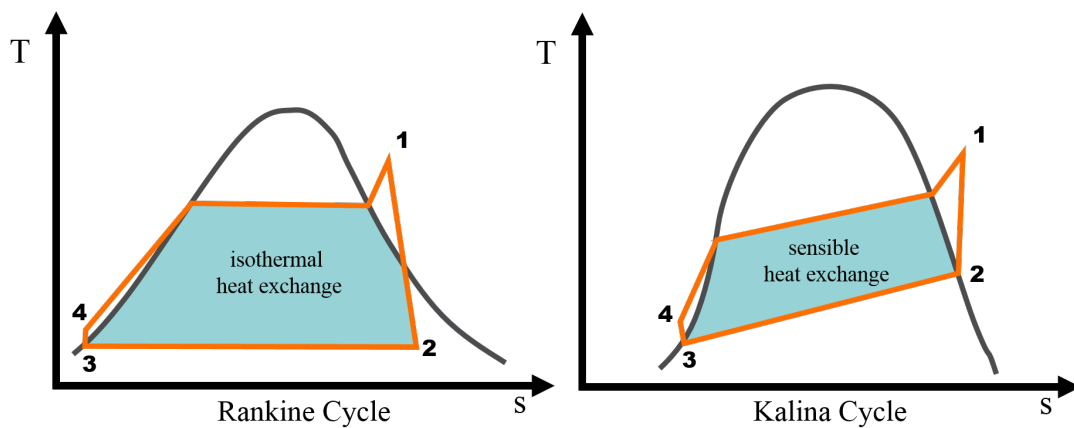


Figure 2.7: Temperature-entropy diagrams of a simple Rankine and Kalina cycle. Main difference between the cycles is during the boiling and condensation process, the Rankine cycle is isothermal, while the Kalina cycle changes temperature due to a zeotropic mixture.

Since the introduction of the original Kalina cycle there has been multiple variants of the cycle introduced with differing complexities. Studies have shown that Kalina cycles typically result in higher efficiencies when compared to Rankine cycles, but at the detriment of added complexity and cost [30].

According to a doctoral thesis by Thorin [31], comparisons were made between a steam Rankine cycle and Kalina cycles with four different configurations. The results indicated that Kalina cycles can have 30% more power output than the Rankine cycle for the targeted waste heat recovery application. However, as the amount of thermal energy recovery decreased (higher exhaust stream outlet temperature), the efficiency advantage for the Kalina cycle diminished. Preliminary cost/economic analysis was also made to compare the two cycles with the Kalina cycle requiring additional cost associated with

large heat exchangers and cycle complexity.

Modi et al. [32] took into account the economic aspect and the part-load performance to evaluate the Kalina cycle 12 (KC12). A thermoeconomic optimization was performed by minimizing the levelized cost of electricity. The different Kalina cycle simulations resulted in the levelized costs of electricity between \$212.2 per MWh and \$218.9 per MWh. This compared to a levelized cost of electricity of \$181.0 per MWh when compared to the state-of-the-art steam Rankine cycle with the same rated capacity. Therefore, suggesting the Kalina cycle is not beneficial for higher temperature applications around 500 °C.

Analysis of the Kalina cycle was performed by NuScale prior to this project. The analysis used the configurations presented by Modi and Haglind of KC234 and KC1234 [33]. NuScale’s analysis resulted in efficiencies lower than that of the current baseline regenerative Rankine cycle [34], and with the added Kalina cycle complexity economic benefit is not likely.

Alternative Kalina cycle designs could provide higher efficiencies such as KC6 presented by Kalina in 1987 [35] or the similar split cycle from Nguyen et al. [36]. These Kalina variants have been presented as higher efficiency cycles due to better matching of temperature profiles throughout the heating cycles. The downside of these cycles is additional added complexity by splitting the Ammonia-Water concentrations into 5 different levels.

2.6 Combined Cycle

Combined cycles typically use two different power cycles for electrical power generation. The cycles are setup where a topping cycle acquires heat from the primary heat source. Once power is converted in the topping cycle, the remaining heat is transferred to a bottoming cycle for additional power generation. As some cycles work best under different temperature ranges, the combined cycle allows two different cycles to take advantage of the different temperatures within the cycle.

Combined cycle plants in current operation use bottoming steam Rankine cycles coupled with gas turbine/Brayton topping cycles [37]. These combined plants can operate a combined efficiency as high as 60% [38], but require the topping cycle to have exit temperatures around 370°C. For combined cycles with lower topping exit temperatures,

bottoming cycles such as the Kalina [39] and ORC [40], [41] have been proposed. Both cycles work well to maximize efficiencies in lower temperature cycles and could provide higher efficiencies, but at the added cost and complexity of an additional cycle.

As the Kalina cycle adds significant complexity, the higher efficiencies are not likely to justify the additional costs and development. Alternatively, ORC systems are commercially available and relatively simple cycles. One potential setup is depicted in figure 2.8. This cycle shows a sCO_2 regenerative topping cycle with an ORC bottoming cycle. The added efficiency from the bottoming cycle occurs when the additional heat leaving the low pressure side of the low temperature regenerator is utilized for heat input into the ORC system (states 3-4 & 13-8). In the sCO_2 regenerative cycle, this energy goes unused, as the temperature of the high pressure fluid at state 6 is too high to capture any additional heat from state 3.

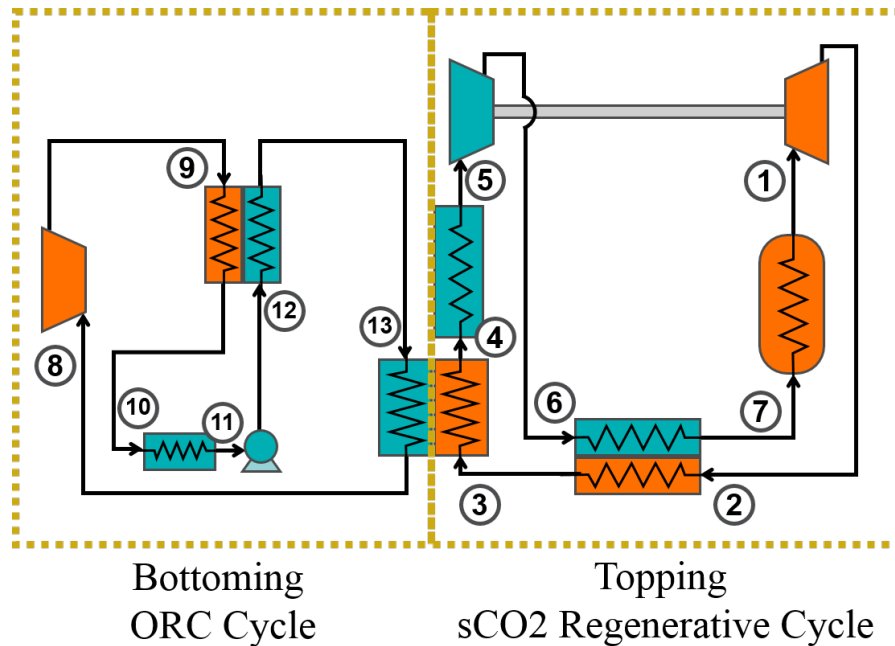


Figure 2.8: Diagram for a combined cycle with a sCO_2 regenerative topping cycle and a ORC bottoming cycle.

Work from [37] has shown the combined cycle efficiencies of 40-50% for ORC bottoming cycles. To obtain these values, much higher temperatures of 560-860°C at turbine

inlet were used, but the analysis also used lower sCO_2 turbine efficiencies of 80% compared with current research trending toward 90% [17], [21], [42].

The NuScale setup is not likely to benefit from a combined cycle due to the low maximum temperature of $300^\circ C$. The question is will the added work from the ORC be able to reach efficiencies currently seen in the regenerative Rankine cycle, and if so will the additional efficiency justify the costs and added cycle complexity.

2.7 Trilateral Flash Cycle

The trilateral flash cycle is a novel power cycle that introduces a two phase expander. The main benefit of the cycle is in increasing thermal efficiencies from a sensible primary heat source [43]. This is shown figure 2.9, as other cycles undergo phase changes during the heat addition process, the flash cycle sensibly heats the working fluid as a liquid. Therefore, it is much easier to design a heat exchanger that matches the heat capacity rates of both fluid streams. As the NuScale setup uses sensible heating in the primary heat exchanger, the flash cycle would greatly reduce exergy losses.

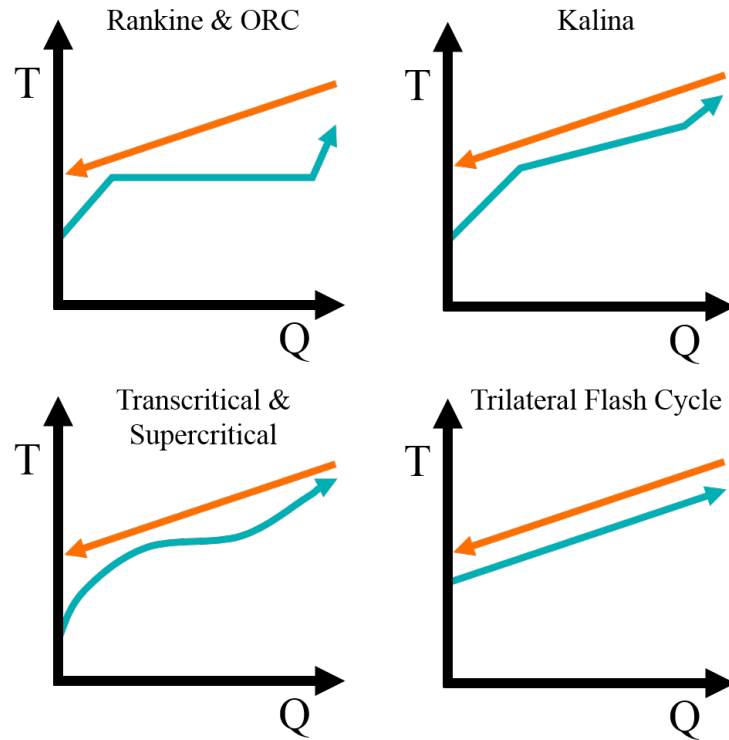


Figure 2.9: Heat addition temperature profile for different cycles. Top line represents primary heat source temperature. Bottom line is the power cycle working fluid temperature. The organic or trilateral flash cycle has the best profile match due to sensible heating of a liquid working fluid. Image adapted from [43].

A generic T-s diagram of the cycle is shown in figure 2.10. When the fluid reaches the maximum temperature at a design saturated liquid pressure (state 1) it undergoes a two-phase expansion process to an intermediate pressure (state 2). This generates cycle work and the two phase fluid is then separated to its liquid (state 9) and vapor components (state 3). The vapor is then sent through an additional expansion process producing cycle work (state 4), and the expanded low pressure vapor (states 4-5) is then used to reheat the liquid stream. After regeneration, the vapor is condensed (state 6), pumped to an intermediate pressure (state 7), and regenerated (states 8-9). At this point the flashed saturated liquid stream is merged with the main stream and pumped to high pressure (state 10) where it is heated to max temperature (state 1).

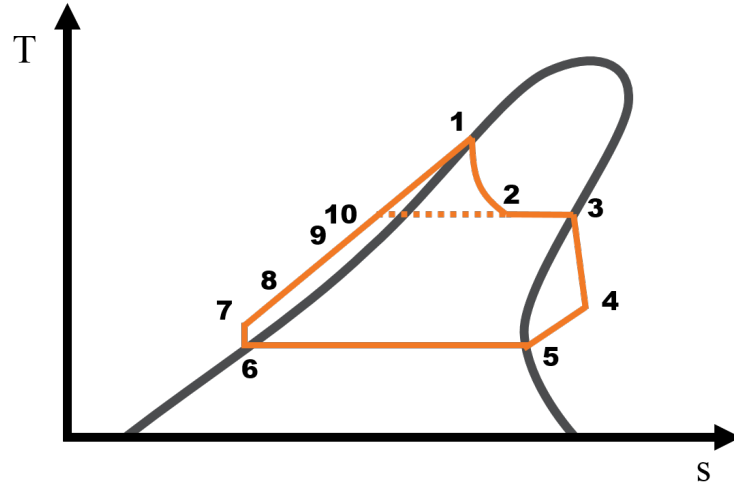


Figure 2.10: T-s diagram for trilateral flash cycle.

While not a requirement of a trilateral flash cycle, dry or isentropic fluids are best suited. Using these fluids prevents condensation during the expansion of the saturated vapor at state 3 [43].

The major drawback of this cycle is in the losses generated from the two phase expander. Current methods to develop an efficient and reliable expander have at best shown isentropic efficiencies of 52-76% range [44]. Here Smith et al. developed a screw expander to handle the two phase expansion process. Even though they found no evidence of detectable wear on components, there currently is no commercial use of a two phase expander for large scale power generation. With more research on two-phase expanders the flash cycle may become a more attractive setup, but the overall efficiency of the cycle currently would not make it an attractive option to proven cycles.

Chapter 3 Methods

3.1 Overview

The selection of candidate power cycles for matching to the small modular reactor (SMR) design was performed with a process that systematically reduced the options in order to find promising alternatives. An overview of the process is depicted in figure 3.1 where the operating conditions and the baseline setup found in NuScale’s SMR design were taken as inputs.

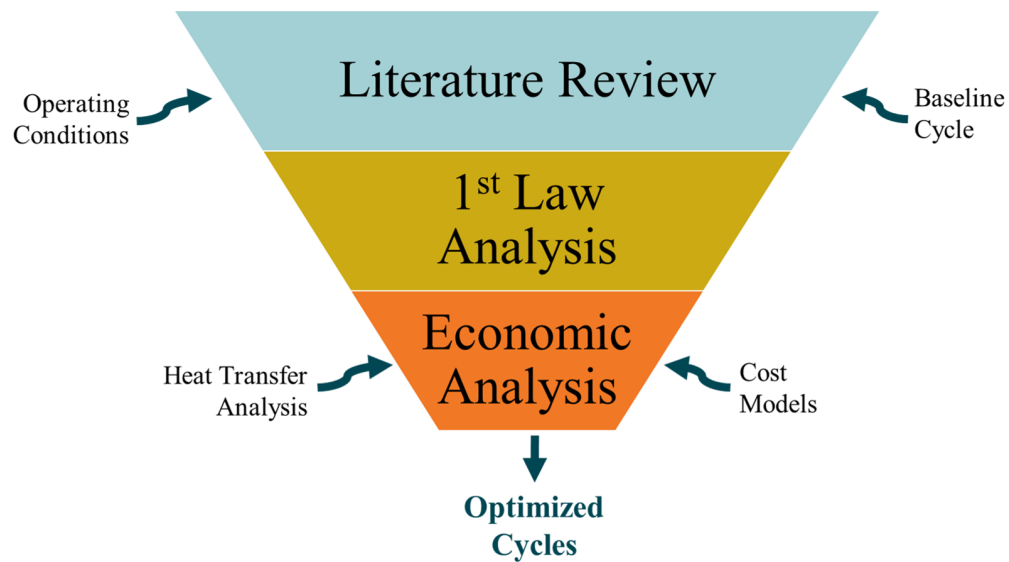


Figure 3.1: Diagram of cycle selection process.

The selection process began with a literature review of power cycles, where cycles that did not fit with NuScale’s current design were removed. After literature review,

the power cycle candidates underwent a 1st law analysis to determine the overall cycle efficiency compared to the baseline cycle efficiency. If cycles showed lower efficiency without potential reduction in cost, the cycle was discarded. Finally, the remaining cycles underwent an economic analysis with optimization to determine if the cycle could produce a positive financial impact compared to the baseline cycle.

The methods used to complete the 1st law and economic analysis are presented in the subsections below where the equations, cost models, and process are discussed.

3.2 1st Law Analysis

Estimated work output (electrical power) from a power cycle can be determined using the principles outlined in the 1st law of thermodynamics. The 1st law dictates that energy can be converted into different forms, and must always be conserved. By using the 1st law, individual cycle components (turbines, heat exchangers, pumps, etc.) can be analyzed to determine the overall work produced by the cycle for a given heat input.

Equations used to solve for cycle efficiencies are discussed in the subsection below. Equations are standard and can be found in any introductory thermodynamics textbook such as [27].

3.2.1 Equations

All equations used for 1st law analysis are derived from the steady state open system general equation. The kinetic energy terms have been removed as the changes have a small impact on overall cycle efficiency and require a detailed design of component geometry to quantify, which is beyond the scope of this study. The change in gravitational potential energy is assumed to be negligible:

$$0 = \dot{Q} - \dot{W} + \Sigma \dot{m}_{in} \left(i_{in} + \frac{V_{in}^2}{2} + gz_{in} \right) - \Sigma \dot{m}_{out} \left(i_{out} + \frac{V_{out}^2}{2} + gz_{out} \right) \quad (3.1)$$

Where the remaining terms \dot{Q} , \dot{W} , \dot{m} , and i are the heat transferred, work produced or consumed, fluid mass flow rate, and specific enthalpy respectively. The convention

used assumes heat transferred into the system and work produced by the system are *positive* values. Conversely, heat transferred out of the system and work consumed by the system are *negative* values. The specific component equations are found in the following subsections.

3.2.1.1 Turbine

Turbines are used to generate work by expanding a higher pressure fluid to a lower pressure. This expansion extracts mechanical work due to the change in the fluid volume.

The turbine model accounts for both dry expansion of a superheated vapor and wet expansion of a saturated vapor. When a turbine undergoes wet expansion the turbine efficiency degrades as the fluid quality lowers due to moisture development [12]. To account for the expected turbine efficiency drop, the Baumann model was incorporated into the standard turbine model. The Baumann model adjusts the isentropic efficiency of the turbine based on the quality of the saturated vapor undergoing isentropic expansion:

$$\dot{W}_t = \eta_a \dot{m} (i_{in} - i_{isen,out}) \quad (3.2)$$

Where the adjusted efficiency, η_a , and adjusted quality, x_a , are:

$$\eta_a = \eta_t (1 - a(1 - x_a)) \quad (3.3)$$

$$x_a = \frac{x_{in} + x_{isen,out}}{2} \quad (3.4)$$

As can be seen in equation 3.3 if the fluid remains a superheated vapor during expansion, the quality will always equal 1. Therefore, the turbine efficiency will equal the original assumed turbine efficiency. If the fluid undergoes condensation, the turbine efficiency will be degraded based on the isentropic expanded fluid quality and the Baumann factor, a . The value of the Baumann factor typically varies between 0.4 to 2.0 [12]. Baumann originally suggested a value of 1.0 in 1921, but experiments since then have shown blade design was an important factor in the efficiency drop, and therefore values lower than 1.0 are typically used. The analysis used a value of 0.72 based on [13].

3.2.1.2 Pumps and Compressors

Pumps and compressors utilize work input to pressurize an incoming fluid stream. Even though actual pumps and compressors vary greatly in design, both components can be modeled the same for 1st law analysis. The work required for a pump or compressor is equal to the change in fluid enthalpy of an isentropic pump/compressor divided by the pump's/compressor's efficiency:

$$\dot{W}_p = \frac{\dot{m}(i_{in} - i_{isen,out})}{\eta_p} \quad (3.5)$$

3.2.1.3 Heat Exchangers

Heat exchangers transfer heat energy from a hot fluid stream to a cold fluid stream. Within each power cycles there consists of many different types of heat exchangers such as condensers, steam generators, and regenerators. The design of these components vary greatly but the 1st law analysis is the same. All heat exchangers within this analysis assume fluid streams remain separated during the heat transfer process.

Equations for the heat exchangers in 1st law analysis were done for two types. The first was for internal heat exchange where the working fluid within the cycle exchanges heat at different state points. This type of heat exchange is done in regeneration processes. The equation for two fluid heat transfer is:

$$\dot{m}_h(i_{h,in} - i_{h,out}) = \dot{m}_c(i_{c,out} - i_{c,in}) \quad (3.6)$$

The second type is for heat exchange with an external fluid. This type of heat exchange is done in the condensers and the primary heat exchanger. As these components involve heat exchange with fluids outside of the power cycle, only the heat transferred into/out of the fluid is required as shown in equation 3.7:

$$\dot{Q} = \dot{m}(i_{in} - i_{out}) \quad (3.7)$$

Heat exchangers are one of the major design points for a power cycle. A designer can adjust performance to improve or reduce the effectiveness of the heat exchanger. Improving heat exchanger effectiveness can improve overall cycle efficiency, but typically

comes with increased capital and operating costs.

One method used to define overall heat exchanger performance is the NTU-effectiveness method [14]. NTU-effectiveness can be used to constrain a heat exchanger to a specific effectiveness (ϵ) or conductance (UA) value. This can be a useful means for evaluating power cycle performance as conductance is directly related to heat exchanger cost [21].

To determine the conductance, effectiveness, and NTU, equations 3.8 - 3.15 are used along with the inlet and outlet fluid thermodynamic states.

First the average heat capacity rate is found for both the hot and cold streams:

$$\dot{C}_h = \dot{m}_h \frac{i_{h,in} - i_{h,out}}{T_{h,in} - T_{h,out}} \quad (3.8)$$

$$\dot{C}_c = \dot{m}_c \frac{i_{c,out} - i_{c,in}}{T_{c,out} - T_{c,in}} \quad (3.9)$$

During condensing and boiling processes the the temperature difference between the inlet and outlet can equal zero. In this case, the heat capacity rate was assumed to be a large value approximating infinity. The maximum and minimum heat capacity rate values are selected from the hot and cold pair and effectiveness was determined by the following two equations:

$$\dot{Q}_{max} = \dot{C}_{min}(T_{h,in} - T_{c,in}) \quad (3.10)$$

$$\epsilon = \frac{\dot{Q}}{\dot{Q}_{max}} \quad (3.11)$$

Where \dot{Q} is the actual heat transferred and can be found through evaluation of the cold or hot stream. For the hot stream the equation is:

$$\dot{Q} = \dot{m}_h(i_{h,in} - i_{h,out}) \quad (3.12)$$

The dimensionless number of transfer units, NTU , is found by the following equation for a counterflow arrangement:

$$NTU = \begin{cases} \frac{\epsilon}{1-\epsilon} & C_r = 1 \\ \ln\left(\frac{1-\epsilon C_r}{1-\epsilon}\right) \frac{1}{C_r-1} & C_r \leq 1 \end{cases} \quad (3.13)$$

Where C_r is the heat capacity ratio and is defined as:

$$C_r = \frac{\dot{C}_{min}}{\dot{C}_{max}} \quad (3.14)$$

Finally, conductance is simply the minimum heat capacity rate multiplied by NTU:

$$UA = NTU \cdot \dot{C}_{min} \quad (3.15)$$

3.2.1.4 Throttle Valves

Throttle valves are used to reduce the pressure of a fluid stream. Some cycles within this analysis use throttle valves to combine a high pressure fluid stream with a lower pressure fluid stream. This analysis assumes all throttle valves undergo isenthalpic expansion as no work is generated and no heat is transferred. The equation for a throttle valve is:

$$i_{in} = i_{out} \quad (3.16)$$

3.2.1.5 Mixing Valves

Mixing valves occur when two fluid streams at the same pressure are mixed together. As no work is generated and no heat is transferred outside of the fluid streams, the mixing valve only needs to account for the change in enthalpy that occurs when the two streams are mixed:

$$i_{out} = \frac{\dot{m}_{in,1}i_{in,1} + \dot{m}_{in,2}i_{in,2}}{\dot{m}_{out}} \quad (3.17)$$

Where the mass flow out is:

$$\dot{m}_{out} = \dot{m}_{in,1} + \dot{m}_{in,2} \quad (3.18)$$

3.2.1.6 Flow Splitting

For cycles that include regeneration the working fluid is sometimes split during or after expansion to heat up the cold fluid stream prior to gaining energy from the external heat source. This is done to improve cycle efficiencies by reducing exergy losses. The splitting process does not undergo any energy transfer, but each stream has an associated energy due to its enthalpy and flow rate. To account for the splitting of streams a split ratio, ϕ , is used where:

$$\dot{m} = \dot{m}_1 + \dot{m}_2 \quad (3.19)$$

$$\dot{m}_1 = \phi \dot{m} \quad (3.20)$$

$$\dot{m}_2 = (1 - \phi) \dot{m} \quad (3.21)$$

3.2.1.7 Cycle Efficiency

To determine overall cycle efficiency, the net work of the cycle is divided by the cycle heat input. The net work is found by summing all work produced and consumed by the cycle:

$$\dot{W}_{net} = \Sigma \dot{W}_t + \Sigma \dot{W}_p \quad (3.22)$$

The overall 1st law efficiency is:

$$\eta_I = \frac{\dot{W}_{net}}{\dot{Q}_{in}} \quad (3.23)$$

3.3 Exergy Analysis

Exergy is the maximum amount of energy within a system that can be used for useful work. By quantifying exergy, inefficiencies within individual components are more easily seen. This can lead to better designs by focusing on the largest exergy destruction processes.

To perform an exergy analysis, the exergy of the fluids streams is determined for each

state point using the equation:

$$\dot{E} = \dot{m}(i - i_o - T_o(s - s_o)) \quad (3.24)$$

Where i_o , T_o , and s_o are the specific enthalpy, temperature, and specific entropy at the reference dead state condition respectively.

The exergy from the reactor was determined using a simplified model from [45], which specifies total exergy based on the heat generated and reactor temperature:

$$\dot{E}_r = \dot{Q}_{in} \left(1 - \frac{T_o}{T_r}\right) \quad (3.25)$$

With the exergy values from each state point, the lost or destroyed exergy can be found for each component. The exergy destroyed (\dot{E}_d) quantifies the amount of energy that theoretically could have been converted into useful work, but was not due to cycle component limitations such as turbine efficiency and heat exchanger effectiveness. These values can be compared within each component as well as across different cycles to determine where losses are occurring within the cycle.

To determine the exergy destroyed in each component the inlet exergy fluid streams are summed, the outlet exergy fluid streams are subtracted, and the work produced or consumed is subtracted. The equations for each component are:

Turbine

$$\dot{E}_d = \dot{E}_{in} - \dot{E}_{out} - \dot{W}_t \quad (3.26)$$

Pump/Compressor

$$\dot{E}_d = \dot{E}_{in} - \dot{E}_{out} - \dot{W}_p \quad (3.27)$$

Reactor Secondary Exchanger

$$\dot{E}_d = \dot{E}_{in} - \dot{E}_{out} + \dot{E}_r \quad (3.28)$$

Heat Exchanger

$$\dot{E}_d = \Sigma \dot{E}_{in} - \Sigma \dot{E}_{out} \quad (3.29)$$

Condenser/Precooler/Throttle Valves

$$\dot{E}_d = \dot{E}_{in} - \dot{E}_{out} \quad (3.30)$$

In equation 3.30, The exergy removed in the condenser and precooler in the form of heat rejection to the environment was characterized to be destroyed exergy. As the temperature of the working fluid stream is near the condensing temperature it was assumed no attempt would be made to capture the rejected heat for any downstream process utilization.

3.4 Component Costing Models

To cost each power cycle, estimates were determined for each of the major components in each cycle (heat exchangers, turbines, compressors, and pumps) using first order costing models. The first order models allow for quick estimates based on cost correlated factors, but the models can have errors of 30-50% [46] if not higher. These first order models take into account a capacity or size parameter such as turbine power or heat exchanger surface area to compute the baseline component costs. The costs can then be adjusted for factors such as pressures and material considerations. Some models are correlated to vendor data and are typically logarithmic in nature due to economies of scale [47].

To adjust cost estimates to today's dollars, each model was scaled by a cost index ratio as seen in equation 3.31.

$$C_{2018} = C_{baseline} \frac{I_{2018}}{I_{baseline}} \quad (3.31)$$

Where $C_{baseline}$, $I_{baseline}$, I_{2018} , and C_{2018} are the baseline cost generated by the model, the index value corresponding to the baseline model year, the index value for 2018, and the adjusted cost in 2018 dollars. The Chemical Engineering Plant Cost Index [48] was used as it includes items such as equipment, construction, and engineering for similar components found in power cycles.

In the following subsections cost model comparisons are first discussed for turbines, compressors, pumps, and heat exchangers. This is followed by the selection of the specific cost models based on the comparison. Finally, the method used to determine heat exchanger surface area is outlined due to it being required for all heat exchanger costing models.

3.4.1 Costing Model Comparison

To determine appropriate costing models a comparison was performed on three similar methods developed by Peters et al. [49], Turton et al. [47], and Loh et al [46]. One exception was made for supercritical CO_2 cycles, which use the model developed by Carlson et al. [20]. The sCO_2 cycle is expected to use costlier printed circuit heat exchangers and require much different turbines/compressors. Therefore, separate costing models were selected.

For the rest of this paper the cost models will be referred to only by the last name of the first author (e.g. Turton et al. will be referred as Turton). The comparisons for turbines, compressors, heat exchanger, and pumps are shown in the following subsections.

3.4.1.1 Turbine and Compressor Cost Model

Turbine costs estimates for all models are shown in figure 3.2. The plot depicts the purchased costs based on the expected turbine power output. Costs are shown in 2018 dollars and the material is assumed to be stainless steel. Material selection is based on NuScale turbines stated to a type of stainless steel [9] and scaled costs by a factor of 3. The region of interest in figure 3.2 is between 10^4 and 10^5 kW where the NuScale turbine is expected to produce around 50 MW of power. All of the cost models required data to be extrapolated in the region of interest as models maxed out at values close to 20 MW. While extrapolation is not ideal, the curves generally show smooth transitions as costs typically scale with a power-law behavior. One exception to this is the gas - Turton model which shows declining costs at higher turbine power. This is unrealistic, and shows how the Turton model breaks down at higher power outputs. The steam Loh model is a piece-wise function that accounts for different cost slopes for specific turbine ranges.

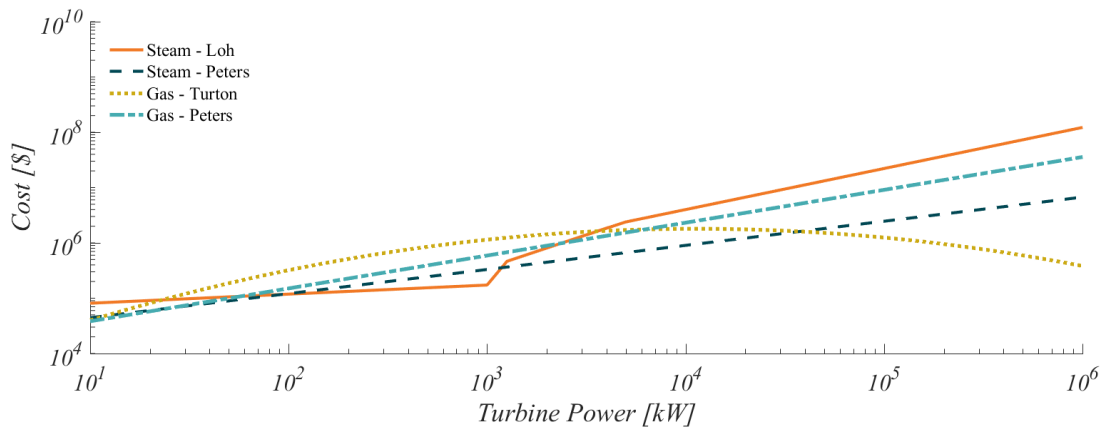


Figure 3.2: Comparison of turbine costing models.

As seen in figure 3.2 costs widely vary in the region of interest with models in disagreement by factors of 15 when comparing similar style turbines. It's important to note the Loh model for a steam turbine includes condenser and "accessories" cost, but this should not account for all of the discrepancy seen between the steam Loh and steam Peters models. For gas turbines used in Brayton cycles, the Turton model widely varies from the Peters gas turbine model by a factor of 40.

For the sCO_2 cycles the the Carlson cost models for the turbine and compressor along with the Loh - steam turbine model are shown in figure 3.3. For larger capacity turbines the Carlson turbine is less than the Loh steam turbine model by a factor of 3 - 4. This does show that comparable sCO_2 turbines project lower costs as component sizes are believed to be 25% less than the size of comparable steam Rankine cycles and therefore have smaller costs [50], [51].

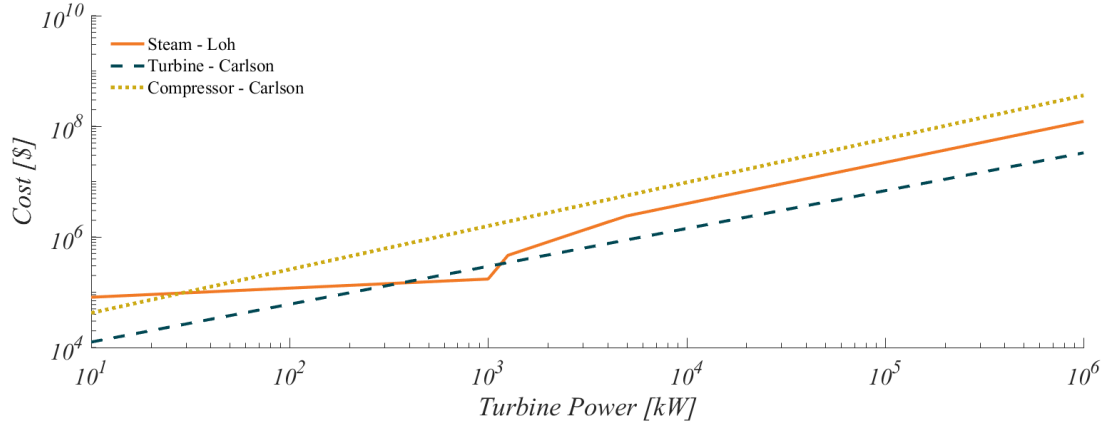


Figure 3.3: Comparison of sCO_2 turbine and compressor costing models developed by Carlson et al. The model from Loh et al. for steam turbines is shown for comparison.

The Carlson compressor cost model estimates even higher costs compared to the turbine. The Carlson model does mention a density adjustment factor from 0.2 to 0.8 depending on the CO_2 density at the compressor inlet, but the method of application was not detailed. Therefore it is unknown how the density adjustment factor is applied in the model shown in figure 3.2. Other reasons for the high cost could be due to the difficulty of designing compressors operating near the critical point. As fluid properties rapidly change in this region, designs could be difficult to optimize [50].

3.4.1.2 Heat Exchanger Cost Model

Heat exchanger cost estimates typically vary linearly with heat transfer surface area [20]. All cost models use surface area as the size parameter with adjustment factors for different materials and higher operating pressures. Shell and tube heat exchangers were selected as the best type of heat exchanger for all power cycles, except the sCO_2 cycle. Shell and tube heat exchangers are widely available and well understood by manufacturers. These heat exchangers are versatile as they can handle a variety of flow configurations, heat transfer modes, and intermediate operating pressures.

The sCO_2 cycle operates at pressures much greater than the maximum pressure of 70 bar for shell and tube heat exchangers [52]. For this reason, a printed circuit heat exchangers (PCHE) was selected as it can handle very high pressures.

Shell and Tube Cost Models:

Figure 3.4 show purchase cost estimates for a stainless steel fixed/floating head shell and tube heat exchanger based on the Loh, Peters, and Turton models. Pressure was held to a constant value of around 1 bar for all models in the figure.

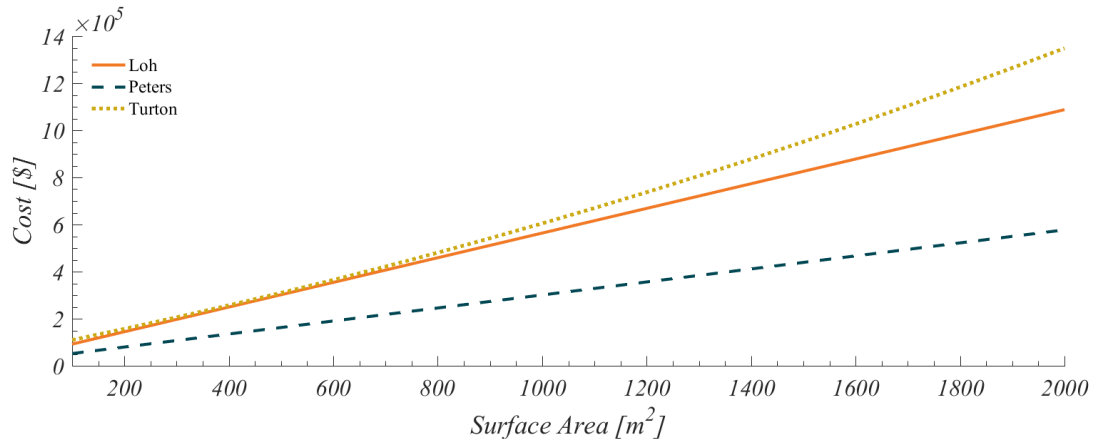


Figure 3.4: Comparison of shell and tube heat exchanger costing models.

The Loh and Turton model show good agreement until around $1000 m^2$ at which point they diverge. The Peters model underestimates the costs compared to the Loh and Turton models by around a factor of 2.

Printed Circuit Cost Models:

For the sCO_2 recompression cycle, higher pressure capable heat exchangers are required. Printed circuit heat exchanger (PCHE) are considered the likely candidates for these cycles, due to pressure and temperature capabilities as well as compactness [15], [20], [50]. Two cost models for these types of heat exchangers were evaluated, one recently developed from Carlson et al. [20] uses vendor data along with the Engineering Sciences Data Unit (ESDU) dataset [53]. The other model was developed by Dostal et al. in 2004 [15] where Dostal estimated the weight of the heat exchanger and used quoted values of from the company Heatric, at \$30 per kg for stainless steel in 2004.

The Carlson model presents cost estimates based on overall heat exchanger conductance (UA), where U is the overall heat transfer coefficient and A is the heat transfer

surface area. Carlson’s model assumes the value of U remains relatively constant. The constant assumption could be a problem for cycles operating near the critical point as fluid properties rapidly change.

To compare the Carlson and Dostal models an estimated constant overall heat transfer coefficient, U , of $1 \frac{kW}{m^2K}$ was assumed based on [17] for PCHE’s using sCO_2 . The surface area, A , can then be determined by dividing UA by U .

The Dostal model relates cost through the heat exchanger weight. To determine weight, heat transfer surface area found above was used with the assumptions presented in table 3.1.

Table 3.1: Printed circuit geometry assumptions used to determine heat exchanger weight.

Parameter Name	Variable	Value	Source
Hxer metal fraction	f_m	0.564	[15]
Area to Volume ratio	A/V	850 [m^2/m^3]	[17]
Metal density	ρ	8027 [kg/m^3]	[54]
Cost	C_{PCHE}	30 [$\$/kg$]	[15]

Surface area relates to weight through the volume of the heat exchanger multiplied by a metal fraction, f_m , which is found by the equation:

$$W_{metal} = \frac{\rho A f_m}{A/V} \quad (3.32)$$

Results from the two models are shown in figure 3.5 where both the Carlson and Dostal models are based on stainless steel material and have been adjusted to 2018 dollars. As seen in figure 3.5 the Carlson model estimates costs to be about 4.5 times that of the Dostal model.

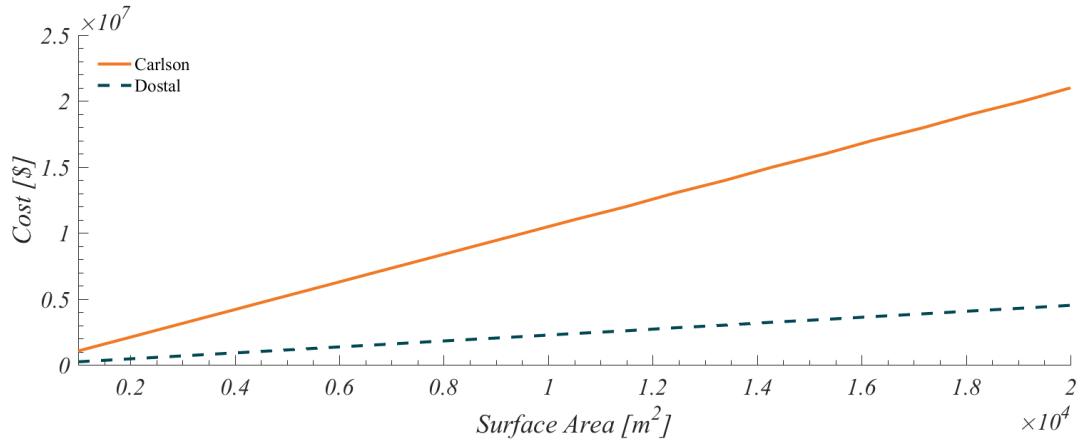


Figure 3.5: Comparison of PCHE costing models.

Evaluating the models to cost per heat exchange surface area, the Dostal model is about 230 per $\$/m^2$ and the Carlson model is about 1000 $\$/m^2$. Comparing to the shell and tube models from the Loh, Peters, and Turton models, costs ranged from 580 to 600 per $\$/m^2$ for stainless steel material. As PCHEs are a newer technology and considered costlier, it is likely the Dostal model under predicts the current cost.

3.4.1.3 Pump Cost Model

Pump costing models from Peters, Turton, and Loh differ with the capacity parameter, making direct comparison more difficult. The Peters model uses flow rate multiplied by pump pressure, the Turton model uses the pump power, and the Loh model uses only flow rate.

To compare costing models, stainless steel pumps at different flows, pressures, and power were compared and shown in table 3.2. Costs *highlighted* in the table represent extrapolated values generated outside of the model bounds. The table is sorted by flow rate and increasing costs generally follow the increasing flow rate for all models. Exceptions to this is seen in row 7 where the Turton model cost is much lower than Loh and Peters as pump power is low, but flow is high.

Comparing the three models, the Loh model estimates pump costs on the lower end and the Peters model estimates on the higher end, while Turton typically is found in

the middle. At high pressures and flow rates, as seen in rows 4, 8, 9, 10, the Peters model diverges greatly in cost estimates when extrapolating values outside of the model bounds.

Table 3.2: Pump cost estimates for three first order costing methods. Each costing method uses a different capacity parameter with Loh using flow, Turton using power, and Peters using flow and pressure. The *highlighted* costs values represent extrapolated values for parameters outside of the model bounds.

	Flow [m^3/s]	Power [kW]	Pressure [bar]	Loh	Turton	Peters
1	4.73E-02	3.2	2.0	\$8,743	\$2,855	\$7,630
2	5.07E-02	15.3	2.9	<i>\$9,121</i>	<i>\$4,667</i>	<i>\$9,886</i>
3	5.64E-02	33.3	7.3	\$9,749	\$6,720	\$22,427
4	6.25E-02	333	47.3	\$10,423	\$31,846	\$144,767
5	6.77E-02	99.5	11.0	\$11,000	\$12,883	\$37,969
6	7.15E-02	246	36.9	<i>\$11,416</i>	<i>\$24,926</i>	<i>\$128,926</i>
7	15.5E-02	52.1	2.6	\$20,646	\$8,601	\$17,292
8	19.0E-02	331	15.7	<i>\$24,514</i>	<i>\$31,651</i>	<i>\$140,096</i>
9	27.4E-02	1558	58.3	<i>\$33,760</i>	<i>\$134,269</i>	<i>\$760,788</i>
10	57.8E-02	2229	82.7	<i>\$67,444</i>	<i>\$196,222</i>	<i>\$2,281,139</i>

3.4.2 Costing Model Selection

As discussed in section 3.4.1 costing models show wide variation in costs for turbines, heat exchangers, and pumps. To determine the selection of each model for specific components a number of factors were considered.

Table 3.3 lists each component and the costing model selected for use in the analysis. The primary factor for evaluating the selection of cost models was based on internal NuScale component costs. These costs are proprietary and cannot be disclosed within this paper, but allowed for selection of models that would provide a similar relative

percentage cost of the components. Other factors contributing to the cost model selection are listed within table 3.3.

Table 3.3: Costing model selection for power cycle analysis.

Component	Model Selection	Justification
Steam Turbine	Loh	Includes condenser, magnitude fits best with known turbine costs, costs remains well behaved for extrapolated values, and total installation costs can be estimated.
sCO ₂ Turbine	Carlson	Only model found for sCO ₂ and was designed using vendor data.
sCO ₂ Compressor	Carlson	Only model found for sCO ₂ and was designed using vendor data.
Shell and Tube Heat Exchanger	Turton	Incorporates pressure correction best, and total installation costs can be determined.
PCHE Heat Exchanger	Carlson	Most recent model for PCHEs and uses the EDSU database with vendor data.
Pumps	Turton	Model remains well behaved for extrapolated values, model accounts best for both pressure and flow, and total installation costs can be estimated.

Out of the selected models the steam turbines, shell and tube heat exchangers, and pumps all assume stainless steel construction, which increased costs by a factor of 3. This is based on the NuScale components all listed as stainless steel to improve safety due to potential material corrosion [9]. The models were scaled to include installation costs based on the method or data provided by the author, with the exception of the

Carlson model. The Carlson model install costs were not provided and typical methods of multiplying by a factor of 2 or 3 are not applicable as the costs vastly overshadow the size and weight of the components.

Some model limitations are present that are of importance to note for this analysis:

- The Loh turbine model accounts only for steam turbines, but was used for organic fluids (i.e. ethanol) as well.
- The Loh turbine model does not differentiate between turbines with dry expansion or with moisture development. Moisture degrades efficiency and can require reinforced blades which leads to increased costs [55].
- Both the Loh turbine model and Turton pump model required extrapolated points based on the operating conditions of the power cycle.

3.4.3 Heat Exchange Surface Area

To determine estimated costs for heat exchangers, surface area estimates are required for all costing models evaluated in this analysis. The heat transfer surface area correlates well with cost as it directly determines the overall size and amount of material required.

For all cycles except the sCO_2 it was assumed the heat exchangers used would be a shell and tube type. The procedure outlined by [52] was implemented to estimate the heat transfer surface area and is:

1. Determine mode of heat transfer for both the hot stream and the cold stream (sensible liquid, boiling, condensing, or sensible gas).
2. Determine the fluid type (water, light organic, etc.) and pressure.
3. Look up estimated convection coefficients, h , for the hot and cold streams from [52] based on steps 1 and 2.
4. Find the overall heat transfer coefficient for the outer heat transfer surface area (tube outer surface) using equation 3.33 and assuming 1 [in] schedule 40 stainless steel tubes.
5. Calculate log mean temperature difference for a counterflow heat exchanger using equation 3.34.

6. Find surface area using the known total heat transferred and values determined from steps 1-5 along with equation 3.37.

3.4.3.1 Heat Transfer Area Equations

The overall heat transfer coefficient for the outer surface of the tube in a shell and tube heat exchanger is:

$$\frac{1}{U_o} = \frac{1}{h_o} + \frac{d_o \ln(d_o/d_i)}{2k_w} + \frac{d_o}{d_i h_i} \quad (3.33)$$

The log mean temperature difference in a counterflow heat exchanger is found by:

$$\Delta T_{lm} = \frac{\Delta T_1 - \Delta T_2}{\ln(\Delta T_1/\Delta T_2)} \quad (3.34)$$

Where ΔT_1 and ΔT_2 are:

$$\Delta T_1 = T_{h,in} - T_{c,out} \quad (3.35)$$

$$\Delta T_2 = T_{h,out} - T_{c,in} \quad (3.36)$$

Surface area is found using:

$$A = \frac{\dot{Q}}{U_o \Delta T_{lm}} \quad (3.37)$$

3.4.3.2 Different Heat Transfer Modes In Single Heat Exchanger

The procedure listed above can be readily used when each fluid stream undergoes only one mode of heat transfer within the heat exchanger. A problem occurs when the mode changes within the heat exchanger, which can impact convection coefficient estimates by a factor of 10 or more. These differences can significantly change surface area estimates as area decreases when convection coefficients increase.

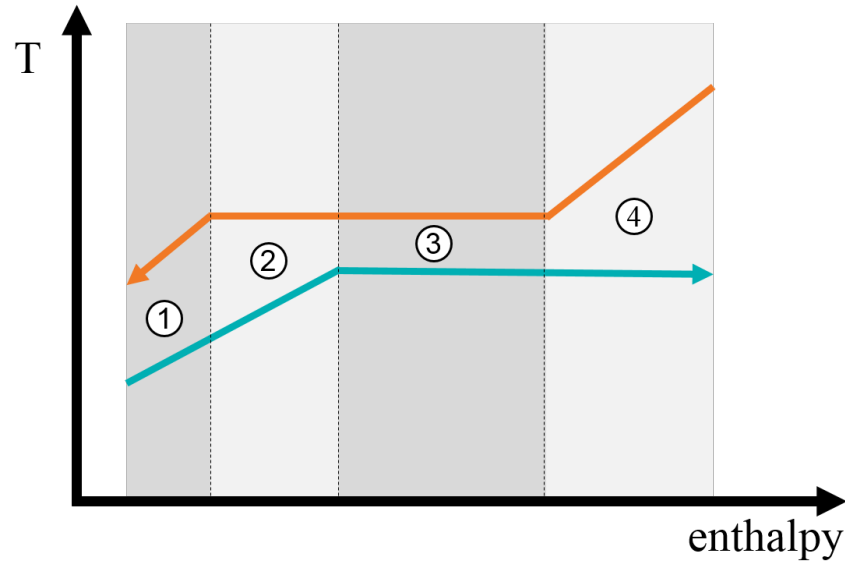


Figure 3.6: Temperature/enthalpy diagram of a two fluid heat exchange in counterflow orientation. Regions 1-4 depict different heat transfer modes. Region 1 shows sensible heat transfer of two liquid streams. Region 2 shows condensation in the hot stream and sensible liquid heat transfer in the cold stream. Region 3 shows condensation and boiling heat transfer. Region 4 shows boiling heat transfer in the cold stream and sensible cooling of gas in the hot stream.

To illustrate the issue, figure 3.6 represents the change in temperature of a hot and cold stream undergoing heat transfer in a counterflow arrangement. The two fluids are generic fluids and undergo phase changes during heat transfer. As seen in figure 3.6 the pair of fluids have 4 different types of heat transfer modes which are numbered 1-4 in figure 3.6. A description of each mode along with an estimate of the overall heat transfer coefficient for water at 1 bar are:

1. Sensible heat transfer of two liquid streams ($U_o = 2.3 \frac{kW}{m^2K}$).
2. Condensation in the hot stream and sensible liquid heat transfer in the cold stream ($U_o = 2.9 \frac{kW}{m^2K}$).
3. Condensation in the hot stream and boiling in the cold stream ($U_o = 3.4 \frac{kW}{m^2K}$).

4. Boiling heat transfer in the cold stream and sensible cooling of vapor in the hot stream. ($U_o = 0.2 \frac{kW}{m^2K}$)

As heat transfer surface area is found by using equation 3.37, by holding heat transfer, \dot{Q} and log mean temperature difference, ΔT_{lm} constant, the difference in areas between two overall heat transfer coefficients is:

$$A_2 = A_1 \frac{U_{o,1}}{U_{o,2}} \quad (3.38)$$

Using equation 3.38 with the estimated U values for water, the difference in surface area between region 1 and region 3 is a reduction of 33% and the difference between region 3 and region 4 is an increase by a factor of 17. This can lead to vastly different surface area estimates which lead to vastly different cost estimates. To account for these different heat transfer modes, an algorithm was developed to discretize along the heat exchanger and determine if the heat transfer mode changes. When a mode change occurs, the surface area is determined for each region. The areas for each region are summed to get the overall heat exchanger surface area.

To find when the heat transfer mode changes the known inlet conditions and overall heat transfer rate are used to find the specific heat transferred between the hot and cold streams by using:

$$q_c = \frac{\dot{Q}}{\dot{m}_c} \quad (3.39)$$

$$q_h = \frac{\dot{Q}}{\dot{m}_h} \quad (3.40)$$

The specific heat transferred represents the change in specific enthalpy each fluid stream undergoes between the inlet and outlet. To see if the heat transfer mode changes, the heat exchanger is discretized into a specified number of sections, N , and the specific enthalpy change for each section is found by:

$$\Delta i_c = \frac{q_c}{N} \quad (3.41)$$

$$\Delta i_h = \frac{q_h}{N} \quad (3.42)$$

With the specific enthalpy change, the specific enthalpy for each fluid can be found for each discretized section by adding Δi to the previous specific enthalpy value:

$$i_c^{j+1} = i_c^j + \Delta i_c \quad (3.43)$$

$$i_h^{j+1} = i_h^j + \Delta i_h \quad (3.44)$$

As pressure is known and assumed constant in the heat exchanger, the heat transfer mode for each discretized section can be readily found by using the pressure and specific enthalpy to find the fluid quality. Quality is a function of pressure and specific enthalpy for any fluid and when using software such as Engineering Equation Solver can easily be determined with its large database of fluids. In EES, for a liquid the quality is returned as -100, for a vapor the quality is returned as 100, and for a saturated fluid the quality is between 0 and 1. With a quality value, the heat transfer mode can be found for each stream, and therefore an estimate of surface area can be determined using the procedure outlined at the beginning of section 3.4.3.

3.5 Levelized Cost of Electricity

To integrate cost with cycle efficiency, the levelized cost of electricity (LCOE) was incorporated. The LCOE is an estimation of all costs associated with the building and operation of the power plant divided by the total energy produced over its lifetime [56]. The LCOE allows for direct economic comparison of different technologies, as it accounts for projects that have different life spans, capital costs, and capacities.

To estimate each power cycle's LCOE, public values from NuScale were used to determine the percentage of the LCOE that contributed to the cost of the power cycle components. In 2016, the overall NuScale plant which hold 12 power cycle modules is estimated to have overnight costs of \$2.9 billion [57]. The LCOE of the NuScale plant ($LCOE_{NuScale}$) is estimated to be at 85 \$/MWh [6], of which about 50% of those costs are the plant capital costs (f_{cap}) [57].

To estimate the LCOE of each modeled power cycle, first the estimated cost of the baseline cycle used in NuScale's analysis was determined using the cost models specified in section 3.4.2 and multiplied by 12 to get the total power cycle plant component costs.

The equipment cost fraction, f_{equip} , of capital costs was then estimated by dividing the total power cycle plant component costs by the total plant cost of \$2.9 billion.

A percentage change between the new cycle costs and the baseline cycle costs was calculated using the equation:

$$\%C = \frac{C_{new} - C_{baseline}}{C_{baseline}} \quad (3.45)$$

With all of the values from above and the 1st law cycle efficiencies, η_I , for the baseline and new cycles, the new LCOE estimate is found using:

$$LCOE_{new} = \frac{\eta_{I,baseline}}{\eta_{I,new}} \left[LCOE_{NuScale} (1 + f_{cap} \cdot f_{equip} \cdot \%C) \right] \quad (3.46)$$

$$LCOE = \frac{\Sigma \text{ Costs Incurred}}{\Sigma \text{ Energy Produced}} \quad (3.47)$$

One important note is the levelized cost value from NuScale, $LCOE_{NuScale}$, was adjusted for 2018 dollars by increasing from 85 to 89 \$/MWh.

3.6 Assumptions

For all cycles analyzed the following assumptions were used when deriving the models:

- Cycles operates at a steady-state condition
- No heat losses within and between components
- No pressure losses in the system
- Changes in fluid kinetic energy is negligible
- No changes in gravitational potential energy
- Completely uniform mixing of fluids
- Plant lifetimes are equal for all cycles
- Plant overhead, maintenance, and ancillary costs are all equal for all cycles

To solve for the overall cycle efficiency, the models were constrained by anticipated operating conditions such as the condensing temperature, maximum temperature, and maximum pressure. Other assumptions such as turbine and pump efficiency were based

on literature. The list of all assumptions used for each cycle is listed in tables 3.4 and 3.5.

Table 3.4: Overall assumptions used in the analysis of potential replacement power cycles.

Parameter Name	Variable	Value	Source
Power Cycle Heat Input	\dot{Q}_{in}	160 MW	Current Reactor Design Heat Output.
Max Pressure	P_{max}	125 bar	Maximum allowable pressure allowed in primary heat exchanger.
Max Temperature	T_{max}	301 °C	Maximum temperature of power cycle working fluid
Min Temperature	T_{min}	25 °C	Minimum condensing or cooling temperature available for heat transfer with the working fluid.
Heat Exchanger Pinch Point Temperature	T_{pinch}	5 °C	Minimum temperature difference allowed between the hot and cold streams within the heat exchanger.
Min Turbine Quality	x_{min}	0.87	Minimum amount of quality allowed during turbine expansion to prevent blade erosion.

The minimum temperature, T_{min} , specified in table 3.4 is the ambient outdoor temperature. The minimum cycle temperature was set at 30 °C for all power cycles except for the steam Rankine cycles which was set to 42 °C. This change is due to condensing pressures in the Rankine cycles are much lower than atmospheric pressure causing high volume flow rates.

Table 3.5: Overall efficiency of turbines, compressors, and pumps used in the analysis of potential replacement power cycles.

Parameter Name	Variable	Value	Source
Turbine Isentropic Efficiency	η_t	0.85	Turbine efficiency for all cycle except the sCO_2 cycles.
sCO_2 Turbine Isentropic Efficiency	η_{t,sCO_2}	0.90	Turbine efficiency for the sCO_2 cycles.
sCO_2 Compressor Isentropic Efficiency	η_c	0.89	Compressor efficiency for the sCO_2 cycles.
Pump Efficiency	η_p	0.75	Pump efficiency used in all cycles.

3.7 Software

All cycles were evaluated used Engineering Equation Solver (EES) version 10.369. EES is a numerical equation solver that can solve thousands of coupled non-linear algebraic equations. EES also determines thermophysical properties for fluids using high accuracy equations of state given reference inputs such as temperature and pressure. The fluids used in the analysis and the references for each equation of state are listed in table 3.6.

Table 3.6: References to equations of state used to determine thermophysical properties in EES.

Fluid	Equation of State Reference
Ammonia (NH_3)	Tillner-Roth, Harms-Watzenberg, and Baehr, "Eine neue Fundamentalgleichung für Ammoniak", DKV-Tagungsbericht 20:167-181, 1993.
Carbon Dioxide (CO_2)	R. Span and W. Wagner, A New Equation of State for Carbon Dioxide Covering the Fluid Region from the Triple-Point Temperature to 1100 K at Pressures up to 800 MPa, J. Phys. Chem, Ref. Data, Vol. 25, No. 6, 1996.
Ethanol (C_2H_6O)	J. A. Schroeder, S. G. Penoncello, and J. S. Schroeder, "A Fundamental Equation of State for Ethanol", Journal of Physical and Chemical Reference Data 43, 043102 (2014)
Water (H_2O)	Wagner and Pruss (J. Phys. Chem. Ref. Data, Vol. 31, No. 2, 387, 2002).

3.8 Solution Process

Optimization of power cycle efficiency was first performed to determine which cycles had promise over the current baseline Rankine cycle. Selected cycles were chosen over the potential to produce more power or slightly less power at an assumed lower cost. The final analysis of the project focused on quantifying and integrating power cycle costs using levelized cost of electricity to better understand economic factors.

To solve for cycle efficiencies and costing, the model was constrained using values for the assumed likely operating conditions of the power plant. This included values such as the ambient temperature (condensing temperature), maximum temperature of the cycle, and maximum pressure as stated in tables 3.4 and 3.5. Heat exchangers were typically constrained in one of two ways that would determine optimal solutions for the cycles being analyzed. For the Rankine cycles, where pinch points will develop due to

condensation heat exchange, an outlet enthalpy of the cold stream was determined using pinch point analysis as done by Nellis and Klein [58]. The second method used to for all other cycles, selected an effectiveness value (ϵ) and solved for the outlet temperatures using the equations described in section 3.2.1.3.

Independent variables used to determine an optimal solution were selected from variables not fixed from design assumptions. The independent variables selected for each cycle included the following:

- Hot side heat exchanger outlet enthalpy (i_{out})
- Mass flow split ratio (ϕ)
- Heat exchanger effectiveness (ϵ)
- Pressure ratios between turbine expansion stages
- Degree of superheat exiting the primary heat exchanger

Independent variables differed for each cycle depending on the system setup. The values for the independent variables were initially estimated and then optimized using the optimization procedure outlined in the next section.

3.9 Cycle Optimization

Design optimization is a process methodology seeking to find optimal values for a function given a set of independent variables and constraints. Engineering Equation Solver (EES) incorporates a series of optimization algorithms which include single and multi-variable optimization algorithms. For most power cycle optimization, multi-variable optimization was utilized, where independent variables are selected based on either heuristic rules or by computing function gradients. The process iterates until a minimum/maximum value is found for the objective function.

In design optimization, problems are considered to be unconstrained or constrained. In an unconstrained problem, the objective function min/max is found for the entire solution space. On the other hand, a constrained problem is bound to a set of equality and inequality constraints which prevent the solution from moving beyond the constrained bounds.

To find optimal values for each power cycle, inequality constraints were required to check for specific conditions. These constraints ensured 2nd law violations did not occur

in heat exchangers, turbine expansion did not drop below a quality limit, and saturated liquid is not pumped.

EES does not formally handle constrained optimization problems with inequality constraints. To combat this issue, the constrained problem was transformed into an unconstrained optimization problem using the penalty method outlined in [59]. The penalty method works by incorporating the inequality constraints into the objective function in order to unfavorably adjust the value when constraints are violated. The magnitude in which the penalties affect the objective function is determined by the scaling of the constraints using both a scaling coefficient and constraint value normalization.

To perform a transformation via the penalty method, the following equation is applied:

$$T(\vec{x}) = f(\vec{x}) \pm R(\sum [g_i^+(\vec{x})]^2) \quad (3.48)$$

Where T is the transformed objective function, f is the objective function, \vec{x} are the independent variables, R is the scaling penalty parameter, and g_i^+ are the penalty inequality constraints defined as:

$$g_i^+ = \max(0, g_i(\vec{x})) \quad (3.49)$$

The inequality constraints defined above are required to be in negative null form, which means when constraints are valid, the constraint solution is either zero or negative. Conversely, when the constraint is violated the solution will be positive. For the penalty method, as equation 3.49 takes the maximum of zero or the constraint value, only constraints that are violated will adversely impact the objective function.

The \pm in equation 3.48 is based on whether the optimization is to find a maximum or minimum value. For maximization problems, the \pm is changed to a subtraction sign ($-$), for minimization, the sign is addition ($+$). In the case of power cycle optimization, when optimizing for cycle efficiency, a maximum was sought after and therefore a subtraction sign was used. When optimizing for levelized cost of electricity, a minimum was desired and therefore an addition sign was used.

Normalization of constraints is performed so all constraint penalties are applied with the same magnitude. The normalization is done by dividing the constraint by its violation threshold value. This sets each constraint to a value of 1 when the constraint is considered

to be in violation. For positive values close to zero the constraint is still in violation, but the solution is still considered to be somewhat feasible.

The scaling penalty parameter, R , is set so it properly adjusts the objective function when a violation occurs. If R is set to high, steep solution gradients will occur when a violation occurs. A large R value will help ensure optimization algorithms do not violate constraints, but could steer the algorithm away from optimal solutions that lie on or near the constraint boundaries. If R is set to low, optimal values may be found that lie well within the infeasible region. To account for both problems, R was set to a value of 1 for all cycles. This value was chosen as the objective function was normalized to produce a value around 1 within the expected range, and the setting was found to have the proper sensitivity in applying penalties.

With the constrained problem transformed to an unconstrained problem, cycles were optimized using a selection of multi-variable optimization algorithms provided by EES. The algorithms use different methods to find optimal solutions. The optimization algorithms are outlined in the EES user guide from [54], a brief description of each are:

- Variable Metric: only multi-variable method within EES that computes the numerical gradients to provide a search direction.
- DIRECT Optimization: a global optimization method which is best used when local optimal values exist.
- Genetic Method: a robust global optimization method that mimics biological processes to hone in on optimal solutions.

The order and usage of each algorithm selected was cycle dependent. Where one or more methods were used based on algorithm success rate and ability to function without error. Typically, global algorithms such as the DIRECT and Genetic methods were first used. The best values from those algorithms were then used as the starting position for the Variable Metric algorithm which would further optimize the solution around the point of interest.

3.10 Uncertainty

To quantify the uncertainty present in the cost models and the assumptions used around the turbine, pump, and compressor efficiencies an uncertainty analysis was performed

for the levelized cost of electricity (LCOE) estimates. The uncertainty analysis used the method describe in NIST Technical Note 1297 [60] where uncertainty is propagated using the variance formula:

$$u_f = \sqrt{\left(\frac{\partial f}{\partial x}\right)^2 u_x^2 + \left(\frac{\partial f}{\partial y}\right)^2 u_y^2 + \left(\frac{\partial f}{\partial z}\right)^2 u_z^2 + \dots} \quad (3.50)$$

Where u_f is the uncertainty of f and u_x , u_y , u_z are the uncertainty values for the independent variables x , y , and z .

The uncertainty method was implemented using the uncertainty propagation method contained in Engineering Equation Solver (EES). This methods computes the numerical partial derivatives of the function, f , for the given independent variables.

The uncertainties shown for the selected independent variables found in table 3.7 were used to propagate uncertainty for both an overall cycle efficiency value and LCOE. The uncertainty used in the cycle efficiency is an absolute uncertainty value while the cost uncertainty and Baumann coefficient is relative to the value.

Table 3.7: Uncertainty values for independent variables used to determine overall uncertainty of LCOE and cycle efficiency.

Independent Variable	Uncertainty
Turbine Efficiency	0.02
Pump Efficiency	0.02
Compressor Efficiency	0.02
Baumann Coefficient	10%
Component Cost	50%

Chapter 4 Results

Based on the literature review cycles were selected to first perform a 1st law analysis in order to determine overall cycle efficiency. Based on this cycles were pared down and an exergy, costing, and LCOE analysis was performed. The results from this analysis are presented in the sections below.

4.1 1st Law Analysis

Based on the literature review, the following cycles were considered to have potential benefit when matched with the NuScale SMR:

- Regenerative Reheat Rankine Cycle - potential higher efficiencies and is an easy replacement to the baseline cycle.
- Transcritical Cycles - have advantages of low pumping power and sensible heat transfer with the primary source.
- sCO_2 Regenerative Cycle - not likely to have high efficiencies, but will provide insight on the most basic sCO_2 cycle fit with a SMR.
- sCO_2 Recompression Cycle - outside of the sCO_2 reheat recompression cycle. This cycle is the most likely to have high enough efficiencies to compete with the baseline cycle.
- Combined Cycle - Coupling a sCO_2 regenerative cycle with an ORC could provide reasonable efficiencies.

For each of the cycles above a first law analysis was performed to determine the cycle efficiencies to be compared with baseline regenerative Rankine cycle. The following subsections present the results from the analysis for each cycle as well as comparing the overall efficiency of all cycles.

4.1.1 Cycles

4.1.1.1 Regenerative Rankine Cycle

Results from the optimization of the baseline regenerative Rankine cycle are shown in table 4.1. The first column of values shows the optimized results, the second column of values show the results when using NuScale’s values for independent variables prior to optimizing, and the last column provides the stated or estimated NuScale values determined from [9].

Table 4.1: Regenerative Rankine cycle overall values for 1st law analysis. The optimized model column are values found via optimization. The model with NuScale parameters is the model ran with independent variables provided by NuScale [9]. The estimated NuScale values column contain the estimated values from the stated NuScale design.

Value Name	Variable	Optimized Model	Model with NuScale Parameters	Estimated NuScale Values
Cycle Efficiency	η_I	0.312	0.307	0.318
Mass Flow Rate Through Primary Hxer [kg/s]	\dot{m}	70.6	67.8	67.1
Net Cycle Work [kW]	\dot{W}_{net}	50,000	49,000	50,800
Turbine Work [kW]	\dot{W}_p	50,300	49,400	51,400
Pump Work [kW]	\dot{W}_t	353	323	555
Turbine Efficiency Adjusted for Moisture	η_a	0.812	0.814	0.862
Total Regenerator Conductance [MW/K]	UA	3.6	1.8	1.8

The overall cycle efficiency for the optimized model is at 31.2%. When running

the model using NuScale's values prior to optimization the overall efficiency was found to be 30.7%. This under predicts the estimated value from NuScale at 31.8%. The difference appears to originate from the turbine moisture model, which degrades the turbine efficiency more than the values predicted by NuScale.

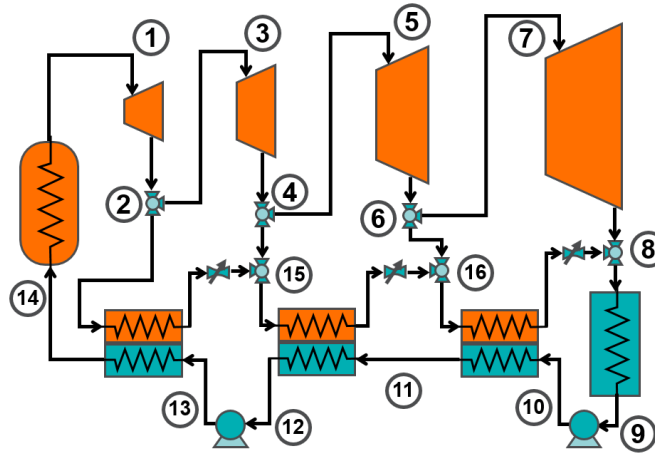


Figure 4.1: Cycle diagram of the NuScale regenerative Rankine cycle.

The independent variables used to solve for the results in table 4.1 are shown in table 4.2. Table 4.2 contains the independent variables for the optimized solution in the first column of values, and the independent variables based on the NuScale setup in the second column. The state points for the pressure values labeled in table 4.2 correspond to the state points on the diagram in figure 4.1. The low, medium, and high temperature regenerators refer to the heat exchangers between states 10-11, 11-12, 13-14 respectively.

Table 4.2: Independent variables used to solve the regenerative Rankine cycle for maximum efficiency. The first column of values are from the optimized model, the second column is NuScale setup found from [9].

Value Name	Variable	Optimized Model	Model with NuScale Parameters
Max Pressure	P_1	37	34
Turbine Stage One Exit Pressure [bar]	P_2	9.2	5.1
Turbine Stage Two Exit Pressure [bar]	P_4	1.9	2.4
Turbine Stage Three Exit Pressure [bar]	P_6	0.40	0.61
First Pump Exit Pressure [bar]	P_{10}	25	25
High Temperature Regenerator Effectiveness	ϵ_{high}	0.92	0.84
Medium Temperature Regenerator Effectiveness	ϵ_{med}	0.90	0.89
Low Temperature Regenerator Effectiveness	ϵ_{low}	0.85	0.89

Significant differences between the independent variables used in the optimized model and the model ran with the NuScale parameters include the maximum pressure, turbine stage exit pressures, high temperature regenerator effectiveness, and low temperature regenerator effectiveness. The maximum cycle pressure has a direct effect on cycle efficiency, as boiling temperature is increased with maximum pressure reducing entropy generation within the primary heat exchanger. The turbine stage exit pressures influence cycle efficiency through the feedwater regeneration process. As exit pressure determines the condensing temperature of the regeneration stream these variables determine the maximum temperature limit of the feedwater when exiting each regenerator. Regenerator effectiveness will increase the maximum amount of heat used in power generation versus heat rejection from the condenser.

It is unclear why the NuScale maximum pressure is set at a lower value unless it is expected a lower boiling temperature is required to ensure fluid quality expansion limits are not reached. Additionally, reasons the optimized values differ from the NuScale param-

ters could be due to how the model handles liquid separation and moisture development within turbine stages. Not explicitly shown in the diagram, but part of the NuScale setup, is liquid separation that occurs between the turbine stages between states 4-7 on figure 4.1. This process separates moisture from the saturated vapor, which increases quality by 0.05 points. The regenerative Rankine model for both the optimized and NuScale parameter setups account for this liquid separation by increasing the turbine quality at state 5 by 0.05. Then the exiting quality at state 15 is found by performing an energy and mass balance at the valve splitter (states 4, 5, 15).

The turbine moisture model can indirectly change the quality of the exiting vapor between stages via the adjusted efficiency. This along with simplified liquid separation only occurring at state 5, can effect the final quality of the fluid when exiting out of the last turbine stage. The final quality would affect optimization due to expansion quality limits.

The turbine stage exit pressures could be affected by design trade offs from turbine manufacturers. These designs may require fluid bleed stages can only occur at specific pressures and therefore the model may require adjustments based on turbine manufacturer input.

4.1.1.2 Reheat Regenerative Rankine Cycle

For the reheat cycle two different configurations were compared as shown in figure 4.2. The cycle on the left is a regenerative reheat Rankine cycle with three regenerators, the cycle on the right removes the low and medium temperature regenerators. All of the regeneration fluid streams are mixed with the feedwater stream at the same pressure at states 9-10, 12-13, and 15-16. Both cycles contain two reheaters shown on the top of the diagram. The first reheater is between states 2-3 and the second is between states 4-5.

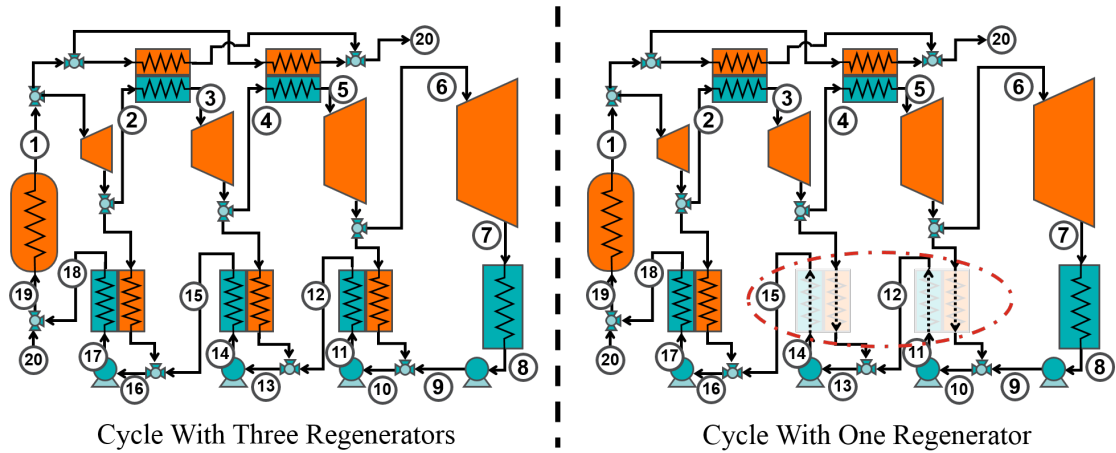


Figure 4.2: Cycle diagram of two regenerative reheat Rankine cycles. The cycle on the left has 3 regenerators, while the cycle on the right has only 1. All regenerative streams are mixed with the feed water during the heating process.

Results from the optimization of the two cycle setups along with the optimized baseline cycle values are shown in table 4.3. The overall cycle efficiency for both cycles were equal at 33.1%, compared to 31.2% for the baseline regenerative Rankine cycle. The main reason for the higher efficiency when compared to the baseline setup is due to a higher turbine efficiency from dry expansion and higher boiling temperature and pressure within the primary heat exchanger.

Table 4.3: Regenerative reheat Rankine cycle values optimized for maximum efficiency.

Value Name	Variable	With Three Regen	With One Regen	Optimized Baseline Model
Cycle Efficiency	η_I	0.331	0.331	0.312
Mass Flow Rate Through Primary Hxer [kg/s]	\dot{m}	75.3	75.2	70.6
Net Cycle Work [kW]	\dot{W}_{net}	52,900	53,000	50,000
Turbine Work [kW]	\dot{W}_t	53,400	53,400	50,300
Pump Work [kW]	\dot{W}_p	441	445	353
Turbine Efficiency Adjusted for Moisture	η_a	0.837	0.834	0.812
Total Regenerator Conductance [MW/K]	UA	6.4	3.0	3.6

The reheat cycle with only one regenerator shows a lower regenerator conductance value of 3.0 [MW/K] versus 3.6 [MW/K] compared to the baseline cycle. The model shows the high temperature regenerator for both the reheat cycles and baseline cycle has a similar conductance value around 1.8 [MW/K]. The reheater regenerators have a combined conductance value around 1.1 [MW/K] for both the 3 regenerator and 1 regenerator reheat cycle designs.

The independent variables used to solve for the results above are shown in table 4.4. The table shows the independent variables for both the three and one regenerator setups. The state points for the pressure values labeled in table 4.4 correspond to the state points on the diagram in figure 4.2. The low, medium, and high temperature regenerators refer to the heat exchangers between states 11-12, 14-15, 17-18 respectively. The reheat pinch point temperature refers to the minimum ΔT between the hot and cold fluid streams within reheaters. As the reheat stream is a superheated vapor, a larger ΔT is desired to minimize the heat exchanger size.

Table 4.4: Independent variables used to solve the regenerative reheat Rankine cycle for maximum efficiency. The columns contain the independent variables used for the three regenerator setup and the one regenerator setup.

Value Name	Variable	With Three Regen	With One Regen
Max Pressure [bar]	P_1	49	49
Turbine Stage One Exit Pressure [bar]	P_2	13.7	13.8
Turbine Stage Two Exit Pressure [bar]	P_4	5.7	5.5
Turbine Stage Three Exit Pressure [bar]	P_6	0.97	0.91
Reheat Pinch Point [C]	T_{pinch}	10.0	10.0
1st Reheater Effectiveness	$\epsilon_{1st,RH}$	0.95	0.95
2nd Reheater Effectiveness	$\epsilon_{2nd,RH}$	0.96	0.96
High Temp Regenerator Effectiveness	ϵ_{high}	0.88	0.87
Medium Temp Regenerator Effectiveness	ϵ_{med}	0.86	-
Low Temp Regenerator Effectiveness	ϵ_{low}	0.91	-

4.1.1.3 Transcritical Cycle

The transcritical cycle was optimized using the two different fluids ethanol and ammonia. The results from the optimization are shown in table 4.5. In table 4.5 the first column of values provide the optimized results for the ethanol cycle, the second column of values provide the optimized results for the ammonia cycle, and the last column provides the optimized results for the baseline regenerative Rankine cycle.

Table 4.5: Transcritical cycle overall values for optimized maximum efficiency. The Values are for transcritical cycles using ethanol and ammonia working fluids. The baseline model is the optimized regenerative Rankine cycle for comparison.

Value Name	Variable	Ethanol	Ammonia	Optimized Baseline Model
Cycle Efficiency	η_I	0.341	0.264	0.312
Mass Flow Rate Through Primary Hxer [kg/s]	\dot{m}	269	151	70.6
Net Cycle Work [kW]	\dot{W}_{net}	54,600	42,300	50,000
Turbine Work [kW]	\dot{W}_t	58,100	45,700	50,300
Pump Work [kW]	\dot{W}_p	3,530	3,440	353
Total Regenerator Conductance [MW/K]	UA	6.7	2.7	3.6

The results from table 4.5 reveal the transcritical ethanol cycle has the highest efficiency at 34.1% compared to 26.4% and 31.2% for the transcritical ammonia and baseline regenerative Rankine cycle respectively. The higher efficiency for the ethanol cycle does require mass flow rates about 4 times that of the baseline cycle which contribute to the large increase in pumping power and regenerator conductance values.

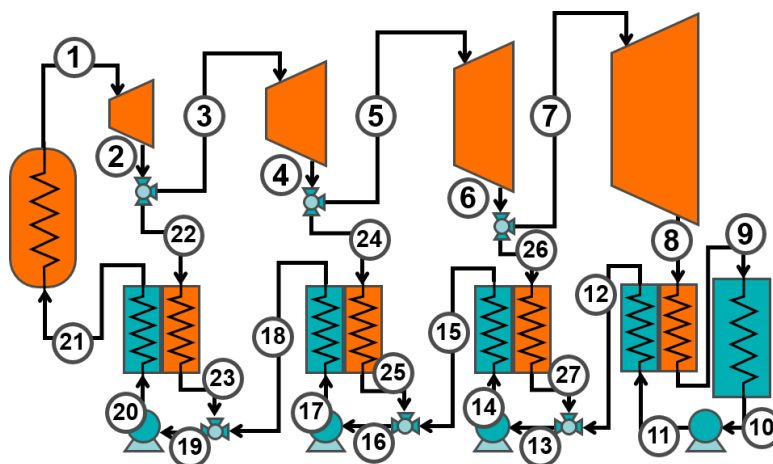


Figure 4.3: Diagram of transcritical cycle. The cycle contains 3 main regenerators between states 14-21 and one condenser regenerator between states 11-12. The condenser regenerator is only used if the fluid at state 8 is a superheated vapor.

The independent variables used to solve for the results in table 4.5 are shown in table 4.6. The table shows the independent variables for both the ethanol and ammonia cycles. The state points for the pressure values labeled in table 4.6 correspond to the state points on the diagram in figure 4.3. The low, medium, and high temperature regenerators refer to the heat exchangers between states 14-15, 17-18, 20-21 respectively. The condenser regenerator is located between states 11-12, and was only used for the ammonia cycle.

Table 4.6: Independent variables used to solve the transcritical cycle for maximum efficiency. The columns contain the independent variables used for the three regenerator setup for the ethanol cycle and the four regenerator setup for the ammonia cycle.

Value Name	Variable	Ethanol	Ammonia
Max Pressure	P_1	83	125
Turbine Stage One Exit Pressure [bar]	P_2	40	107
Turbine Stage Two Exit Pressure [bar]	P_4	9.4	69
Turbine Stage Three Exit Pressure [bar]	P_6	1.35	43
High Temp Regenerator Effectiveness	ϵ_{high}	0.77	0.97
Medium Temp Regenerator Effectiveness	ϵ_{med}	0.94	0.97
Low Temp Regenerator Effectiveness	ϵ_{low}	0.91	0.96
Condenser Regenerator Effectiveness	ϵ_{cond}	-	0.92

The low value of the high temperature regenerator effectiveness for the ethanol cycle is based on the internal pinch point that develops from the cooling of the superheated vapor to a saturated fluid. This requires a higher mass flow rate from the hot fluid bled from the first turbine stage to prevent the decrease in the cold stream outlet temperature. The mass flow rate creates a trade off between lower regenerator effectiveness and higher feed stream temperatures in order to seek optimal values.

4.1.1.4 sCO_2 Regenerative Cycle

The results for the sCO_2 regenerative cycle optimization are shown in table 4.7 along with the baseline regenerative Rankine cycle. Results show the sCO_2 regenerative cycle has a significantly lower efficiency of 24.5% compared to the baseline cycle of 31.2%. The cycle is much simpler with only one regenerator, a compressor, and a turbine, but the regenerator conductance value of the sCO_2 cycle is almost three times as high as the baseline cycle which indicates the size of the heat exchanger will be around 3 times higher if heat transfer coefficients are within the same range as other cycle regenerators. The large regenerators are required due to the small pressure ratio in the sCO_2 regenerative

cycle. Compared to the Rankine cycle which expands to condensing temperature, the sCO_2 regenerative cycle has significantly higher exiting temperatures out of the turbine which require internal regeneration in order to maximize cycle efficiency.

Table 4.7: sCO_2 regenerative cycle overall values optimized for maximum efficiency.

Value Name	Variable	Optimized Cycle	Optimized Baseline Model
Cycle Efficiency	η_I	0.245	0.312
Mass Flow Rate Through Primary Hxer [kg/s]	\dot{m}	1,220	70.6
Net Cycle Work [kW]	\dot{W}_{net}	39,200	50,000
Turbine Work [kW]	\dot{W}_t	75,800	50,300
Compressor Work [kW]	\dot{W}_c	36,700	353
Back Work Ratio	bwr	0.48	-
Total Regenerator Conductance [MW/K]	UA	9.7	3.6

The back work ratio, which is the ratio of compressor power to turbine power, requires almost one half of the power generated by the turbine to be used in the compression process. The large back work ratio is required as the cooled low pressure fluid is a superheated vapor prior to compression at state 4. Compressing the fluid back to a supercritical state requires a 62% decrease in specific volume of the fluid.

The independent variables used to solve for the results in table 4.7 are shown in table 4.8. The state points for the pressure values labeled in table 4.8 correspond to the state points on the diagram in figure 4.4.

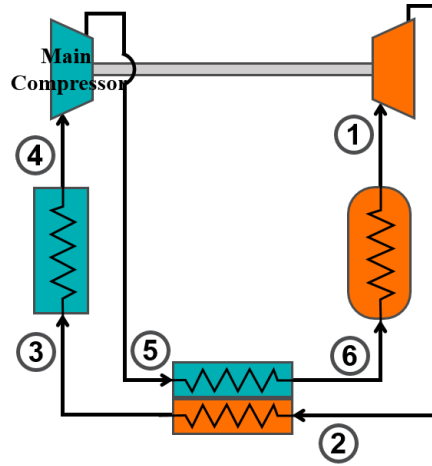


Figure 4.4: sCO_2 regenerative cycle diagram.

Table 4.8: Independent variables used to solve the sCO_2 regenerative cycle for maximum efficiency.

Value Name	Variable	Optimized Cycle
Max Pressure [bar]	P_1	125
Min Pressure [bar]	P_2	61
Min Temperature [C]	T_4	30.0
Regenerator Effectiveness	ϵ	0.95

As the sCO_2 regenerative cycle is a simpler cycle compared to the previous cycles, optimized values can be better visualized. The effect on efficiency by varying the minimum pressure of the cycle is shown in figure 4.5, while holding other independent variables constant. Maximum efficiency for the cycle is shown to be in the pressure range below the critical point, making the optimized cycle a type of transcritical cycle. As the pressure increases cycle efficiency significantly drops upon crossing the critical point. There are multiple reasons for this, one is by raising the minimum pressure above the critical point more heat is rejected in the pre-cooler due to the spike in specific heat. Another reason is by raising the minimum pressure less power is produced by the turbine from the smaller volume expansion. These deficiencies are somewhat offset by reduced back work ratio and higher regeneration temperature at state 6, but not enough to prevent

the reduction in overall cycle efficiency.

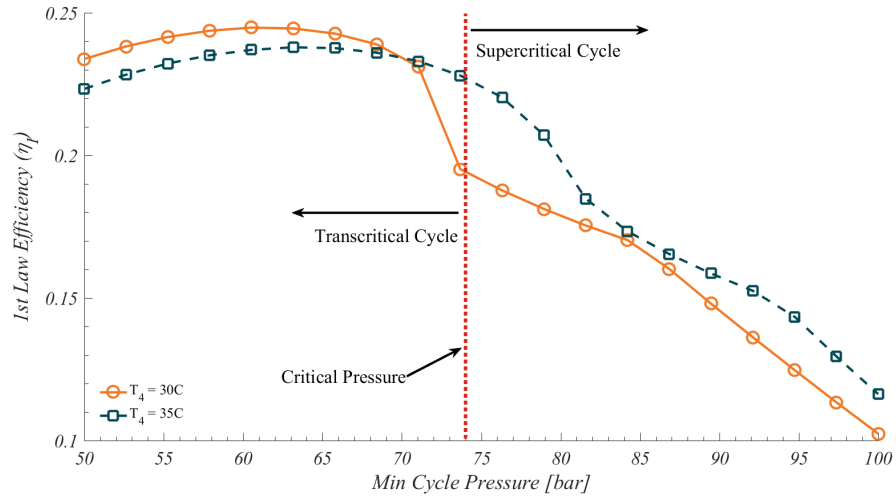


Figure 4.5: sCO_2 regenerative cycle efficiency vs. minimum pressure.

4.1.1.5 sCO_2 Recompression Cycle

The results for the sCO_2 recompression cycle optimization are shown in table 4.9 along with the baseline regenerative Rankine cycle. Results show the sCO_2 recompression cycle has a slightly lower efficiency of 29.9% compared to the baseline cycle of 31.2%.

Table 4.9: sCO_2 recompression cycle overall values optimized for maximum efficiency. Table contains values for the sCO_2 regenerative cycle and the baseline regenerative Rankine cycle for comparison.

Value Name	Variable	Optimized Recomp Cycle	Optimized Regen Cycle	Optimized Baseline Model
Cycle Efficiency	η_I	0.299	0.245	0.312
Mass Flow Rate Through Primary Hxer [kg/s]	\dot{m}	1,680	1,217	70.6
Net Cycle Work [kW]	\dot{W}_{net}	47,865	39,172	49,959
Turbine Work [kW]	\dot{W}_t	78,548	75,826	50,312
Main Compressor Work [kW]	\dot{W}_{c1}	8,035	36,654	353
Recompressor Work [kW]	\dot{W}_{c2}	22,648	-	-
Back Work Ratio	bwr	0.39	0.48	-
Total Regenerator Conductance [MW/K]	UA	46.5	9.7	3.6

The increased efficiency of the sCO_2 recompression cycle from the simpler sCO_2 regenerative cycle (24.5%) is due to the second regenerator and compressor. These added components allow for better matching of heat capacity rates between the high and low pressure fluid streams when performing regeneration. The increased efficiency of the cycle does come at a significant increase of regenerator conductance, which is about 5 times higher than the sCO_2 regenerative cycle and 13 times as high as the baseline regenerative Rankine cycle. The large increase in conductance is can be attributed to the increased internal heat exchange which rose from 190 MW to 410 MW. The increased heat exchanger duty is due to better temperature matching in the regenerators, and less heat rejection by directing flow away from the precooler into the recompressor.

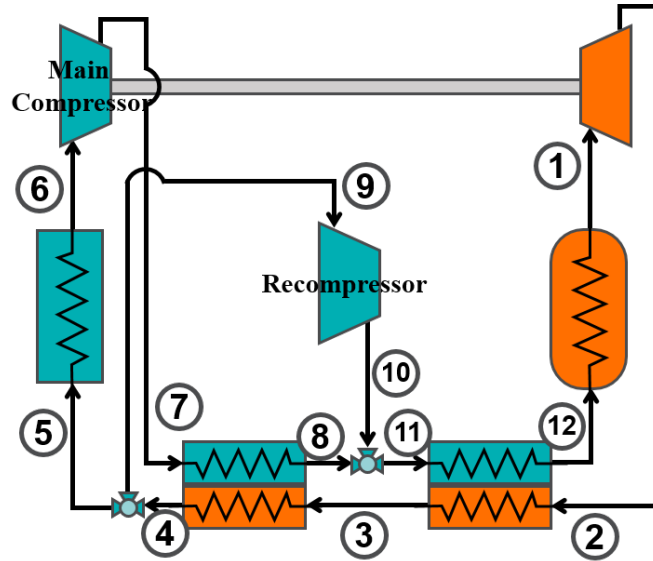


Figure 4.6: sCO_2 recompression cycle diagram.

The independent variables used to solve for the results in table 4.9 are shown in table 4.10. The state points for the pressure values labeled in table 4.10 correspond to the state points on the diagram in figure 4.6.

Table 4.10: Independent variables used to solve the sCO_2 recompression cycle for maximum efficiency.

Value Name	Variable	Optimized Cycle
Max Pressure [bar]	P_1	125
Min Pressure [bar]	P_2	74
Min Temperature [C]	T_6	31.1
Flow Split Ratio	ϕ	0.48
High Temp Regenerator Effectiveness	ϵ_{HTR}	0.97
Low Temp Regenerator Effectiveness	ϵ_{LTR}	0.91

A visual of optimized efficiency can be shown for both the flow split ratio and minimum cycle pressure. Cycle efficiency as a function of split ratio (ϕ) is shown in figure 4.7.

The other independent variables are held constant at the optimized values, except for minimum pressure which was set to the optimized pressure of 74 bar and two different pressures above and below this value. The flow split ratio (ϕ) is the percentage of the fluid that is directed to the pre-cooler (state 5-6) from state 4, while the rest of the fluid is directed to the recompressor at state 9.

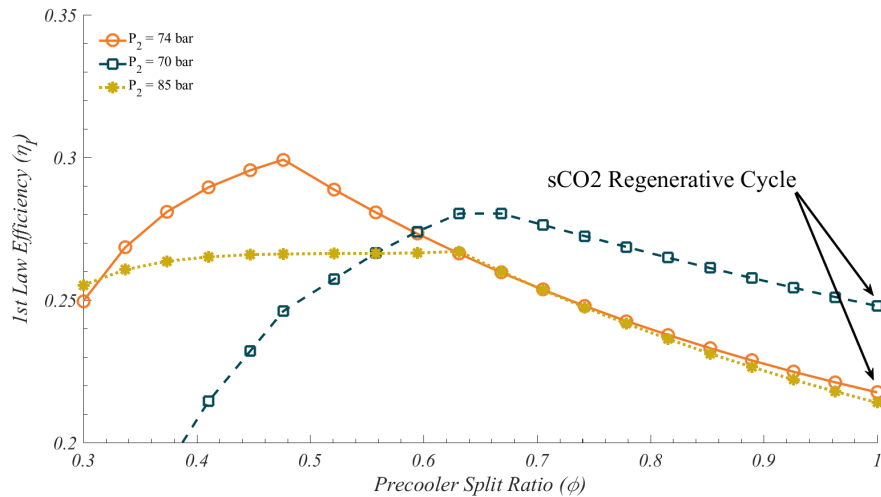


Figure 4.7: sCO_2 recompression cycle efficiency vs. flow split ratio.

Efficiency for the cycle in figure 4.7 peaks between 0.45 and 0.7 depending on the minimum pressure. For pressures above the critical point (85 bar) cycle efficiency is less sensitive to split ratio. This is due to less variation of fluid properties when moving further away from the critical point. As split ratio is increased to 1, the recompression cycle becomes the standard regenerative cycle as the recompressor is no longer used. It's important to note the efficiency value of 24.8% for the cycle with a minimum pressure of 70 bar and split ratio of 1 is higher than the value stated for the sCO_2 regenerative cycle (24.5%). This is due to the regenerator effectiveness being increased from 0.95 to 0.97.

Cycle efficiency as a function of minimum pressure (P_2) is shown in figure 4.8. The other independent variables are held constant at the optimized values, except for split ratio which was set to the optimized value of 0.476 and two different values above and below this value.

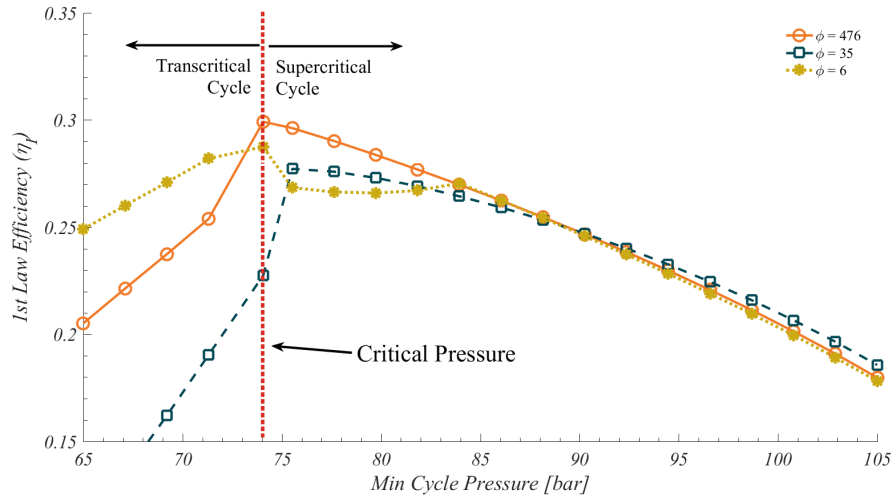


Figure 4.8: sCO_2 recompression cycle efficiency vs. minimum cycle pressure.

The plot clearly shows the recompression cycle efficiency is optimal around the critical pressure for each of the split ratios shown. This means the sCO_2 recompression cycle operates best as a supercritical cycle unlike the sCO_2 regenerative cycle which is most efficient as a transcritical cycle. The switch is due to the capability of the recompression cycle to recapture the waste heat from internal regeneration. This allows the cycle to better take advantage of a lower back work ratio by compressing the fluid near the critical point. Additionally, the turbine overcomes the lower volume expansion with higher mass flow rates, which is produced from a higher regeneration temperature at state 12.

4.1.1.6 Combined Cycle

For the combined cycle, the values found from the sCO_2 regenerative topping cycle in section 4.1.1.4 were used as inputs for the bottoming cycle and are listed in table 4.11. The state points for the temperature and pressure values labeled in table 4.11 correspond to the state points on the diagram in figure 4.6.

Table 4.11: sCO_2 regenerative topping cycle input values used for combined cycle analysis.

Value Name	Variable	sCO_2 Regen
sCO_2 Regen Cycle Efficiency	η_{I,sCO_2}	0.245
sCO_2 Mass Flow Rate [kg/s]	\dot{m}	1,220
sCO_2 Inlet Temperature [C]	T_3	94.1
sCO_2 Pressure [bar]	P_3	61.4
sCO_2 Regen Net Cycle Work [kW]	\dot{W}_{net,sCO_2}	39,200

Decoupling of the topping and bottoming cycle was done to simplify the combined cycle model. This allowed the program to only solve the conditions for one cycle, rather than coupling both together at the same time. The decoupling improved performance and reduced solving errors.

To solve the decoupled combined cycle model, the optimizer would select independent variables that included the sCO_2 regenerative cycle outlet temperature (state 4 in figure 4.9). As the sCO_2 regenerative cycle flow rate and inlet temperature (state 3) are known and constant (table 4.11), the heat into the bottoming cycle could be determined. The cycle conditions were then solved and the penalty method used to check the conditions within the bottoming/topping cycle heat exchanger. If a temperature violation was found, a penalty was added to steer the optimizer to a valid solution.

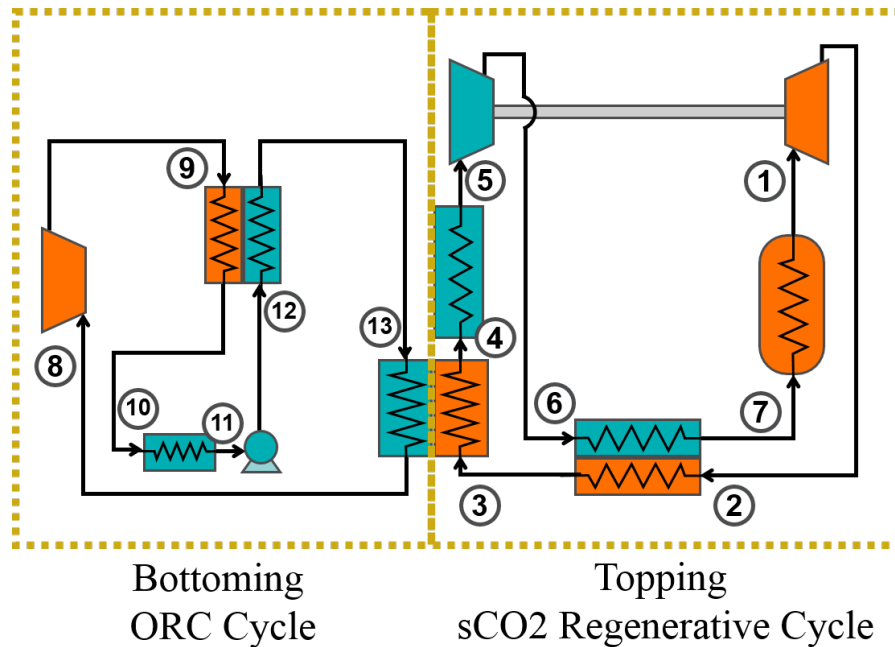


Figure 4.9: Diagram for a combined cycle with a sCO_2 regenerative topping cycle and an ORC bottoming cycle.

The combined cycle model was ran using different working fluids. The first was R245fa, which is the most widely studied working fluid for an organic Rankine cycle (ORC), due to its dry expansion and optimal condensing pressures near atmospheric pressure. Other fluids modeled included propane, ethane, R41, and R23. Propane is another fluid that has been proposed for use in ORCs. Ethane and R41 have critical pressures between the minimum and maximum pressures of the cycle, making the cycle transcritical rather than ORC. The last fluid, R23, has its critical pressure above the condensing pressure and therefore was operated as a supercritical cycle.

The results for the combined cycle optimization are shown in table 4.12. The row named "cycle type" in the table refers to the power cycle type where ORC is an organic Rankine cycle, TC is a transcritical regeneration cycle, and SC is a supercritical regeneration cycle. The table reveals overall cycle efficiency had minor increases compared to the single sCO_2 regenerative cycle efficiency of 24.5%, with R245fa showing the largest increase at 25.6%.

Table 4.12: Combined cycle overall 1st law analysis values for different working fluids. The cycle type represents whether the cycle was an organic rankine cycle (ORC), transcritical cycle (TC), or supercritical cycle (SC).

Value Name	Variable	R245fa	Propane	Ethane	R41	R23
Cycle Type	-	ORC	ORC	TC	TC	SC
Combined Cycle Efficiency	$\eta_{I,comb}$	0.256	0.255	0.253	0.248	0.250
ORC Cycle Efficiency	$\eta_{I,ORC}$	0.070	0.055	0.021	0.053	0.033
Mass Flow Rate Through ORC [kg/s]	\dot{m}	124	81.4	360	37.1	347
Net ORC Work [kW]	$\dot{W}_{net,ORC}$	1,780	1,560	1,260	491	852
Total Regenerator Conductance [MW/K]	UA	0.12	1.3	6.4	0.3	1.1

The independent variables used to solve for the results in table 4.12 are shown in table 4.13. The state points for the temperature and pressure values labeled in table 4.13 correspond to the state points on the diagram in figure 4.6.

Table 4.13: Independent variables used to solve the combined cycle for maximum efficiency with different working fluids.

Value Name	Variable	R245fa	Propane	Ethane	R41	R23
Maximum ORC Temperature [C]	T_8	65.0	63.1	51.9	74.5	72.0
Maximum Pressure [bar]	P_8	4.55	18.8	58.9	71.5	71.3
Minimum Pressure [bar]	P_9	1.77	10.8	46.6	42.9	54.9
Heat In From sCO ₂ Regenerative Cycle [kW]	\dot{Q}_{in}	25,600	28,300	60,400	9,300	26,100
ORC Regenerator Effectiveness	ϵ_{sCO_2}	0.53	0.95	0.85	0.71	0.72

The maximum heat available from the topping sCO_2 regenerative cycle is 121 MW for which the bottoming cycles extracted between 6 - 18% of that heat for power generation. The low extraction percentage is due to lack of temperature profile matching in the cycles, where pinch points are created preventing the cycle from extracting additional heat.

4.1.2 Cycle Comparison

Comparison of all cycles modeled and optimized for efficiency are shown in figure 4.10. The current baseline regenerative Rankine cycle is highlighted in the figure and is found to be near the midpoint of cycles analyzed.

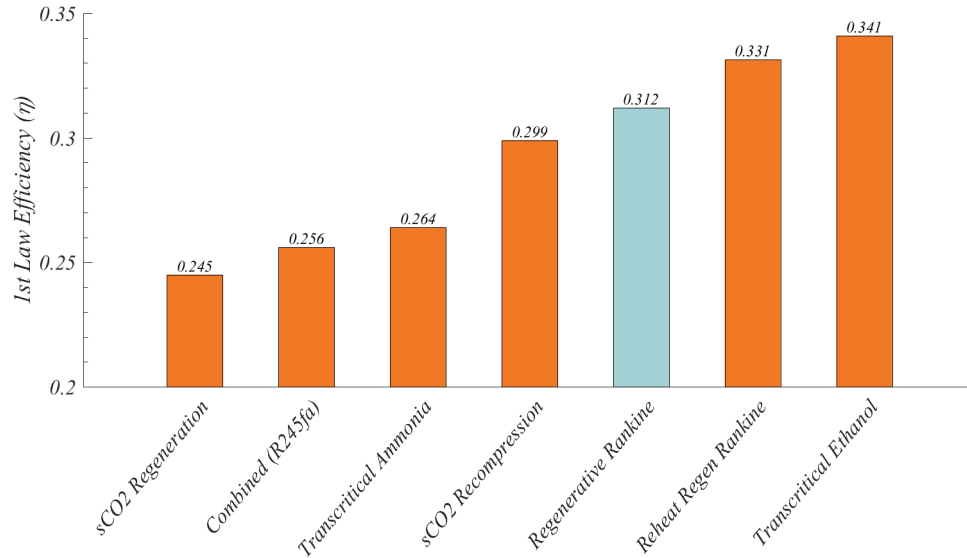


Figure 4.10: Overall first law cycle efficiency comparison. Highlighted regenerative Rankine cycle is the baseline cycle used to compare all other cycles to.

The transcritical ethanol cycle shows the highest efficiency, followed by the regenerative reheat Rankine cycle. The sCO_2 recompression cycle is slightly below the efficiency of the baseline cycle, while all other cycles are significantly below the baseline cycle.

Based on the first law analysis the sCO_2 recompression cycle, transcritical ethanol cycle, and regenerative reheat Rankine cycle were all determined worth further exploration using the exergy, costing, and levelized cost of electricity (LCOE) methods. The sCO_2 regenerative cycle, combined cycles, and transcritical ammonia cycle were removed from further analysis as the efficiency was too low and would not improve the LCOE of the NuScale setup regardless of costs.

4.2 Exergy Analysis

Exergy analysis was performed on the four cycles: sCO_2 recompression cycle, transcritical ethanol cycle, regenerative reheat Rankine cycle, and baseline regenerative Rankine cycle. The exergy analysis determined the percentage of exergy destroyed from the exergy inputted into the cycle which was a constant 78.2 MW for all cycles. The exergy

destroyed was found for each of the cycle components, which is summed to obtain the total percentage of exergy destroyed.

Overall exergy destroyed for the four cycles is shown in figure 4.11. In agreement with the 1st law cycle efficiency shown in figure 4.10 the cycles with the least exergy destroyed have the highest cycle efficiencies.

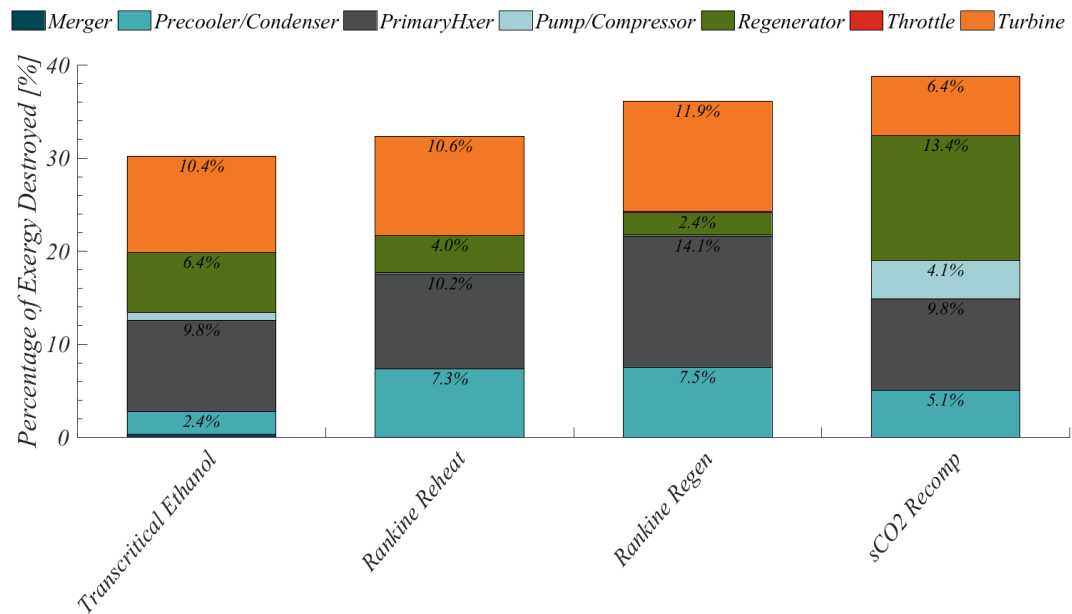


Figure 4.11: Percentage of exergy destroyed by cycle and component.

As seen in figure 4.11, the "mix" of where exergy is destroyed within each cycle varies considerably. By looking at each of the major components separately it can be more easily seen how each cycle differs.

For the heat exchangers, figure 4.12 shows the percentage of exergy destroyed for the internal heat exchangers (regenerators), the heat rejected (precooler/condenser), and the heat addition from the reactor. The baseline cycle shows the lowest exergy destroyed in the regenerators, but at the cost of more exergy destroyed in the reactor. The sCO_2 recompression cycle has most losses occurring within the two regenerators. The high losses is interesting in that the cycle was developed to minimize regenerator losses, but due to the high amount of heat transfer (410 MW) within the regenerators, there is still

a large amount of entropy generation.

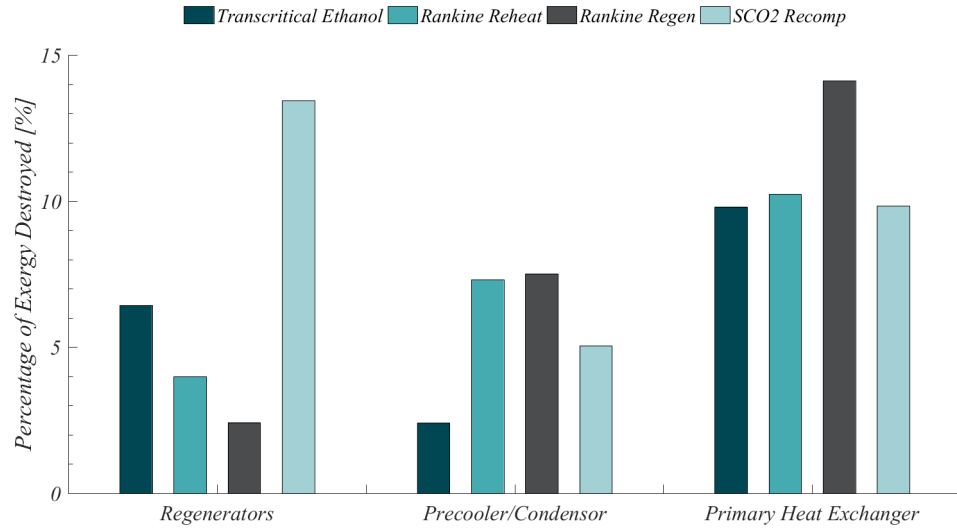


Figure 4.12: Percentage of exergy destroyed for heat exchangers.

The percentage of exergy destroyed within the turbines and pumps/compressors is shown in figure 4.13. In the figure the sCO_2 recompression cycle shows the largest deviation between the two cycles. The exergy lost in the turbine is less in the sCO_2 cycle due to the higher expected turbine efficiencies of 90% expected based on literature referenced in section 2.3.

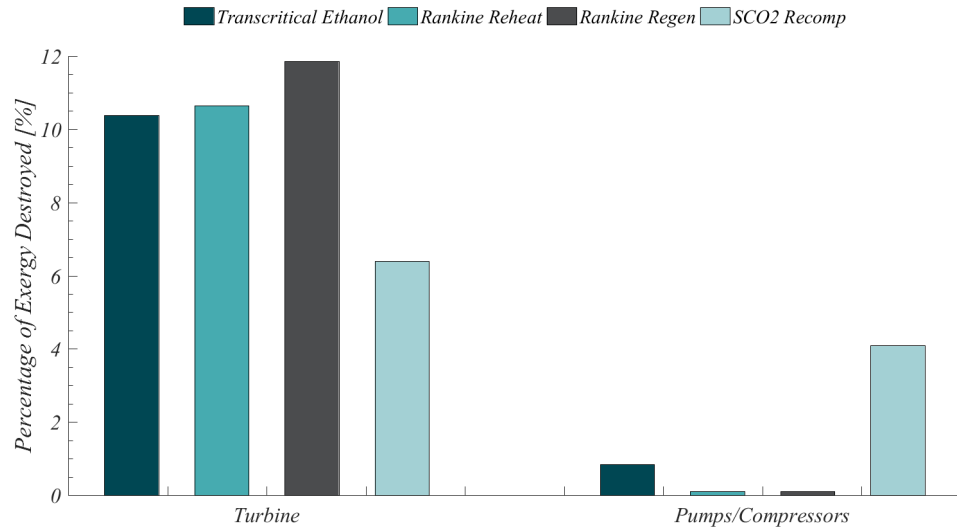


Figure 4.13: Percentage of exergy destroyed for turbines and pumps.

The higher exergy loss in the sCO_2 recompression cycle from the compressor is due to the other cycles pumping an incompressible liquid while the recompression cycle is compressing a supercritical fluid. Most of the compressor exergy loss occurs in the recompressor as the temperature is well above the critical point and require a larger portion of work energy input to the compressor. This results in a 43% decrease in specific volume of the fluid in the recompressor compared to a 14% decrease in specific volume of the fluid in the main compressor. As flow rates are similar for both compressors the additional work required by the recompressor produces higher percentage of exergy destruction as a result.

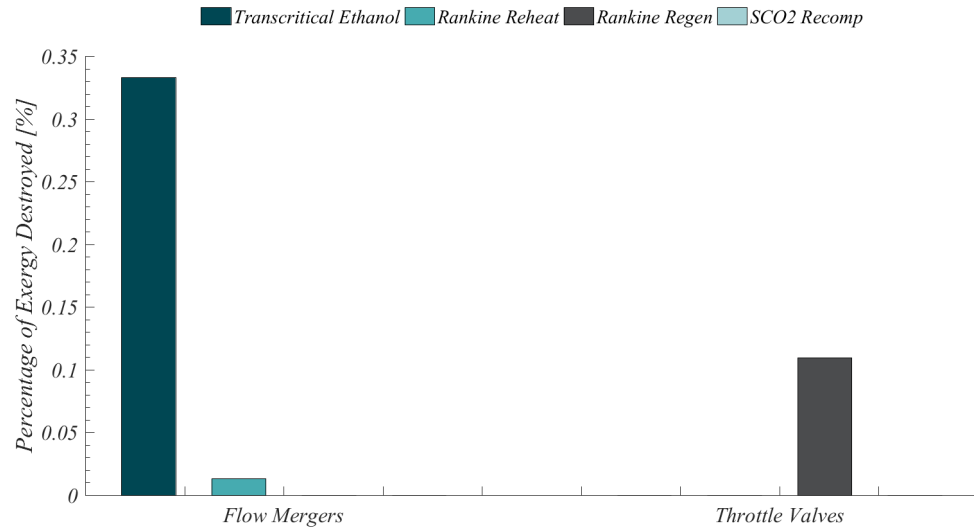


Figure 4.14: Percentage of exergy destroyed for flow mergers and throttle valves.

The percentage of exergy destroyed within the fluid mergers and throttle valves is shown in figure 4.14. While the overall percentage of exergy destroyed is very small ($< 1\%$), the effect of throttling and merging is quantified and does have small losses associated with it.

4.3 Costing and LCOE Analysis

Costing analysis utilized first order costing methods to estimate the major components of the power cycle (heat exchangers, turbines, pumps, and compressors). The cycle capital cost along with the cycle efficiency were used to estimate an updated levelized cost of electricity (LCOE). Uncertainty analysis was performed on both the cycle efficiency and LCOE. The uncertainty propagation provides a range of both upper and lower values to compare with the estimated values. In this section each of the cycle's capital component costs and LCOE are discussed, and an overall cycle comparison of LCOE and efficiency is presented.

4.3.1 Cycles

4.3.1.1 Regenerative Rankine Cycle

The regenerative Rankine cycle is the baseline design from which all other cycles have been compared. As the specific costs for this setup are not disclosed publicly by NuScale, the cycle costs were estimated at the optimized efficiency point. These cost estimates were then used to determine the fraction of equipment costs (f_{equip}) for use in equation 3.46.

The cost for the optimized baseline regenerative Rankine cycle was estimated at \$20.8 million for the major components. A breakdown of the costs by component estimated from the costing models is shown in figure 4.15. The majority of the power cycle cost is from the turbine and condenser which represent over 90% of the cycle's cost.

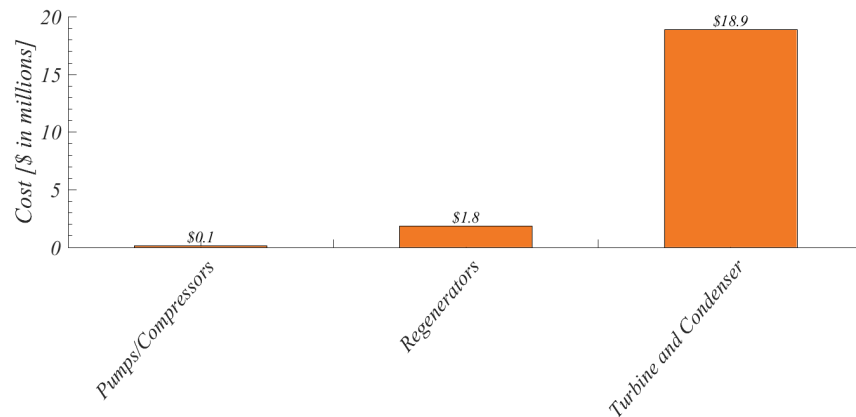


Figure 4.15: Regenerative Rankine cycle estimated cost by component.

As the regenerative Rankine cycle is the baseline cycle used to compare all other cycles it is assumed the optimized efficiency of 31.2% produces the LCOE value from NuScale of 89.04 \$/MWh. Setting the baseline cycle to the cited NuScale value provides a method to easily compare all other cycles by calculating a new LCOE value using the method described in section 3.5.

With total cycle costs of \$20.8 million, the fraction of equipment costs to total plant costs was found to be 8.6%. This value along with the optimized efficiency value of 31.2%

was used in all other cycle LCOE calculations.

To see how LCOE and cycle efficiency are related with the regenerative Rankine cycle, the average regenerator effectiveness is varied and shown in figure 4.16. By improving the effectiveness of the regenerator heat exchangers the efficiency of the power cycle typically improves.

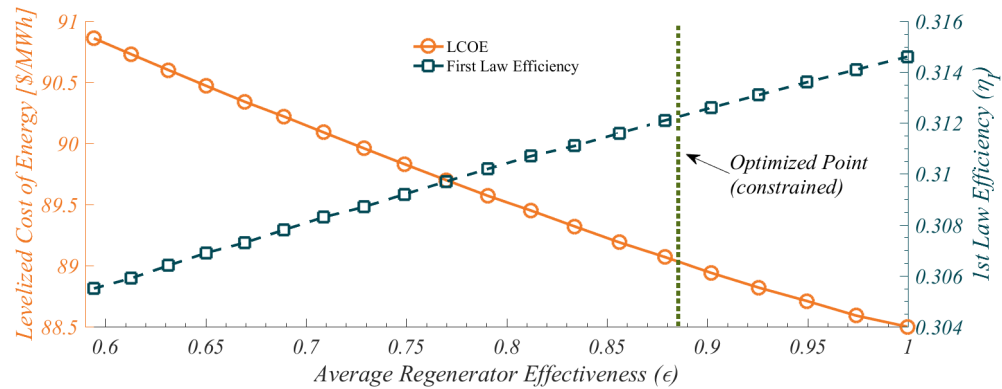


Figure 4.16: Regenerative Rankine cycle levelized cost of electricity and 1st law efficiency vs. average regenerator effectiveness.

For the baseline cycle, it shows the LCOE and efficiency both improve as effectiveness is increased. This holds even at an effectiveness values close to 1 (a value of 1 represents a perfect heat exchanger). This is due to the additional cost of the larger regenerators not exceeding the benefit in additional power produced. The optimized point for cycle efficiency is shown with the green dotted line in figure 4.16. This point was constrained to the value of 31.2% due to the pinch point temperature assumption of 5°C within all heat exchangers. Uncertainty calculations determined the cycle efficiency value of 31.2% has a plus/minus range 0.6% due to the uncertainty of the turbine and pump efficiency values.

4.3.1.2 Regenerative Reheat Rankine Cycle

The cost for the regenerative reheat Rankine cycle is estimated at \$24.3 million for the major components. The cycle used for costing only included one regenerator with the other two fluid streams mixing with the feedwater. A breakdown of the costs by

component is shown in figure 4.17. The majority of the power cycle cost is from the turbine and condenser which represent over 81% of the cycle's cost.

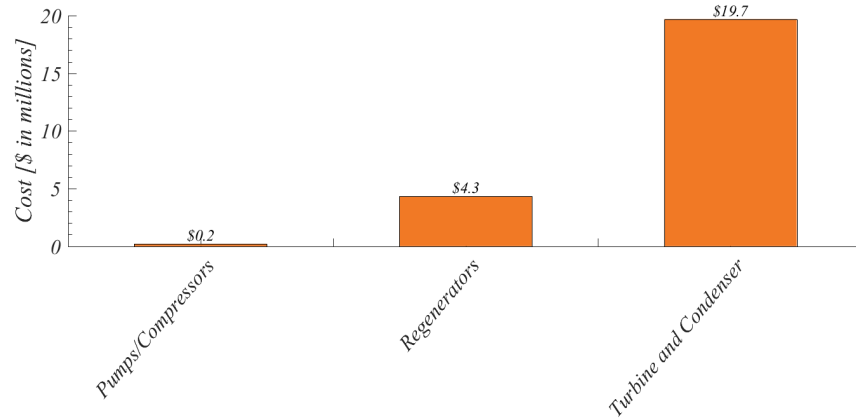


Figure 4.17: Regenerative reheat Rankine cycle estimated cost by component.

The optimized LCOE value was found to be at 84.47 ± 3.60 \$/MWh which coincided with the optimized efficiency value of $33.1\% \pm 0.6\%$. The reason both values were found at the same point is shown in figure 4.18 where average regenerator effectiveness is varied. The green dotted line in figure 4.18 represents the optimized LCOE and efficiency point. This point was constrained from seeking better values due to the pinch point temperature assumption of 5°C within all heat exchangers.

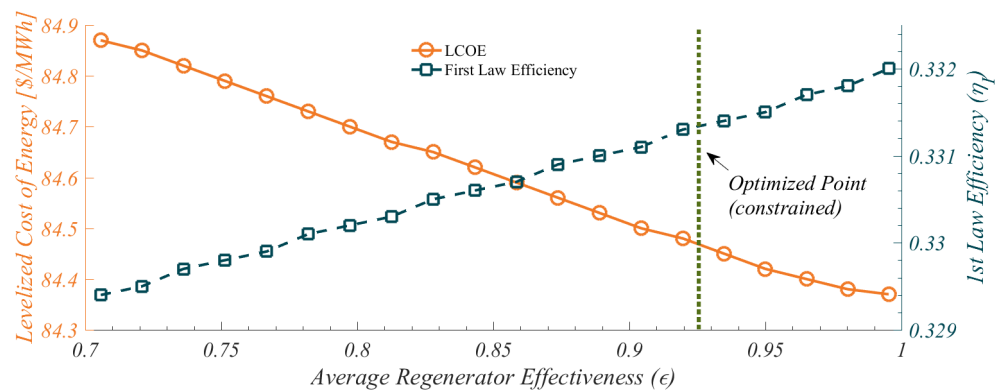


Figure 4.18: Regenerative reheat Rankine cycle levelized cost of electricity and 1st law efficiency vs. average regenerator effectiveness.

While not explicitly seen in figure 4.18, the LCOE value does reach an optimal point before reaching an effectiveness of 1 at around 0.995, when the heat exchanger cost begins to outweigh the additional power produced.

The independent variables used to solve for the optimized LCOE point are found in table 4.4 located in section 4.1.1.1, as both the optimized point for LCOE was the same as the optimized point for cycle efficiency.

4.3.1.3 Transcritical Ethanol Cycle

The cost for the transcritical ethanol cycle is estimated at \$37.6 million for the major components. The cycle used for costing included 3 regenerators. A breakdown of the costs by component is shown in figure 4.19. The power cycle costs are split between the turbine and heat exchangers which represent around 50% of the costs each.

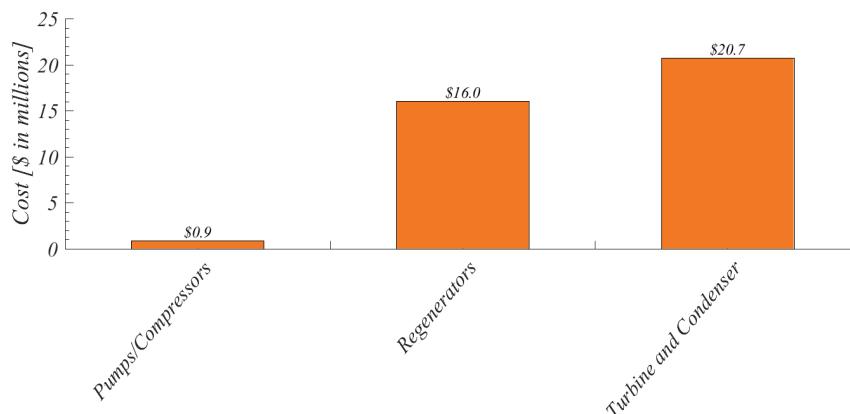


Figure 4.19: Transcritical cycle estimated cost by component.

The large cost in the regenerators is due to the lower ethanol convection coefficients for heat transfer which require larger heat exchanger surface area. Additionally, the high and medium temperature regenerators contain a large degree of superheated vapor coming from the turbine. The heat exchanger surface area model considered the vapor stream as a gas heat transfer mode which lowers the convection coefficient by a factor of 10 or more.

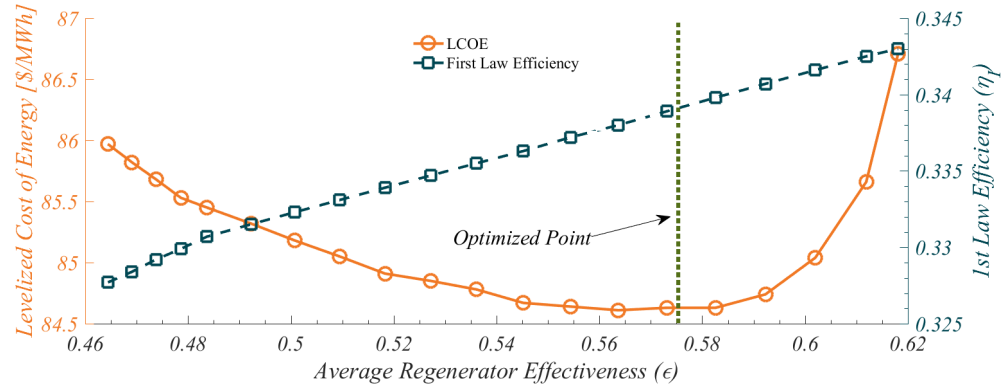


Figure 4.20: Transcritical cycle levelized cost of electricity and 1st law efficiency vs. average regenerator effectiveness.

The optimized LCOE value was found to be at 84.63 ± 4.28 \$/MWh which produces an overall efficiency of $33.9\% \pm 0.6\%$ and differs from the efficiency as optimized without considering LCOE with a value of 34.1%. The difference between the two is driven by the increasing cost of the regenerators which is shown in figure 4.20 where average regenerator effectiveness is varied. The green dotted line in figure 4.20 represents the optimized LCOE point. As the average regenerator effectiveness is increased beyond the optimal point, the cost of the regenerators outweighs the increase cycle efficiency. The high cost of the heat exchangers lowers the overall average regenerator effectiveness to a value of 57%. This is quite low compared to other cycles with averages of 90% or greater, and is due to two reasons. The first, as mentioned, is the cost of the regenerators due to the large increase in estimated surface area to accommodate the increased regenerator effectiveness. The second is the phase changes occurring during regeneration develop pinch points, which prevent more effective heat transfer from occurring.

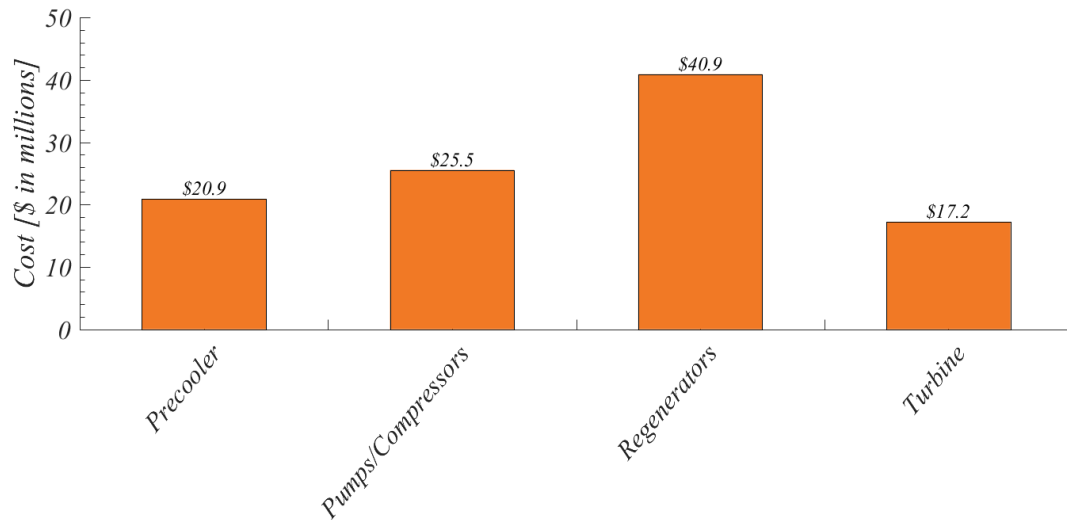
The independent variables used to solve for the optimized LCOE point are found in table 4.14. The state points for the pressure values labeled in table 4.14 correspond to the state points on the diagram in figure 4.3.

Table 4.14: Independent variables used to solve the transcritical ethanol cycle for minimum LCOE.

Value Name	Variable	Value
Max Pressure [bar]	P_1	74
Turbine Stage One Pressure [bar]	P_2	25
Turbine Stage Two Pressure [bar]	P_4	7.5
Turbine Stage Three Pressure [bar]	P_6	1.15
High Temp Regenerator Effectiveness	ϵ_{high}	0.59
Medium Temp Regenerator Effectiveness	ϵ_{high}	0.54
Low Temp Regenerator Effectiveness	ϵ_{low}	0.60

4.3.1.4 sCO_2 Recompression Cycle

The cost for the sCO_2 recompression Cycle is estimated at \$105 million for the major components. A breakdown of the costs by component is shown in figure 4.21.

**Figure 4.21:** sCO_2 recompression cycle estimated cost by component.

The regenerators make up the largest portion of the costs at 39%. The compressor is the next largest contributing to 24% of costs, and is followed by the precooler and turbine at 20% and 16% respectively. The large cost for the regenerators is due to the large conductance value of 40.9 MW/K and the heat exchanger requirement to be a printed circuit design (PCHE).

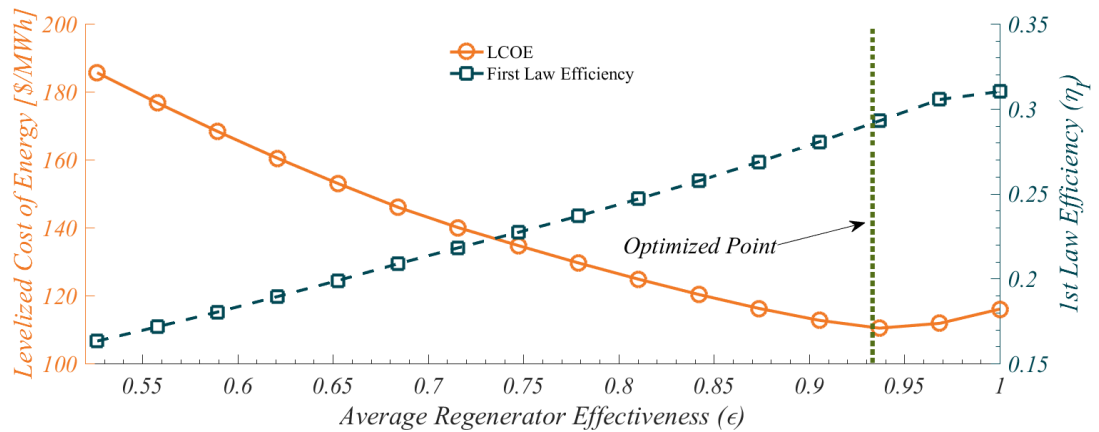


Figure 4.22: sCO_2 recompression cycle levelized cost of electricity and 1st law efficiency vs. average regenerator effectiveness.

The optimized LCOE value was found to be at 108.41 ± 11.44 \$/MWh which produces an overall efficiency of $29.8\% \pm 0.8\%$ and differs from the optimized efficiency value of 29.9%. The difference between the two is driven by the increasing cost of the regenerators which is shown in figure 4.22 where average regenerator effectiveness is varied. The green dotted line in figure 4.22 represents the optimized LCOE point. As the average effectiveness is increased from the optimal point, the cost of the regenerators outweighs the increased cycle efficiency.

The independent variables used to solve for the optimized LCOE point are found in table 4.15. The state points for the pressure values labeled in table 4.15 correspond to the state points on the diagram in figure 4.6.

Table 4.15: Independent variables used to solve the sCO_2 recompression cycle for minimum LCOE.

Value Name	Variable	Value
Max Pressure [bar]	P_1	125
Min Pressure [bar]	P_2	74
Min Temperature [C]	T_6	30.7
Flow Split Ratio	ϕ	0.48
High Temp Regenerator Effectiveness	ϵ_{HTR}	0.97
Low Temp Regenerator Effectiveness	ϵ_{LTR}	0.91

4.3.2 Cycle Comparison

Comparison of all cycles modeled and optimized for LCOE are shown in figure 4.23. The figure includes the cycle efficiency at the optimized LCOE value and the quantified uncertainty. Uncertainty calculations quantify the uncertainty found in the first order component costing models and the efficiency for the turbines, pumps, and compressors. The LCOE value for the regenerative Rankine cycle is the stated estimated value from NuScale [9] (adjusted for 2018 dollars), while all other cycle LCOE values were determined based on this value.

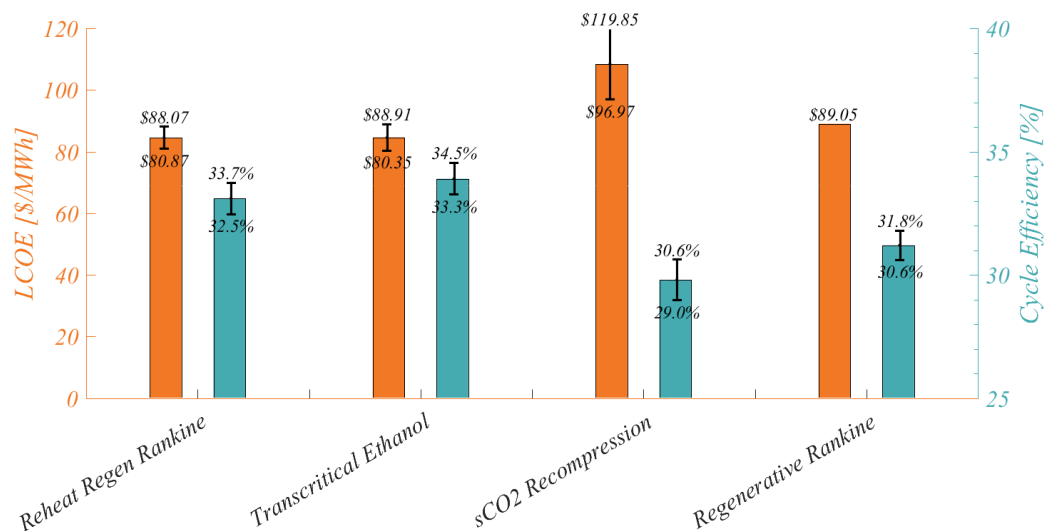


Figure 4.23: Estimated levelized cost of electricity (LCOE) cycle efficiency comparison. Error bars represent the uncertainty in the cost models and turbine, pump, and compressor efficiencies. Highlighted value is the estimate provided by NuScale [9] for the baseline regenerative Rankine cycle.

The regenerative reheat Rankine cycle shows the lowest (best) LCOE, followed by the transcritical ethanol cycle. These two cycles show a percent change decline of 5% below that of the baseline regenerative Rankine cycle with a LCOE of 89.05 \$/MWh. The upper end of the uncertainty in regenerative reheat Rankine cycle still places it below the baseline LCOE value due to a relatively small increase in cost along with the increase in cycle efficiency. The upper end of the uncertainty in the transcritical ethanol cycle estimates to be slightly above the baseline cycle, due to the higher costs of the cycle magnifying the cost uncertainties.

The sCO_2 recompression cycle is projected far above all other cycles with a percent change increase of 22.5%. This is both due to significantly higher estimated costs while producing less power than the baseline cycle. To break even with the baseline cycle LCOE value, the sCO_2 recompression cycle would need to produce an additional 11 MW of power, if holding costs constant. Conversely, holding power production constant and reducing cycle costs to zero, the sCO_2 recompression cycle would still be unable to break even with the baseline cycle.

Chapter 5 Discussion

The overall results from the cycle analyses from section 4 has been summarized in table 5.1. Only the two cycles, regenerative reheat Rankine and transcritical ethanol, estimated to have higher efficiencies and a lower levelized cost of electricity (LCOE) when compared to the baseline regenerative Rankine cycle. It was found that increasing power produced is the best method for lowering LCOE. This is due to the estimated power cycle costs contributing only 4% to the LCOE value.

The sections contained in the discussion provide some insight into the main results presented in the previous section on cycle efficiency, exergy efficiency, and LCOE.

Table 5.1: Summary of potential NuScale power cycles to replace the current regenerative Rankine cycle.

Cycle	Efficiency [%]	LCOE [\$/MWh]	Replacement	Notes
Combined	25.6	-	No	Cycle unable to generate high efficiency
Kalina	-	-	No	Cycle efficiency too low based on NuScale analysis
Regenerative Rankine	31.2	89.05	N/A	Baseline cycle for the NuScale SMR
Regenerative Reheat Rankine	33.1	84.47	Good	Higher efficiency offsets the additional cost. Potential to increase reactor power out.
Regenerative sCO_2	24.5	-	No	Cycle efficiency too low
sCO_2 Recompression	29.9	108.41	Unlikely	Cycle cost is 5 times higher. Only potential is based on increasing reactor power out.
Transcritical NH3	26.4	-	No	Cycle efficiency is too low
Transcritical Ethanol	34.1	84.63	Good	Highest cycle efficiency offsets the doubling of cycle costs. Potential to increase reactor power out.
Trilateral Flash Cycle	-	-	No	Potential low efficiencies and lack of commercial two phase expander

5.0.1 Cycle Efficiency

Comparing the results to literature the efficiencies found for both the steam Rankine cycles and sCO_2 cycles compare well with the results from Dostel et. al shown in figure 2.5. By extrapolating the values in figure 2.5 to the 300 °C temperature range, the plot projects cycle efficiencies of 34.6% for the steam cycle and 29.3% the sCO_2 cycle (model determined 33.1% for the reheat cycle and 29.9% for the sCO_2 recompression cycle). Santini et al. showed cycle efficiencies of 30.9% for the sCO_2 recompression cycle at comparable operating temperatures and pressures. The higher efficiency value is likely due to the condensing temperature and turbine efficiency assumptions used. When using Santini et al's condensing temperature of 24 °C and increasing turbine efficiency to 0.93, the model determined a higher efficiency of 31.7% for the recompression cycle.

The uncertainty for cycle efficiency consists only of the assumed efficiencies for the turbine, pumps, and compressor components along with the Baumann factor used in the turbine moisture model. For all cycles, except the sCO_2 recompression cycle, 95% or more of the uncertainty is due to the uncertainty within the turbine. For the uncertainty in the sCO_2 recompression cycle, it is still dominated by the turbine efficiency uncertainty, but less so in that it contributes to 88% of the uncertainty.

5.0.2 Exergy Efficiency

Comparing the exergy losses within the four cycles analyzed showed large shifts in which components contributed the most losses. If the turbine and pumps/compressors are combined, the total exergy destroyed varied little from 10.5%-12.0% across all cycles. The main differences found within the cycles comes from the losses found within the heat exchangers. When summing up the regenerators, precooler/condenser, and primary heat exchanger, the range of exergy destruction is 19%-28% compared to the cycle's overall total percentage of exergy destroyed of 31%-39%.

The ethanol cycle has the lowest overall losses due to a large reduction in the condenser, and a smaller but significant decline in the primary heat exchanger. This reduction is somewhat offset by an increase in exergy destruction within the regenerators.

The baseline cycle has the largest losses within the primary heat exchanger at 14.1%. Conversely, the similar reheat cycle lowers losses by almost 4%, which shows the benefit

of higher boiling pressures.

5.0.3 Levelized Cost of Energy (LCOE)

The LCOE results show the transcritical ethanol and the regenerative reheat Rankine cycle produce lower LCOE results compared to the baseline cycle. This would make the NuScale power plant more attractive to investment as it would better compete with the cleaner alternatives of gas combined cycles with carbon capture and solar PV, making nuclear a stronger option out of sources with low greenhouse gas emissions.

The high costs found for the sCO_2 recompression model were unexpected based on literature. Where turbine sizes are expected to be 25% of traditional steam turbines. This analysis found the turbine and compressors doubled in cost compared to the Rankine pumps and turbine, but the biggest cost driver was the printed circuit heat exchangers (PCHEs). As the sCO_2 recompression cycle has a small pressure ratio of 1.7 a large amount of internal heat exchange is required to maintain adequate efficiency. As sCO_2 power cycles become more available, the costs of the cycle should lower due to economies of scale. Even with cost reductions, the NuScale SMR design, with a maximum temperature around 300 °C and pressure at 125 bar, makes the cycle an unlikely candidate for use in the NuScale SMR.

It's important to reiterate the model limitations when interpreting these results. The uncertainty of the costing models and component efficiencies was quantified in the LCOE optimized values. The costing models are first order models that can have errors of 50% or more and uncertainty calculations show the costs contribute between 60% - 80% of the total uncertainty shown in figure 4.23. The remaining 20% - 40% of the uncertainty is found in the cycle efficiency. The range of uncertainty in LCOE for the regenerative reheat Rankine cycle and transcritical ethanol cycle is between 4% - 5% of the estimated value. This places the upper-bound of the estimated reheat cycle LCOE value still below the baseline LCOE value, while the transcritical ethanol LCOE value is slightly above the baseline value.

One other important limitation is the models do not include ancillary items such as piping and differences in operating and maintenance costs. These can vary significantly due to large pressure and flow rate differences between the cycles and would need to be further assess against the baseline cycle.

5.0.4 Efficiency vs. LCOE

As shown in the results in section 4, the optimal points for efficiency and LCOE were the same for both the baseline and reheat Rankine cycles, but differed for the transcritical ethanol and sCO_2 recompression cycles. The main contributor for the difference in the two points is due to the estimation of the heat exchange surface area.

For the transcritical cycle the high and medium temperature regenerators both contain superheated vapor at the regenerator inlet. The heat exchanger area model considers this to be a gas/vapor heat exchange which lowers the heat transfer convection coefficient by a factor of 10 or more. This mode of heat transfer significantly increases the required area to the point where it dominates the overall area required. This effect can be described by viewing figure 5.1 which shows the temperature profile during heat exchange within the high temperature regenerator for the transcritical ethanol cycle.

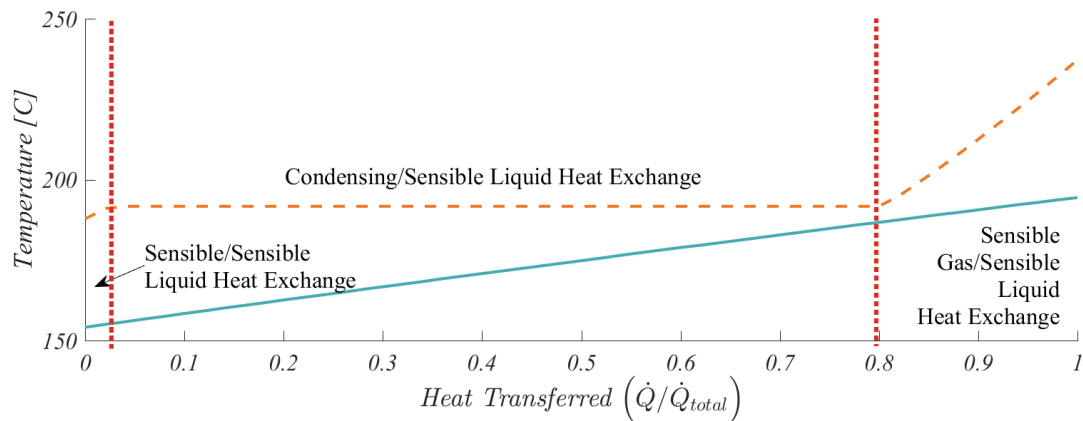


Figure 5.1: Temperature profile within the high temperature regenerator in the transcritical ethanol cycle.

The high temperature regenerator undergoes 3 different modes of heat transfer as shown in figure 5.1. The cold stream is always performing sensible liquid heat transfer, but the modes switch when the hot stream undergoes phase changes. From left to right, the first mode has the smallest amount of heat transferred when both fluids are performing sensible liquid heat transfer. The second mode contains the largest portion of heat transferred within the middle stage where condensation takes place. The last

mode seen on the right side of the figure is when the hot stream is a superheated vapor undergoing a sensible gas heat exchange.

The convection coefficient in the sensible gas heat exchange mode are much smaller than the other modes of heat exchange and therefore require about 33% of the total surface area to transfer 20% of the heat. This area determined during the third mode of heat exchange is potentially much greater than required. This is due to the superheated vapor likely to undergo local condensation if temperature gradients exist between the tube wall and bulk fluid temperature. Much like seeing water condensation on a cold glass in a room with low relative humidity. If this is the case, the convection coefficients would be significantly higher, and would reduce the estimated costs of the heat exchangers.

5.0.5 Reactor Power

The sensibly heated transcritical and supercritical cycles show the smallest losses within the primary heat exchanger. This is driven by better temperature profile matching with the primary source which is sensibly cooled. The highest entropy generation in the primary heat exchanger occurs when paired with the regenerative Rankine cycle. This cycle has a low boiling temperature to facilitate the large amount of superheat required for turbine expansion. The regenerative reheat Rankine cycle is able to raise the boiling temperature which decreases exergy destruction.

When looking at the power production side of the LCOE equation, a decrease in LCOE can be performed in one of two ways. The first as discussed throughout this paper is to increase the efficiency of the power cycle. The increased cycle efficiency generates more electricity for the same amount of heat from the nuclear reactor. The second is to increase the power from the nuclear reactor. By generating more heat for the nuclear reactor the power cycle can then generate more electricity at a given cycle efficiency.

The caveat of increasing reactor power is the power cycle needs to possess the capability to extract the additional heat from the reactor within the NuScale SMR. As the NuScale SMR cools via natural convection, to extract more heat, the difference between the maximum and minimum coolant temperatures must be increased. Since the maximum temperature cannot be increased within the current design, the coolant has to be cooled below the minimum temperature.

The ability for the potential cycles to extract more heat is best shown in figures 5.2 and 5.3, where the temperature profiles of the reactor coolant and power cycle working fluids are shown within the primary heat exchanger. In figure 5.2 the baseline regenerative Rankine cycle and the regenerative reheat Rankine cycle show the difficulty in increasing reactor power. The reheat cycle contains a pinch point where the working fluid begins boiling, while the baseline cycle has a large amount of superheat which can be assumed to take up the remaining surface area within the primary heat exchanger. One possible option to increase reactor power, is to lower the boiling temperature in the optimized regenerative reheat Rankine cycle to somewhere between the baseline cycle and the current optimized level. This action would lower cycle efficiency, but would allow for additional heat generation from the reactor. An optimization would need to be performed by taking into account the adjusted cycle efficiency, reactor power increase, and the heat transfer capability within the primary heat exchanger to assess to best option for the regenerative reheat Rankine boiling pressure.

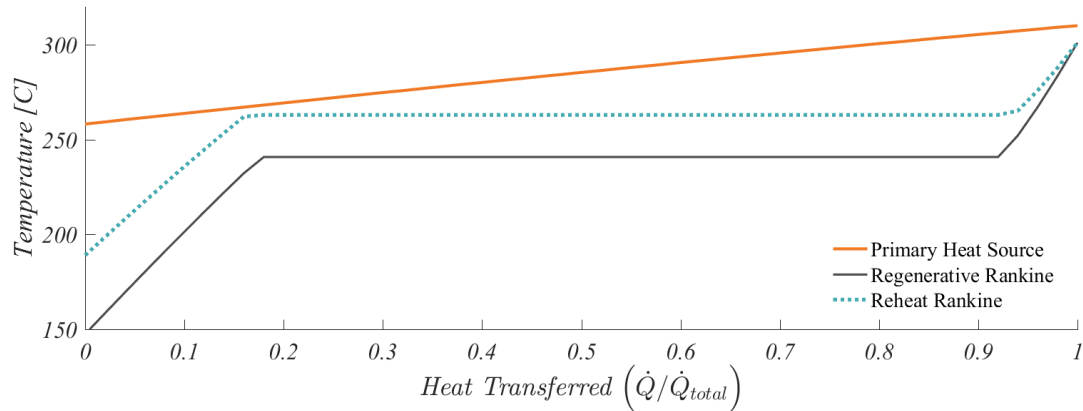


Figure 5.2: Temperature profile of the baseline regenerative Rankine and regenerative reheat Rankine cycles during heat exchange within the primary heat exchanger.

The ability of the transcritical ethanol and sCO_2 recompression cycles to extract additional heat from the nuclear reactor can be seen in figure 5.3. Both cycles can allow for a temperature decrease in the primary coolant as both have a large ΔT between the primary coolant outlet temperature and the fluid's inlet temperature (with no internal pinch points). The potential obstacle for any of these cycles in increasing reactor power

is found in the size of the primary heat exchanger. The reduction in coolant temperature would correspond to a reduction in the mean ΔT between the two streams. This would require larger heat transfer surface areas to handle the additional heat load. To determine if this would be a problem, a heat transfer analysis would need to be performed on the primary heat exchanger.

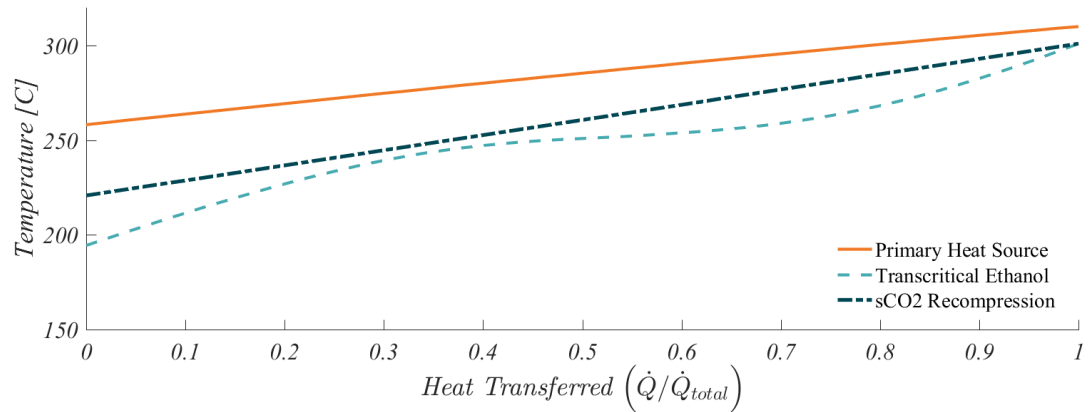


Figure 5.3: Temperature profile of the transcritical ethanol and sCO_2 recompression cycle during heat exchange within the primary heat exchanger.

Chapter 6 Conclusion

This thesis provided an analysis of the fit for thermal power cycles coupled to a small modular reactor (SMR). The SMR was based on the design from NuScale Power where the reactor is sensibly cooled via natural convection. The analysis included a literature review of current power cycles to determine which designs could be well suited for the SMR design. Candidate cycles were then analyzed for overall cycle efficiency, exergy losses, costs, and plant levelized cost of electricity (LCOE).

Results from the analysis used models developed from the first and second law of thermodynamics. Costing and LCOE analysis was performed using first order costing methods where a size or capacity parameter is supplied to estimate cost for the major power cycles components of turbines, compressors, pumps, and heat exchangers. Cycles were optimized using multi-variable optimization algorithms. To handle inequality constraints during optimization, the optimization functions were transformed from constrained problems to unconstrained problems via the penalty method.

Results substantiated the baseline regenerative Rankine cycle is a strong fit for the NuScale SMR due to good cycle efficiency ($31.2 \pm 0.6\%$), low cost, and simple setup. Results also showed two other cycles, regenerative reheat Rankine cycle and transcritical ethanol cycle, would provide higher cycle efficiencies ($33.1 \pm 0.6\%$ and $33.9 \pm 0.6\%$) and a lower LCOE ($5.1 \pm 4.0\%$ and $4.8 \pm 4.8\%$ reduction from baseline).

The regenerative reheat Rankine cycle would be the simplest cycle to integrate into the NuScale SMR. This cycle would not require vastly different components, and the heat transfer interactions within the SMR are already well understood. The regenerative reheat Rankine cycle would require two reheater regenerators, but it was found the low and medium temperature feedwater regenerators could be removed and replaced with mixing valves and pumps. Costs for the reheat cycle components were estimated to

be 17% higher, but this only counts towards a small portion of the overall costs for LCOE (estimated around 4%). Therefore, the increased efficiency more than offsets the increased equipment capital costs when looking at LCOE.

The transcritical ethanol cycle is an attractive replacement due to the higher efficiencies achieved by the cycle. These high efficiencies were somewhat offset by the higher estimated cycle equipment capital costs, but there is potential the costs for the high and medium regenerators are over estimated. Other downsides to the ethanol cycle include the safety risk of using a flammable working fluid, high fluid flow rates, higher system pressures, and less knowledge and experience using ethanol within power cycles.

Future recommended work includes heat transfer analysis of the capability for power cycles to facilitate additional power production from the reactor. As the NuScale SMR circulates coolant via natural convection, working fluids need to reduce pinch points within the primary heat exchanger as well maintain good convection heat transfer coefficients to meet target temperatures within the current heat exchanger geometry.

Additional work includes looking at longer term solutions such as designing the SMR to handle higher temperatures and pressures. This would need to include a cost analysis such as LCOE to account for the increased reactor plant costs in addition to the increase in generated power.

Bibliography

- [1] J. Carl and D. Fedor, *Keeping the Lights on at America's Nuclear Power Plants*. Hoover Institution Press, 2017 (page 1).
- [2] H. J. Yoon, Y. Ahn, J. I. Lee, and Y. Addad, "Potential advantages of coupling supercritical CO₂Brayton cycle to water cooled small and medium size reactor," *Nuclear Engineering and Design*, vol. 245, pp. 223–232, 2012 (pages 1, 13, 14).
- [3] Office of Nuclear Energy, *Benefits of Small Modular Reactors (SMRs) — Department of Energy* (page 1).
- [4] NuScale Power, *NuScale Reactor Diagram* (page 2).
- [5] —, *Small Modular Reactor*, 2018 (page 3).
- [6] —, *SMR Power Plant Operating Costs*, 2016 (pages 4, 43).
- [7] —, *NuScale Power - FAQs*, 2018 (page 4).
- [8] —, *Part 02 - Final Safety Analysis Report (Rev. 0) - Part 02 - Tier 02 - Chapter 04 - Reactor - Sections 04.01 - 04.06*, Corvallis, OR, 2016 (pages 6, 7).
- [9] —, *Part 02 - Final Safety Analysis Report (Rev. 0) - Part 02 - Tier 02 - Chapter 10 - Steam and Power Conversion System - Sections 10.01 - 10.04*, Corvallis, OR, 2016 (pages 6–8, 31, 38, 53, 55, 86, 87).
- [10] S. Klein and G. Nellis, *Thermodynamics*. Cambridge University Press, 2011 (pages 7, 9).
- [11] T. Srinivas, A. V. S. S. K. S. Gupta, and B. V. Reddy, "Generalized thermodynamic analysis of steam power cycles with 'n' number of feedwater heaters," *International Journal of Thermodynamics*, vol. 10, no. 4, pp. 177–185, 2007 (page 8).

- [12] A. Leyzerovich, *Wet-steam Turbines for Nuclear Power Plants*. PennWell Corporation, 2005 (pages 9, 24).
- [13] G. Gyarmathy, *Foundations of a Theory of the Wet-steam Turbine*, ser. FTD-TT-63-785. Translation Division, Foreign Technology Division, 1966 (pages 9, 24).
- [14] F. P. Incropera, T. L. Bergman, A. S. Lavine, and D. P. DeWitt, *Fundamentals of Heat and Mass Transfer*. 2011, p. 567. arXiv: 1105- (pages 10, 26).
- [15] V. Dostal, M. Driscoll, and P. Hejzlar, “A Supercritical Carbon Dioxide Cycle for Next Generation Nuclear Reactors,” *Technical Report MIT-ANP-TR-100*, pp. 1–317, 2004 (pages 10, 12–14, 34, 35).
- [16] Y. Chen, “Thermodynamic Cycles using Carbon Dioxide as Working Fluid - CO2 Transcritical Power Cycle Study,” *PhD Thesis*, 2011 (page 10).
- [17] L. Santini, C. Accornero, and A. Cioncolini, “On the adoption of carbon dioxide thermodynamic cycles for nuclear power conversion: A case study applied to Mochovce 3 Nuclear Power Plant,” *Applied Energy*, vol. 181, no. 2016, pp. 446–463, 2016 (pages 10, 13, 14, 19, 35).
- [18] Budapest University of Technology and Economics, *What is a supercritical fluid?* 2015 (page 10).
- [19] E. G. Feher, “The Supercritical Thermodynamic Power Cycle,” *Energy Conversion*, vol. 8, no. 2, pp. 85–90, 1968 (pages 10, 14).
- [20] M. D. Carlson, B. M. Middleton, and C. K. Ho, “Cycles Using Component Cost Models Baselined With Vendor Data,” in *Proceedings of the ASME 2017 Power and Energy Conference*, Charlotte, NC, 2017, pp. 1–7 (pages 11, 31, 33, 34).
- [21] J. Dyreby, S. Klein, G. Nellis, and D. Reindl, “Design Considerations for Supercritical Carbon Dioxide Brayton Cycles With Recompression,” *Journal of Engineering for Gas Turbines and Power*, vol. 136, no. 10, p. 101701, 2014 (pages 11, 12, 14, 19, 26).
- [22] G. Angelino, “Real Gas Effects in Carbon Dioxide,” *ASME*, pp. 1–12, 1969 (page 11).
- [23] G. Kimzey, “Development of a Brayton Bottoming Cycle using Supercritical Carbon Dioxide as the Working Fluid,” *EPRI Report*, pp. 1–31, 2012 (page 12).

- [24] V. Dostal, P. Hejzlar, and M. J. Driscoll, “The Supercritical Carbon Dioxide Power Cycle : Comparison to Other Advanced Power Cycles,” *Nuclear technology*, vol. 154, no. 3, pp. 283–301, 2006 (page 12).
- [25] Y. Ahn, S. J. Bae, M. Kim, S. K. Cho, S. Baik, J. I. Lee, and J. E. Cha, “Review of supercritical CO₂power cycle technology and current status of research and development,” *Nuclear Engineering and Technology*, vol. 47, no. 6, pp. 647–661, 2015 (page 13).
- [26] R. V. Padilla, R. Benito, and W. Stein, “An Exergy Analysis of Recompression Supercritical CO₂ Cycles with and without Reheating,” *Energy Procedia*, vol. 69, pp. 1181–1191, 2015 (page 14).
- [27] M. J. Moran, H. N. Shapiro, D. D. Boettner, and M. B. Bailey, *Fundamentals of engineering thermodynamics*, English. 2014 (pages 15, 23).
- [28] NIOSH, *CDC - NIOSH Pocket Guide to Chemical Hazards - Ammonia* (page 15).
- [29] A. I. Kalina, “Combined-Cycle System With Novel Bottoming Cycle,” *Journal of Engineering for Gas Turbines and Power*, vol. 106, no. 4, 1984 (page 15).
- [30] X. Zhang, M. He, and Y. Zhang, “A review of research on the Kalina cycle,” *Renewable and Sustainable Energy Reviews*, vol. 16, no. 7, pp. 5309–5318, 2012 (page 16).
- [31] E. Thorin, “Power Cycles with Ammonia-Water Mixtures as Working Fluid: Analysis of Different Applications and the Influence of Thermophysical Properties,” *Department of Chemical Engineering and Technology*, p. 54, 2000 (page 16).
- [32] A. Modi, M. R. Kærn, J. G. Andreasen, and F. Haglind, “Thermoeconomic optimization of a Kalina cycle for a central receiver concentrating solar power plant,” *Energy Conversion and Management*, vol. 115, pp. 276–287, 2016 (page 17).
- [33] A. Modi and F. Haglind, “Thermodynamic optimisation and analysis of four Kalina cycle layouts for high temperature applications,” *Applied Thermal Engineering*, vol. 76, pp. 196–205, 2015 (page 17).
- [34] I. Gawron and D. Botha, “Evaluation of Alternative Power Cycles for a NuScale Reactor,” NuScale, Corvallis, OR, Tech. Rep., 2017, p. 51 (page 17).

- [35] Kalina A.I. and H. Leibowitz, "Applying Kalina Technology to a Bottoming Cycle for Utility Combined Cycles," *Gas Turbine Conference and Exhibition*, 1987 (page 17).
- [36] T. V. Nguyen, T. Knudsen, U. Larsen, and F. Haglind, "Thermodynamic evaluation of the Kalina split-cycle concepts for waste heat recovery applications," *Energy*, vol. 71, pp. 277–288, 2014 (page 17).
- [37] R. Chacartegui, D. Sánchez, J. M. Muñoz, and T. Sánchez, "Alternative ORC bottoming cycles FOR combined cycle power plants," *Applied Energy*, vol. 86, no. 10, pp. 2162–2170, 2009 (pages 17, 18).
- [38] J. M. Muñoz De Escalona, D. Sánchez, R. Chacartegui, and T. Sánchez, "Part-load analysis of gas turbine & ORC combined cycles," *Applied Thermal Engineering*, vol. 36, no. 1, pp. 63–72, 2012 (page 17).
- [39] C. H. Marston and M. Hyre, "Gas Turbine Bottoming Cycles: Triple-Pressure Steam Versus Kalina," *Journal of Engineering for Gas Turbines and Power*, vol. 117, no. 1, pp. 10–15, Jan. 1995 (page 18).
- [40] C. Invernizzi, P. Iora, and P. Silva, "Bottoming micro-Rankine cycles for micro-gas turbines," *Applied Thermal Engineering*, vol. 27, no. 1, pp. 100–110, 2007 (page 18).
- [41] P. Pilavachi, "Mini-and micro-gas turbines for combined heat and power," *Applied Thermal Engineering*, vol. 22, no. 2002, pp. 2003–2014, 2002 (page 18).
- [42] S. Banik, S. Ray, and S. De, "Thermodynamic modelling of a recompression CO2 power cycle for low temperature waste heat recovery," *Applied Thermal Engineering*, vol. 107, pp. 441–452, 2016 (page 19).
- [43] T. Ho, S. S. Mao, and R. Greif, "Comparison of the Organic Flash Cycle (OFC) to other advanced vapor cycles for intermediate and high temperature waste heat reclamation and solar thermal energy," *Energy*, vol. 42, no. 1, pp. 213–223, 2012 (pages 19–21).
- [44] I. K. Smith, N. Stosic, and A. Kovacevic, "Power recovery from low cost two-phase expanders." *Transactions-Geothermal Resources Council*, pp. 601–606, 2001 (page 21).
- [45] J. Sarkar, "Second law analysis of supercritical CO2recompression Brayton cycle," *Energy*, vol. 34, no. 9, pp. 1172–1178, 2009 (page 29).

- [46] H. P. Loh, J. Lyons, and I. I. I. Charles W. White, "Process Equipment Cost Estimation, Final Report," *Other Information: PBD: 1 Jan 2002*, no. January, 2002 (pages 30, 31).
- [47] R. Turton, R. C. Bailie, W. B. Whiting, J. a. Shaeiwitz, and D. Bhattacharyya, *Analysis, Synthesis, and Design of Chemical Processes*, 6. 2012, vol. 40, p. 9823 (pages 30, 31).
- [48] S. Jenkins, *CEPCI Updates: January 2018 (prelim.) and December 2017 (final) - Chemical Engineering — Page 1*, 2018 (page 30).
- [49] M. S. Peters, K. D. Timmerhaus, and R. E. West, *Plant Design and Economics for Chemical Engineers*, ser. Civil Engineering. McGraw-Hill Education, 2003 (page 31).
- [50] M.-J. Li, H.-H. Zhu, J.-Q. Guo, K. Wang, and W.-Q. Tao, "The development technology and applications of supercritical CO₂ power cycle in nuclear energy, solar energy and other energy industries," *Applied Thermal Engineering*, vol. 126, pp. 255–275, 2017 (pages 32–34).
- [51] D. Milani, M. T. Luu, R. McNaughton, and A. Abbas, "Optimizing an advanced hybrid of solar-assisted supercritical CO₂ Brayton cycle: A vital transition for low-carbon power generation industry," *Energy Conversion and Management*, vol. 148, pp. 1317–1331, 2017 (page 32).
- [52] R. K. Shah and D. P. Sekulic, *Fundamentals of Heat Exchanger Design*, 2. 2003, vol. 11, p. 972 (pages 33, 39).
- [53] ESDU, *Selection and Costing of Heat Exchangers 92013*, 1994 (page 34).
- [54] EES, *Engineering Equation Solver Manual* (pages 35, 50).
- [55] J. A. Hesketh and P. J. Walker, "Effects of Wetness in Steam Turbines," *Proceedings of the Institution of Mechanical Engineers, Part C: Journal of Mechanical Engineering Science*, vol. 219, no. 12, pp. 1301–1314, (page 39).
- [56] U.S. Department of Energy Office of Indian Energy Policy and Programs, "Levelized Cost of Energy (LCOE)," *US department of energy*, p. 9, 2015 (page 43).
- [57] NuScale Power, *Construction Cost*, 2014 (page 43).
- [58] G. Nellis and S. Klein, *Heat Transfer*, ser. Heat Transfer. Cambridge University Press, 2009 (page 48).

- [59] J. Arora, *Introduction to Optimum Design*. Elsevier Science, 2011 (page 49).
- [60] B. N. Taylor, “Guidelines for evaluating and expressing the uncertainty of NIST measurement results,” National Bureau of Standards, Gaithersburg, MD, Tech. Rep., 1994 (page 51).

